Electrospinning of Bioactive Dex-PAA Hydrogel Fibers

by

Katherine BoYook Louie

A Dissertation Presented in Partial Fulfillment
of the Requirements for the Degree
Doctor of Philosophy

Approved April 2011 by the
Graduate Supervisory Committee:

Stephen Massia, Chair
Kevin Bennett
Antonio Garcia
Christine Pauken
Brent Vernon

ARIZONA STATE UNIVERSITY

May 2011

ABSTRACT

In this work, a novel method is developed for making nano- and micro-fibrous hydrogels capable of preventing the rejection of implanted materials. This is achieved by either (1) mimicking the native cellular environment, to exert fine control over the cellular response or (2) acting as a protective barrier, to camouflage the foreign nature of a material and evade recognition by the immune system. Comprehensive characterization and *in vitro* studies described here provide a foundation for developing substrates for use in clinical applications.

Hydrogel dextran and poly(acrylic acid) (PAA) fibers are formed via electrospinning, in sizes ranging from nanometers to microns in diameter. While "as-electrospun" fibers are continuous in length, sonication is used to fragment fibers into short fiber "bristles" and generate nano- and micro- fibrous surface coatings over a wide range of topographies. Dex-PAA fibrous surfaces are chemically modified, and then optimized and characterized for non-fouling and ECM-mimetic properties. The non-fouling nature of fibers is verified, and cell culture studies show differential responses dependent upon chemical, topographical and mechanical properties.

Dex-PAA fibers are advantageously unique in that (1) a fine degree of control is possible over three significant parameters critical for modifying cellular response: topography, chemistry and mechanical properties, over a range emulating that of native cellular environments, (2) the innate nature of the material is non-fouling, providing an inert background for adding back specific

bioactive functionality, and (3) the fibers can be applied as a surface coating or comprise the scaffold itself.

This is the first reported work of dex-PAA hydrogel fibers formed via electrospinning and thermal cross-linking, and unique to this method, no toxic solvents or cross-linking agents are needed to create hydrogels or for surface attachment. This is also the first reported work of using sonication to fragment electrospun hydrogel fibers, and in which surface coatings were made via simple electrostatic interaction and dehydration. These versatile features enable fibrous surface coatings to be applied to virtually any material. Results of this research broadly impact the design of biomaterials which contact cells in the body by directing the consequent cell-material interaction.

This dissertation is dedicated to BenBen.

ACKNOWLEDGMENTS

In addition to my husband Dr. Benjamin Bowen, I would like to acknowledge the love and support of my family. Special thanks to my father Dr. Dexter Louie, my mother Patricia Louie, my sisters Elise (ECπ), Jennifer (Dr. JJ) and Barbara Louie, and my brother-in-law Dr. Elliot Botvinick (Robotvinick), for always being there when I needed them and helping me through some rough times. Also thanks to my unforgettable, lovable pets Susie, Shakey, Sammy, Turtle, Jarvey and Fred.

Many thanks to all my committee members - Dr. Stephen Massia, Dr. Kevin Bennett, Dr. Brent Vernon, Dr. Christine Pauken and Dr. Tony Garcia. Special thanks to Dr. Bennett for providing much-appreciated positive inspiration during my last few months at ASU. Special thanks to Professors Neal Woodbury and Stephen Massia for providing the opportunity to pursue a PhD, and Professors Lokesh Joshi and Jim Sweeney for great mentorship during my TA experiences. Special thanks to Dr. Trent Northen and all the LBNL/UCB folks for a fun and inspirational work environment over the last few months.

I also want to thank my good friends and labmates Dr. Jeremy Brower and Dr. Doris Hom Eng, who provided me with tons of help in the lab and outside, as well as my friends Angel Stigen, Dr. Rohit Rosario and Bhavana Ramakrishnan, Anju and Shammi Jayaraj, Dr. Trent Northen and Laura Lee, Stefany and Dr. Gabriel Shaibi, and Chris Cardinal. I also thank the IGERT program for funding me through the majority of my research career at ASU, the Harrington Department of Bioengineering for teaching assistantships, as well as AZTE.

TABLE OF CONTENTS

PAGE

LIST OF FIGURES

FIGURE PAGE

FIGURE PAGE

FIGURE PAGE

FIGURE PAGE

CHAPTER 1

Introduction and Background

1. Introduction

A crucial part of biomaterials design is the optimization of material properties to elicit a specific, desirable cellular response. This is especially true in the design of cellular scaffolds for tissue regeneration or surface coatings for implantable materials. In these applications, specific chemical, mechanical and morphological properties of the biomaterial govern the cellular response. Dextran-based micro- and nano- fibrous hydrogel structures can be created that exhibit highly tunable topography and bioactivity. These can be customized to create novel surface coatings and cellular scaffolds to function as a non-fouling surface or ECM-mimetic material.

2. Background

2.1 Non-fouling materials in biomedical applications

The function of a non-fouling material is implied by the term: the material prevents fouling. Fouling is essentially an irreversible, uncontrolled accumulation of biological material on a surface, a process initiated primarily by non-specific interactions of proteins with a surface. This not only results in an unwanted build-up of protein matter, but the adsorbed proteins themselves also serve as a convenient substrate for undesirable deposition of biological cells or bacteria [1]. Fouling is a challenging problem in the world of biomaterials due to the numerous detrimental consequences that may occur. As result, non-fouling properties are a

crucial design requirement for numerous medical devices and biomaterials. Development of materials with non-fouling characteristics is essential for biomedical applications including dialysis, filtration and drug delivery, as well as the creation of contact lenses, tissue engineered constructs, and implants (stents, catheters, grafts, pacemakers, electrodes, organ transplants, scaffolds, bone screws, etc) [2].

For each of these applications, adsorbed proteins themselves may prevent a device from functioning as intended. Dialysis and filtration devices, for example, require flow through a selective membrane to remove toxic solutes and excess fluid, typically by size exclusion and diffusion principles. When the membrane becomes "clogged" with extraneous protein matter, filtration cannot occur and the device cannot function efficiently[1]. Contact lenses provide another example, as they must be resistant to protein build-up to prevent infection (since adsorbed proteins provide a substrate for bacterial adhesion and proliferation) and blurring of vision (since adsorbed proteins interfere with optical clarity of the lens) [3 4].

Another consequence of fouling may occur on materials implanted in the body, such as electrodes, biosensors, or tissue engineered constructs. Adsorbed proteins may trigger an inflammatory cascade of blood coagulation and recruitment and adhesion of leukocytes, leading to the foreign body reaction and fibrosis [5]. Fibrosis entails the adhesion and overproliferation of fibroblasts on a surface, consequent with a thickened mass of protein matrix components. In the case of skin, the result is scar tissue formation; in the case of implanted devices,

the result is fibrotic encapsulation, in which a fibrotic barrier is formed around the device, thereby limiting device integration and *in vivo* performance [5].

In the specific case of blood-contacting devices, such as stents and vascular grafts, adsorption of certain protein components in the blood initiates a cascade of events leading to platelet adhesion and aggregation, as well as acute thrombus formation [6]. In addition, this may lead to subsequent occlusion of the vessel over time, especially in the case of small-diameter vascular grafts [7]. As a result, non-fouling materials must be designed with properties providing hemocompatibility, as well as resistance to both protein adsorption and cell adhesion.

2.2. Current strategies to create non-fouling materials

In general, two options exist for the construction of non-fouling materials: (a) the *component material* itself may possess non-fouling properties or (b) a *surface coating* can be applied, providing a non-fouling layer that effectively shields the underlying material.

Non-fouling biomaterials can be categorized into two general types based on function, serving as either a (a) *barrier*, in which the non-fouling biomaterial completely prevents protein and cell adhesion or (b) *bridge*, in which the biomaterial induces certain cells and proteins to respond in a specific, desirable manner, thereby directing a favorable response to the material (preventing fouling). Often, a *bridge* material can be constructed by starting with a *barrier* material, and adding back bioactive molecules to elicit specific protein and cellular responses. As a result, a non-fouling biomaterial can be described as

being a *component material* or a *surface coating*, as well as possessing either *barrier* or *bridge* functionality.

Non-fouling biomaterials rely on controlling the interfacial interaction of the biomaterial surface with proteins and cells. In the case of a barrier, the optimal interaction is zero protein adsorption or cell adhesion. In the case of a *bridge*, the optimal interaction is adsorption of desirable proteins or adhesion of desirable cells (aka specific protein adsorption and cell adhesion), while preventing adsorption of undesirable proteins and adhesion of undesirable cells (i.e. non-specific protein adsorption and cell adhesion).

While many protein-resistant surfaces have been identified, the precise nature of the mechanisms involved is still not completely understood. As a result, various research groups spend much time and effort towards understanding and identifying what specific properties endow certain materials with high biocompatibility, thereby exhibiting minimal protein adsorption or fouling behavior. Successful identification and characterization of these properties allows the strategic design of non-fouling surfaces optimized for particular applications.

In general, current strategies to control the interfacial interaction rely on surface chemistry, topography and mechanical properties. Construction of an optimized non-fouling surface is expected to take advantage of each of these mechanisms for control over interfacial interaction.

2.2.1 Non-fouling surface chemistry

The most abundant and well-accepted non-fouling surface coatings are fabricated from poly(ethylene glycol) (PEG) and poly(ethylene oxide) (PEO).

These are biocompatible, synthetic polymers of the same chemical structure (HO-(CH_2-CH_2-O-)$_n$-H), differing only in molecular weight range (PEG < 20 kD < PEO). Numerous studies have demonstrated the low-fouling properties of PEG- and PEO- grafted surfaces [8 9 10 11], as well as hydrogels comprised of PEG or PEO [12 13 14]. The innate protein-repellant capabilities of PEG/PEO appear to be derived primarily from three chemical properties: (a) high hydrophilicity (b) electroneutrality and (c) mobility / flexibility [15 16]. A number of other biocompatible polymers exhibiting similar chemical properties have also been used extensively in non-fouling applications, with comparable performance. These include some natural polysaccharides (e.g. dextran, hyaluronic acid, alginic acid) [17 18] and other synthetic polymers (e.g. polyHEMA) [19].

Hydrophilicity is a property of many macromolecules with non-fouling characteristics. Included among these are PEG, PEO, dextran, pHEMA, PAA, PVA, etc. In general, these are polymeric molecules with a high density of hydrophilic chemical functional groups, such as hydroxyls (-OH), carboxyls (-COOH) or ethers (R-O-R), that results in association with a large number of water molecules. Numerous theories abound as to why this "water-loving" property results in protein repellency. In general, these relate to preferred hydrogen bonding of the hydrophilic polymer with water molecules versus protein groups. This is sometimes described as forming a "hydration barrier" that prevents proteins from reaching the surface. For these systems, the free energy state of the system is minimized, a result due to a combination of factors (synergistic with the hydrophilic chemical functional group), such as chain mobility and

conformational freedom. As a result, protein-repellancy is the more favorable thermodynamic and kinetic outcome [20].

In addition to being hydrophilic in nature, the charge of the molecule has been shown to be another important component. Positively or negatively charged functional groups have electrostatic interactions with proteins or cell-surface groups, promoting either protein adsorption or cell adhesion [21]. As a result, electroneutrality is a co-requisite chemical property to hydrophilicity for non-fouling materials.

It should be noted, however, that some applications require "selective" adsorption of proteins. These may require the selective adsorption of a negatively charged substrate, while repelling positively charged substances (or vice versa); for these, a charged surface is appropriate. Some of these applications include biosensors and filtration devices.

Higher chain mobility has been shown to be associated with increased non-fouling properties. This has been studied extensively with PEG/PEO-grafted surfaces, in which longer chain lengths (higher MW) of these linear polymers have correspondingly higher mobility, resulting in decreased platelet and protein adhesion [16]. In addition, flexibility of the polymer chain is also correlated with increased non-fouling capability versus rigid chains, demonstrated both experimentally and theoretically [22].

However, prevention of protein adsorption may be further enhanced by *branched* (versus linear) chemical structures[23] , provided that high surface coverage is still achieved [24]. For PEG, this includes the branched (3-10 PEG

chains emanating from a central core group), star (10-100 PEG chains emanating from a central core), and comb (multiple PEGs grafted to a polymer backbone) conformations.

For these chemical structures, the generally accepted explanation for non-fouling is due to *steric repulsion / hindrance*, such that the attractive forces between proteins and surface are outweighed by repulsive forces created by (a) favorable interactions between water and the grafted polymer chains as well as (b) thermal motion of the polymer chains [25].

Typically, hydrophobic surfaces tend to foul more readily than hydrophilic surfaces [26] [2]. However, an exception exists for materials characterized as having "superhydrophobic" properties (contact angle >150 degrees), which have been experimentally demonstrated to have hemocompatible properties with minimal platelet adherence [27] [28]. However, this is an emerging field such that a limited number of materials have been developed with superhydrophobicity [29] [30] [31] [32] [33], and even fewer have been experimentally shown to display biocompatibility and non-fouling properties.

2.1.2 Non-fouling surface topography

Interfacial interactions related to surface topography occur at the molecular level as well as larger-scale nano- and micro-topography. In this work, "molecular topography" refers to parameters such as the *grafting density* of a particular polymer monolayer on a surface, or the *thickness* of the monolayer. In contrast, "nano-" and "micro-" topography refer to parameters such as *surface*

roughness, the *surface density of nano- and micro- scale structures* (e.g. particles, fibers), and the distribution of *feature sizes.*

Molecular topography. Steric effects have already been discussed for the specific chemistry and chemical structure of the polymer; however, steric repulsion of a surface to protein is typically enhanced by increased grafting density or thickness of a polymer monolayer [8 16 34]. Longer polymer chains are capable of forming thicker monolayers; also, higher grafting densities results in a higher surface coverage of the underlying material, as well as allowing the grafted chains to have a more extended and oriented conformation [35]. As a result, these features further increase steric hindrance to protein adsorption. This is explained by *physical* exclusion of proteins, according to size, from reaching the underlying surface [36], as well as the enhancement of the steric repulsive effect due to specific polymer chemistry.

It should be noted, however, that long chain length is not a requirement for a non-fouling polymer. This is demonstrated by the fabrication of effective non-fouling surfaces using oligo(ethylene glycol) (OEG) [2]. OEG-grafted surfaces having only 3-6 mers in a chain are effective at protein-repellancy; however, this is dependent on the conformation of the oligoether chains, which is controlled by grafting density. At too high of a graft density, tight packing results in a planar all-trans conformation leading to protein adsorption; at a lower graft density, a helical conformation results, which is associated with protein repellency [37].

Nano- and micro- scale topography. Topographical features at the nano- and micro- scale have been shown to enhance a material's resistance to cell

adhesion. For typical experiments isolating the effect of topography, surface chemistry is unchanged between a planar, nano-featured, or micro-featured topography such that adsorbed proteins are similar between surfaces.

Dalby et al showed that surfaces with planar or 10nm-high islands experienced similar levels of fibroblast cell adhesion, but 50nm-high islands were non-adhesive to fibroblasts [38]. In contrast, nanostructured surface features (50-100nm) were shown to increase smooth muscle and endothelial cell adhesion versus submicron (100nm-1μm) or microstructured (10-15μm) features [39] [40] [41], while fibroblast adhesion was decreased on the same nanostructured surface [42]. A study by Kunzler et al showed that osteoblasts increased proliferation as micro-scale surface roughness increased (R_a = 1-6μm), while fibroblast proliferation decreased with increasing roughness [43]. These examples are just a small sample of the extensive literature examining the cellular response to micro- and nano-topography, and thorough reviews are available on the subject [44] [45] [46].

As a result, cellular response to topography is controlled by feature size, morphology (pillars vs. grooves vs. fibers vs. particles, etc) and surface density or surface coverage, which further determine corresponding surface roughness and surface area. Cell adhesion and proliferation may occur readily on some of these surface topographies, but not on others; the result is highly dependent upon cell type and specific responses to topography.

2.1.3 Non-fouling mechanical properties

Interfacial interactions related to mechanical properties of a material result from the adhesive forces cells are capable of eliciting on a particular material.

Most cells are “anchorage-dependent,” meaning that cell viability is compromised if suspended in a fluid without access to a solid support. The solid support may be rigid, soft, flexible or elastic; however, the specific mechanical properties required for maintaining cell viability varies for each cell type. Mechanical properties determine the capability of the cell to transmit contractile forces; as a result, molecular feedback mechanisms following adhesion allow cells to be able to recognize surface stiffness [47].

Mechanical properties influence cellular phenotype, proliferation and differentiation, as well as limit the capability of an anchorage-dependant cell type to adhere to a particular substrate. Yeung et al showed a differential response between cells cultured on surfaces with increasing stiffness, in which fibroblasts switched from a round to a well-spread form at a particular stiffness level (1000-3000Pa), and endothelial cells showed a stiffness-dependent spreading, while the adhesion and spreading of neutrophils, in contrast, was unaffected by stiffness [48]. Ghosh et al found that the mechanical response of human dermal fibroblasts was modulated to match the substrate stiffness, further resulting in faster migration on softer substrates but increased proliferation on stiffer substrates [49]. Engler et al demonstrated a corresponding increase in spreading of smooth muscles cells with substrate stiffness [50]. Flanagan et al found that motor neurons were able to extend neurites with extensive branches on soft surfaces, but not hard [51].

These results support a generality which dictates that cells tend to be most viable on structures with mechanical properties are similar to those found in the cell’s native environment [52]. As a result, mechanical properties approximating

those of the native tissue can be used to promote the adhesion and proliferation of particular cell types; as follows, mechanical properties can also be used to prevent the adhesion and proliferation of particular cell types.

2.3 Bioactive, biomimetic and ECM-mimetic materials in biomedical applications

"Bioactive materials," loosely defined, are those fabricated to induce a specific biological response from proteins and cells, especially during interaction with the *in vivo* biological environment [53]. "Biomimetic materials," in contrast, are designed to display properties that mimic the native biological environment, with the intent of recapitulating the function of the mimicked property [54]. "ECM-mimetic" materials are more specific, in that properties of the natural ECM are mimicked, such that biological components interacting with the material respond as though interacting with native ECM [54].

For most applications, the ultimate function of the material does not require distinguishing between bioactive, biomimetic and ECM-mimetic. The material is expected to elicit a specific biological response upon contact with a biological system, such as preventing coagulation, promoting adhesion and proliferation of endothelial cells, encouraging angiogenesis and capillary infiltration, or preventing over-proliferation of smooth muscle cells or matrix expression [55]. These types of responses are necessary for many biomedical applications, including scaffolds for tissue regeneration and drug delivery devices, as well as surfaces for improving patency or preventing rejection of implanted materials (e.g. grafts, stents).

2.4 Current strategies to create bioactive materials

For bioactive, biomimetic and ECM-mimetic materials, design is focused on eliciting a specific response when in contact with a biological system. As a result, methods used for fabrication and functionalization are similar between these types of materials. Typically, a material is synthesized to incorporate specialized "cues" (chemical, topographical or mechanical), often derived from native cellular environments, which are recognized by proteins or cells. This recognition directs the biological response toward a desired outcome.

Manipulation of the presented "cues" allows a material to be custom-designed for a specific application. For non-fouling, non-adhesive materials, this has already been discussed with respect to controlling the interfacial interaction with cells and proteins by varying chemical, topographical and mechanical properties. Bioactive materials design also relies on varying these properties, but over a range than emulates native cellular environment. For topography, this often implies fibrous features in the nano- and micro-scale; for surface chemistry, this often implies biologically-derived molecules attached at specific surface densities and distributions; for mechanical properties, this often implies stiffness and elasticity that emulates the environment during which a cell demonstrates a specific response (differentiation, proliferation, etc).

One key design strategy, which is also used in this research plan, is to construct the mechanical and topographical properties using an inert (non-fouling) surface, and then add back bioactive molecules. This strategy allows for the greatest degree of control over the interfacial interaction between a material and

the cells / environment to which it is exposed, allowing for the optimal construction of a material for eliciting a biospecific response.

2.4.1 Bioactive chemical properties

Bioactive chemical modifications refer not only to varying chemical functional groups on molecules (e.g. –COOH, CH_3), but also functionalizing the material with biologically-derived molecules (e.g. peptides, proteins, sugars). In addition, the specific chemical linkages holding the material together also play an important role in determining material characteristics (bulk chemistry, degradation and mechanical properties).

Chemical functional groups. In terms of varying chemical functional groups, different proteins preferentially adsorb on particular chemistries; further, the specific conformation of the adsorbed protein is also determined by surface chemistry [56 57]. Cells adhere to the adsorbed proteins, with the cellular response dependent upon the specific proteins adsorbed and binding motifs consequently exposed (determined by protein conformation). In a representative work, Keselowsky et al showed that the conformation of adsorbed fibronectin varied depending on the terminal chemical functional group of a monolayer surface, resulting in differential integrin-specific binding levels that correlated with cell adhesion strength ($OH>COOH=NH_2>CH_3$) [56]. Chemical functional groups also contribute to determining a material's bulk chemical properties, such as overall hydrophilicity, hydrophobicity, or charge [58 59 26 60 61]. These in turn influence protein adsorption and consequent cellular response [59 26], as well as additional

material properties including pH-responsiveness (e.g. increased or decreased swelling that is pH-dependent) [62].

Chemical linkages. This leads into another important consideration in bioactive material design: the specific chemical linkages used to "hold together" a material. Not only do these influence the bulk chemical properties, but they also modify material characteristics including, but not limited to, (a) degradation rate and (b) mechanical properties (resulting from the degree of cross-linking). A chemical linkage that is acid- or base-labile will degrade faster when immersed in a more acidic (lower pH) or more basic (higher pH) environment, respectively [63]. Alternatively, the linkage may consist of a biological functional group (i.e. enzymatic recognition site) that is cleaved by a specific enzyme, which may be secreted by cells to which the material will be exposed [53]. This contrived material degradation may be used for the controlled release of bioactive molecules (e.g. drugs, growth factors), or to provide a path for cellular infiltration and proliferation into a cellular scaffolding material [53].

Attachment of biologically-derived molecules. Materials are often functionalized with biological small molecules (e.g. peptides) or macromolecules (e.g. proteins, sugars) derived from native cellular environments. With this method, a greater degree of control is possible since the attached molecule may interact directly with a cell adhesion receptor, for instance, versus relying on a secondary mediator (such as protein adsorption). Attached macromolecules often include such proteins native to ECM, including fibronectin, elastin or laminin, as well as natural glycoproteins or polysaccharides. Attached small molecules often

include peptides that have been shown to interact with a particular cell receptor (integrin-specific binding); these may be derived from a particular binding motif present on a larger protein (e.g. RGD derived from matrix protein fibronectin, VAPG derived from matrix protein elastin) [14 55 64], or synthetically identified using processes relying upon a large combinatorial library, such as phage display [53].

The biospecific response elicited from certain cells can be further enhanced when specific molecules are attached on an otherwise inert background material, such as a monolayer or hydrogel comprised of PEG, polyHEMA or dextran. Tugula et al demonstrated that an RGD-functionalized polyHEMA surface required an RGD surface concentration of >1-5.3 pmol/cm^2 for HUVEC adhesion and spreading [19]. Stark et al demonstrated that cyclicRGD immobilized on a dextran monolayer promoted increased adhesion and spreading of endothelial cells versus 3T3 fibroblasts and smooth muscle cells [65]. By preventing non-specific interactions and introducing defined biochemical cues, a fine-tuned biospecific response can be elicited from certain cells [14 66] modulated principally by the characteristics of the surface-attached molecules (specific molecule attached, molecular topography), and secondarily by bulk material properties (chemical, morphology, stiffness, etc).

2.4.2 Bioactive topography

Bioactive modifications for topography occur at the molecular level as well as the larger-scale nano- and micro-topography. In this work, "molecular topography" refers to parameters such as *molecular surface density* (of attached

biological molecules or chemical functional groups) and related *surface distribution* (islands, spacing). In contrast, nano- and micro- topography refers to parameters such as *surface roughness, surface density of nano- and micro- scale structures* (e.g. particles, fibers), and distribution of *feature sizes.*

Molecular topography. While the specific attached molecule (ligand) regulates what interactions are possible between a cell and surface (via integrin-specific binding, receptors present only on certain cell types,etc), studies have shown that the actual resulting biospecific response is further dependent upon the average surface density and surface distribution of the ligands. In terms of ligand surface density, Groll et al showed that the number of adhesive cells on a surface can be controlled by RGD density immobilized on starPEG layers [67], while Lee et al showed that a decrease in spacing of RGD ligands from 78 to 36 nm results in increased osteoblast proliferation and osteocalcin secretion [68]. Maheshwari et al isolated the effect of ligand distribution by keeping the average surface density of RGD constant, while varying the spatial distribution of RGD "clusters" containing either 1, 5 or 9 RGDs/cluster; results showed that RGD immobilized in clusters reduced the minimal surface density required to support fibroblast migration [69].

Nano- and micro- scale topography. Topographical features at the nano- and micro- scale have been shown to modify the cellular response to a given material. This has been discussed already in relation to topographically designing non-fouling materials, as well as using topography to prevent the adhesion of some cells types while promoting the adhesion of others [38 42]. By these same

principles, material topography can also be used to control the biospecific responses of cells. This is often achieved by engineering topographies mimicking native extracellular environments, especially that of natural ECM.

At the most fundamental level, ECM is a 3-dimensional fibrous network comprised primarily of proteins and glycosaminoglycan chains. This not only provides a structural support for adherent cells, but also contains a wide host of molecular signals to which cells respond. These include physical signals from insoluble macromolecules comprising the structural matrix (e.g. cell-binding motifs on collagen, proteoglycans with large glycosaminoglycan side chains), as well as biochemical signals comprised of soluble molecules associated with structural matrix molecules (e.g. growth factors, chemokines, cytokines) [70].

As already discussed, reproducing the effects of these physical and biochemical signals is performed by attaching specific bioactive molecules, and displaying them using a particular molecular topography. However, directing cellular response by mimicking nano- and micro- scale ECM topography is performed by utilizing nano- and micro- fibrous materials. Variations in these topographies generally include *fiber diameter* (ranging from nanometers, hundreds of nanometers, to microns), *porosity and anisotropy* (aligned or random mesh), and can be constructed either as (1) fibers decorating a surface or (2) a "stand-alone" three-dimensional scaffold or membrane. Zong et al showed that cardiomyocytes cultured on scaffolds with sub-micron features, comprised of either aligned or randomly oriented fibers, utilized the external topographical cues for isotropic or anisotropic growth, respectively [71]. In terms of porosity, the

optimal pore size for cell adhesion, proliferation and migration varies from 5 to 500 μm, depending on the particular cell type [72]. A general trend, however, is that for cell migration or proliferation to occur, the pore size should be at least the size of a cell; smaller porosity is associated with reduced cellular infiltration [73]. In addition, cells tend to grow along fibers that are microns in diameters (which approximate or exceed cell size) via contact guidance [74], while spreading and traversing/migrating over sub-micron fibers (nano-scale) [75] [71]. As a result, the topography of a biocompatible fibrous material can be used to create an instructive bioactive matrix for eliciting a desired cellular response by varying the specific fiber properties and morphology.

2.4.3 Bioactive mechanical properties

Mechanical properties have been shown to modify the cellular response to a given material. This has already been discussed in relation to the design of non-fouling materials; these same principles hold true for the design of material mechanical properties for controlling the biospecific responses of cells. Studies point to 2 general trends: (1) cells tend to be most viable on structures whose mechanical properties are similar to those found in the cell's native environment[52] (2) mechanical properties of the cell (e.g. cell stiffness) tend to match that of the surface on which it is attached [49].

2.5 Fabrication methods for nano- and micro- fibrous materials

Numerous methods exist for modifying the nano- and micro-scale topography of surfaces. This includes, but is not limited to, (a) coating a surface with micro- or nano- particles, possibly by spin-coating or chemical attachment

(b) electronics device fabrication including photolithography, electron beam lithography or laser holography (c) polymer demixing (d) chemical etching (e) electrospinning (f) phase separation and (g) self-assembly. Each of these techniques possesses characteristics advantageous for some applications, but not others. For instance, electron beam lithography can be used to create extremely precise geometries and patterns; however, the equipment is expensive, the process is time-consuming, and is limited to being applied over a small surface. In contrast, polymer demixing is simple, fast and inexpensive; however, only sample "features" can be created, such as pits, islands or ribbons – precise control is lacking. For more thorough discussion and analysis of fabrication methods for nano- and micro- scale topographies, extensive review articles are available on the subject [76] [77] [78].

2.6 Electrospinning

In this work, nanofibers and microfibers are fabricated using electrospinning. This technique can be utilized to generate fibers comprised of almost any material. A typical electrospinning experiments yields a non-woven mesh of fibers ranging from nanometers to microns in diameter, with or without "bead" inclusions.

In a typical electrospinning procedure, a polymeric solution is loaded into a syringe, and then pumped slowly out a metal capillary (typically about 0.02" in diameter) with applied high-voltage (typically ranging ~10kV to 25kV). Upon reaching a specific voltage, electrostatic forces exceed that of surface tension; this results in the polymer solution being "pulled" into an elongated, continuous fiber

towards a grounded collecting surface (such as aluminum foil). While traveling towards the surface, the solvent evaporates resulting in the collection of a non-woven mesh of solid fibers [79]. This is illustrated in Figure 1.1 following:

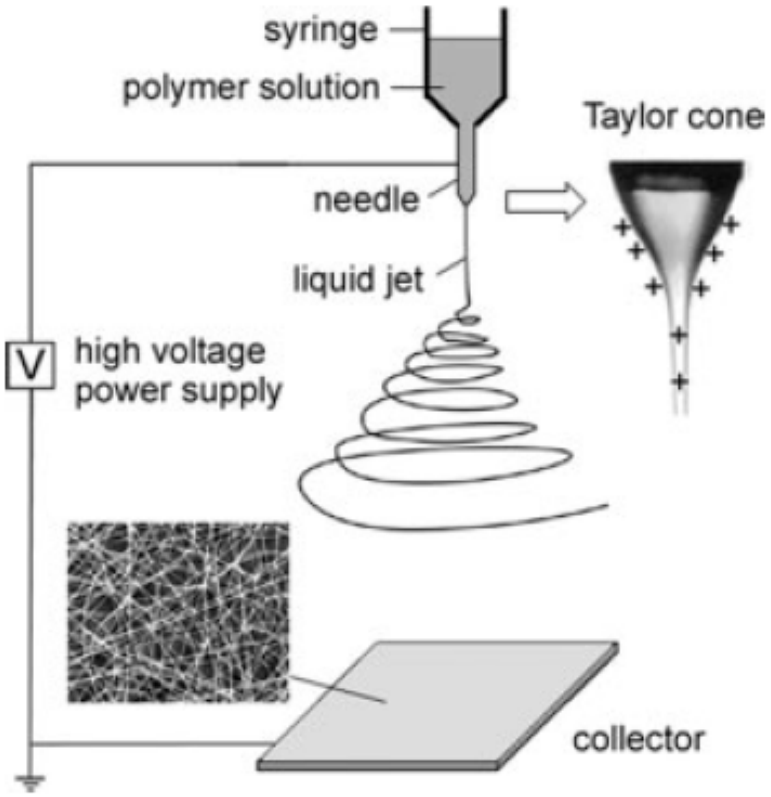

FIGURE 1.1 Schematic of a basic electrospinning set-up [79]. A non-woven mesh of electrospun fibers are collected on a grounded target located a short distance from the tip.

Properties of the resulting fibrous material can be controlled by varying electrospinning parameters related to the electrospinning solution (e.g. concentration, solvent, viscosity, conductivity, molecular weight, surface tension), electrospinning control variables (e.g. flow rate, electric field strength, tip-target distance, inner diameter of metal capillary), or ambient parameters (e.g.

temperature, humidity, air velocity) [80]. Most electrospun materials are polymeric in nature; however, making the appropriate modifications to the electrospinning set-up and post-electrospinning process allows any material to be either electrospun or added to the spun fibers. As a result, a number of different proteins have been electrospun, as well as polysaccharides. In addition, a variety of materials / substances have been successfully incorporated into the spun fibers, such enzymes, proteins, dyes, and other biologically relevant molecules [25].

The biomimetic quality of electrospun fibers promotes a cellular response more similar to what is observed *in vivo.* Due to the innate "porosity" of the scaffolding, cells are capable of infiltrating the material, making it possible to create a 3-dimensional "tissue" composed of multiple cell thicknesses. This is not possible with 2-D surfaces, and although gels have thickness, modifications to porosity or cross-linking mechanisms are necessary to encourage cellular ingrowth. A variety of electrospun materials have been used as substrates for cell culture and assessed for usage as a scaffold in tissue engineering. Cell types grown on electrospun fiber scaffolds include, but are not limited to, neural, endothelial, skeletal, fibroblast, cardiac, and keratinocyte [81]. Substrates have included, but are not limited to, such materials as PLLA, PMMA, PCL, collagen, dextran, PEO, PLGA, hyaluronic acid and gelatin [81]. In addition, the structural alignment of the electrospun fibers can be modified to further direct isotropic cell growth [71]. Numerous review articles on electrospinning are available, especially as the technique is used in tissue engineering and generating ECM-mimetic materials [81 82].

2.7 Dextran-based biomaterials

Dextrans are hydrophilic, biocompatible polysaccharides synthesized by *Leuconostoc* bacteria [83]. They are comprised of glucopyranose subunits, and linked by α(1→6)-polyglucose linkages [84]. Dextrans can be synthesized over a range of molecular weights, often between 1,000 to 2,000,000 daltons, with ~5% branching (via α(1→3) linkages) that increases with molecular weight [85]. Over the molecular weight range of interest in this work (40kD-90kD), dextran behaves as an extended, flexible polymer chain [80].

Advantages of using dextran in biomedical applications relate not only to the polymer's biocompatibility (low toxicity and relative inertness) [86 87], but advantages owing to dextran's chemical nature. First, each subunit (mer) of dextran contains three hydroxyl (-OH) chemical functional groups, giving the polysaccharide hydrophilic properties; as a result, due to this hydrophilicity and flexible nature of dextran, materials fabricated with the molecule are generally non-fouling (resistant to protein adsorption, as previously discussed) [18 88].

This renders the material relatively "inert" in the *in vivo* environment, without eliciting an inflammatory response. Also, the linkages between subunits are resistant to cleavage by most cellular glycosidases [89]; as a result, the polymer has long-term stability, with degradation via slow hydrolysis or via synthetically-introduced enzymatic cleavage by dextranase [89]. In addition, the –OH groups can be exploited under various chemistries for cross-linking [86], or chemically modified for attachment of bioactive molecules or specific functional groups [65]. In terms of using dextran to fabricate a material with fibrous topography, the

polymer has already been successfully electrospun [90]. As a result, cellular environments may be custom-designed using dextran-based biomaterials. Dextran provides a non-fouling background, can be fabricated to have a nano- or micro- fibrous topography, and can be modified with specific bioactive molecules.

CHAPTER 2

Electrospinning of hydrogel nanofibers and microfibers comprised of dextran-poly(acrylic acid) polymer blends

Abstract

Hydrogel nanofibers and microfibers were fabricated by electrospinning and cross-linking polymer blends of dextran (dex) and poly(acrylic acid) (PAA). Aqueous solutions used for electrospinning varied in total polymer concentration, dex:PAA mer ratio, and dex molecular weight. After electrospinning, dex-PAA fibers were subjected to high-temperature thermal dehydration to cross-link reactive hydroxyl (-OH) and carboxyl (-COOH) groups of dex and PAA. Cross-linked dex-PAA fibers subsequently immersed in aqueous solution did not dissolve, but swelled to form *hydrogel fibers*.

Fiber cross-linking was characterized using FTIR, TGA, and assaying for specific chemical reactive groups. Dry fiber and wet hydrogel fiber diameter and morphology were measured using SEM and fluorescence imaging. These properties were correlated with dex-PAA solution properties, both compositional and rheological.

For pure dextran electrospinning solutions, fiber diameter decreased with decreasing solution concentration and lower dextran MW; however, an increasing amount of bead defects were associated with smaller diameter fibers. For pure PAA electrospinning solutions, a similar correlation between bead defects, fiber diameter and polymer concentration was observed. Incorporating PAA into the

dextran-based electrospinning solutions (dex-PAA blends) resulted in smaller diameter fibers as well as fewer bead defects (for a given polymer concentration). Additionally, incorporating PAA made cross-linking possible, and allowed for the formation of hydrogel fibers.

1. Introduction

For materials implanted within the body, eliciting an immune response and consequent rejection is one of the least desirable outcomes. For whatever the intended purpose, it is important for the body to accept the material and potentially integrate the material into normal physiology and structure (e.g. cellular scaffold for tissue regeneration). Therefore, it is important to implant a material with properties designed to elicit a specific, desirable cellular response.

2. Experimental

2.1 Materials

Three MW ranges of dextran from *Leuconostoc mesenteroides* (M_w 35k-45k, M_w 64k-76k, M_w 100k-200k) were purchased from Sigma (St. Louis, MO). Poly(acrylic acid) (M_w ~90k, 25% aqueous solution) was purchased from Polysciences, Inc. (Warrington, PA). Fluorescein dextran (FITC-dex, 70k MW, anionic) was purchased from Invitrogen (Carlsbad, CA).

2.2 Preparation of electrospinning solutions

Solutions were prepared for electrospinning by dissolving dextran and/or poly(acrylic acid) polymer in DI water and stirring overnight. Dextran solutions were prepared varying in concentration between 37.5 to 47.4 wt%, using ~40k,

~70k, or ~160k dextran. PAA solutions were prepared varying in concentration between 37.5 to 44.4 wt%, using ~90k PAA. Dex-PAA solutions were prepared varying in concentration between 37.5 to 47.4 wt% polymer, comprised of dex:PAA solutions with mer ratio varying between 10:1 (10%) and 3:10 (300%), using either ~40k, ~70k or ~160k dextran and ~90k PAA.

2.3 Electrospinning

Electrospinning was performed following the general procedure of Zong et al [91]. Briefly, a polymer solution was prepared by dissolving dextran and/or PAA in DI water and stirring overnight for thorough mixing. The polymer solution was loaded into a syringe and delivered out a stainless steel capillary with an inner diameter of 0.03" using a programmable syringe pump (Harvard Apparatus PHD 2000) at a constant flow rate of 10 µL/min. A voltage of 25kV was applied to the capillary tip and electrospinning solution using a high-voltage power supply (Glassman High Voltage, Inc). Electrospun fibers were collected on a grounded aluminum foil target located 15 cm from the tip. Room humidity was maintained between 14-17%. After electrospinning, fibers were dried under vacuum overnight. To make fluorescent dex-PAA fibers, electrospinning solutions were modified by substituting ~0.4 wt% dextran polymer with 70k FITC-dex.

2.4 Dex-PAA cross-linking and fiber hydrogel formation

Dex-PAA fibers were cross-linked using a thermal dehydration reaction based on the general procedure of Chen and Hsieh, 2004 [92], in which dry electrospun fibers are incubated in a vacuum oven for 1 or 2 hours at 180°C.

Thermal cross-linking was performed on electrospun fibers comprised of varying dex:PAA mer ratios, as well as pure dextran and pure PAA fibers. While untreated fibers completely dissolve in water, thermally cross-linked dex-PAA fibers maintain a fibrous structure and swell to form hydrogel fibers.

2.5 FT-IR spectrum and TGA analysis

To analyze fiber composition and cross-linking kinetics of dex-PAA fibers, FT-IR and TGA analysis were performed on representative fiber samples electrospun using solutions of (a) 70k dex (b) 90k PAA (c) 10:4 dex:PAA and (d) 10:12 dex:PAA (mer ratios). FT-IR spectra of dry electrospun fibers were measured using a Thermo Nicolet Nexus 470 FT-IR spectrometer. Prior to FT-IR analysis, each fiber sample was incubated for 0, 1 or 2 hours in a vacuum oven at 180°C. TGA analysis was conducted using a Setaram TG92 thermal analysis system. Samples were analyzed under an inert helium atmosphere at a heat rate of 20°C/min up to 180°C, held for 2 hours at 180°C, then further heated 20°C/min up to 800°C.

2.6 Quantification of fiber –COOH groups

Quantification of fiber carboxyl groups was determined following the procedure described by Nakajima and Ikada [93]. This assay is based on the assumption that toluidene blue (TB), a small positively charged dye molecule, binds electronegative –COOH groups in a 1:1 ratio [94]. Briefly, fibers are stained with $5x10^{-4}$ M TB (pH=10.0) for 3 hours, then rinsed thoroughly with DI water (pH=10.0) to remove unbound TB. Bound TB is extracted from the fibers using 50 v/v% acetic acid. Absorbance of the extracted TB solution is measured using a

plate reader at 633 nm and used to calculate the number of –COOH groups present.

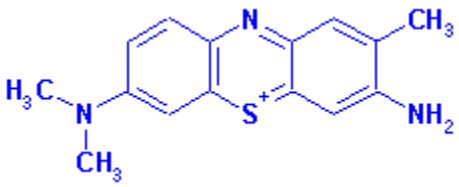

Toluidine blue (MW=305.84)

FIGURE 2.1 Chemical structure of toluidine blue.

2.7 Rheology of electrospinning solutions

To analyze the influence of rheological properties on the electrospinning of dextran and PAA, rheology was performed on electrospinning solutions using an Anton Paar Physica MCR101 rheometer. Oscillatory frequency sweeps were performed at a rate of 0.1 - 100 radians/sec at a controlled strain of 15%. All measurements were maintained at 23°C. Measurements were made using a cone-and-plate geometry to calculate G', G'', tan δ and complex viscosity for each electrospinning solution.

2.8 SEM and epi-fluorescence imaging – dry and wet fiber diameter and morphology

To measure dry fiber diameter and morphology, SEM imaging was performed using an FEI XL-30 EFSEM on dry fibers sputter-coated with Au. To measure wet fiber diameter and morphology, fluorescence imaging was performed using an inverted microscope (Leica Microsystems) on fluorescent wet fibers.

2.9 Enzymatic degradation of dex-PAA fibers

To determine degradation and stability properties, thermally cross-linked dex-PAA fibers were subjected to enzymatic degradation. For these studies, fluorescent dex-PAA fibers were incubated in PBS (phosphate-buffered saline, pH=7.5) or NaP (sodium phosphate, pH=7.5) @ 37°C, with either 0, 1 or 10 μg/mL dextranase enzyme (which catalyzes the endohydrolysis of 1,6-[α]-glucosidic linkages in dextran). To assess degradation, fluorescence intensity of fibers was taken both before and after incubation with dextranase. Since FITC-labeled dextran is the source of fluorescence, and dextranase degrades dextran, relative amount of degradation could be measured as a decrease in fluorescence intensity. Prior to each measurement, fibers were rinsed 3x with PBS to remove degraded fiber components.

Enzymatic degradation was measured on dex-PAA fibers (1) electrospun at 41.2, 42.9,4 44.4 and 47.4 polymer wt% (10:4 dex:PAA), as well as fibers comprised of (2) 10:2, 10:4, 10:6, 10:8, 10:12, 10:30 and 10:50 dex:PAA mer ratio (electrospun at 44.4 polymer wt%).

2.10 Live/Dead Assay

To determine potential cytotoxicity of dex-PAA fibers to mammalian cells, a live/dead assay was performed on fiber-coated surfaces cultured with fibroblast 3T3 cells. This fluorescence-detection assay was performed using a LIVE/DEAD Viability/Cytotoxicity kit for mammalian cells (Invitrogen, L-3224). In brief, live cells show ubiquitous intracellular esterase activity as well as an intact plasma membrane. To discriminate live from dead cells, these

characteristics are probed by staining with green-fluorescent *calcein*, indicating intracellular esterase activity (live), and staining with red-fluorescent *ethidium,* indicating loss of plasma membrane integrity (dead).

3. Results and Discussion

3.1 Electrospinning dextran, PAA and dex-PAA aqueous solutions

Numerous factors determine the resulting morphology and diameter of electrospun fibers, including parameters related to the polymer solution (e.g. concentration, polymer composition, solvent, viscosity, conductivity, molecular weight, surface tension), electrospinning control variables (e.g. flow rate, electric field strength, tip-target distance, inner diameter of metal capillary), or ambient environmental parameters (e.g. temperature, humidity, air velocity) [80]. By modifying these variables, fibers can be electrospun with properties fine-tuned for a specific application.

In this work, aqueous solutions of pure dextran and pure PAA were first electrospun to establish a baseline range of fiber diameters and morphologies possible by varying solution concentration and dextran MW. Next, dex-PAA blends were electrospun to further characterize and optimize fiber properties in terms of fiber diameter, electrospinnability and cross-linking / stability in water.

3.1.1 Fiber diameter and morphology

To create fibers over a wide range of diameters, from nano-scale to micro-scale, fiber properties were controlled by modifying three specific variables of the electrospinning polymer solution: (1) dextran MW, (2) polymer solution

concentration and dex:PAA compositional ratio. SEM images of electrospun fibers were used to measure dry diameter and observe overall morphology such as distribution and size of bead defects.

Effect of dextran MW and solution concentration. Figure 2.2 shows the average diameter of fibers electrospun using solutions of either pure dextran or pure PAA in water, over a range of solution concentrations (wt% polymer). For all dextran and PAA solutions, fiber diameter changed linearly with solution concentration, with smaller diameter fibers electrospun using lower concentrations. Fiber diameter also correlated with dextran MW, as smaller diameter fibers were electrospun using lower MW dextran. These effects are easily visualized in the corresponding SEM images in Figure 2.3. These images also show the bead defects associated with electrospinning smaller diameter fibers. In general, bead defects were observed when the average fiber diameter was less than 400nm. This included, but was not limited to, all fibers electrospun using 40k dextran and pure PAA, with larger bead sizes and numbers occurring at the lowest solution concentration (37.5 wt%). The smallest diameter fibers were electrospun using pure PAA solutions; however, all PAA fibers contained bead defects.

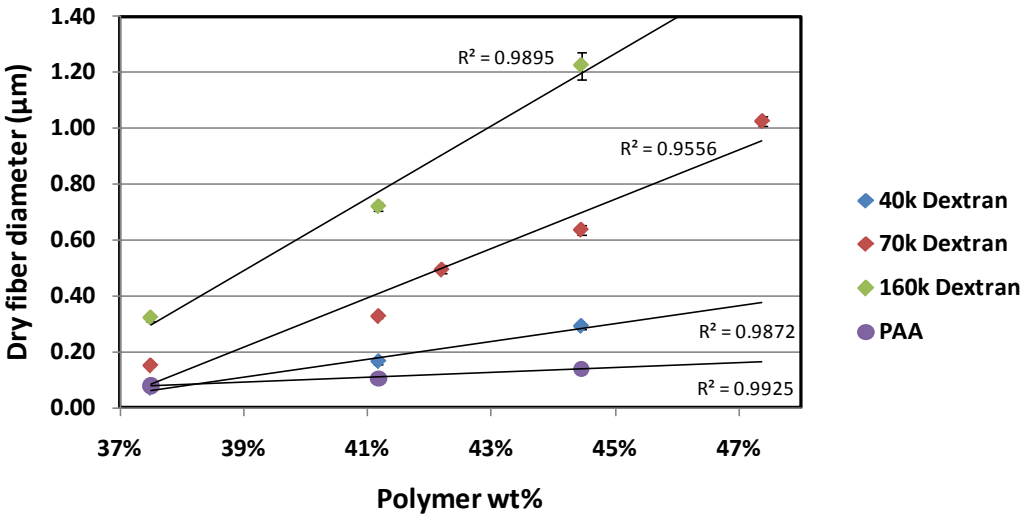

FIGURE 2.2. Dry fiber diameter vs. polymer wt% - dextran and PAA solutions. Average dry diameter of fibers electrospun using solutions varying in polymer type (dextran or PAA), dextran MW (40k, 70k or 160k) and concentration of polymer in solution (polymer wt%). **A linear correlation was found between average fiber diameter and polymer wt% for pure dextran and pure PAA electrospinning solutions. For a given solution concentration, lower dextran MW also corresponded to smaller diameter fibers.** Error bars: standard error.

PAA (37.5%, 41.2%, 44.4% polymer wt%)

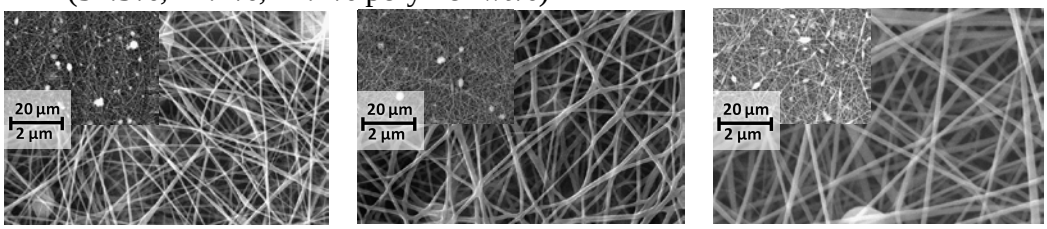

40k Dextran (37.5%, 41.2%, 44.4% polymer wt%)

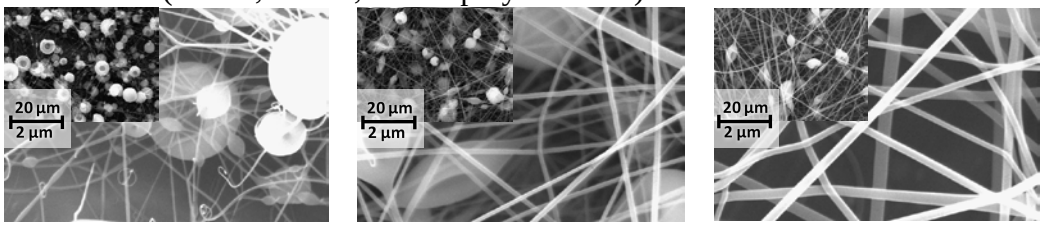

70k Dextran (37.5%, 41.2%, 44.4% polymer wt%)

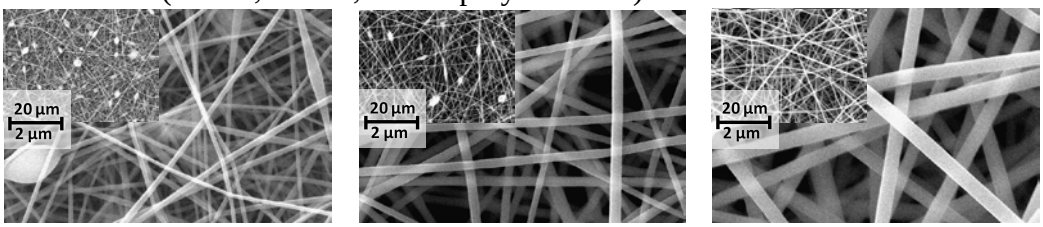

160k Dextran (37.5%, 41.2%, 44.4% polymer wt%)

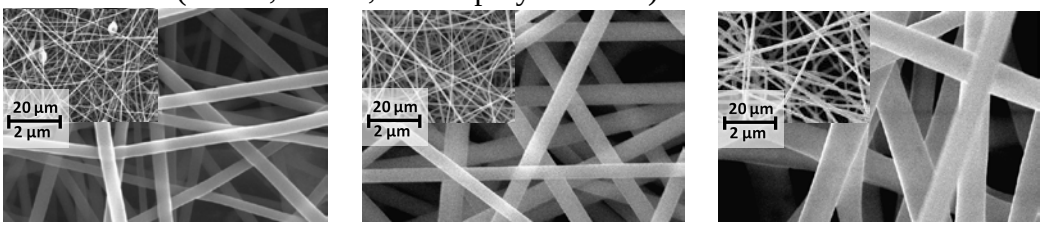

FIGURE 2.3. SEM of electrospun dextran and PAA dry fibers. SEM images are shown of gold-sputtered dextran (MW: ~40k, ~70k and ~160k) and PAA (MW: ~90k) fibers electrospun using different solution concentrations (polymer wt%: 37.5%, 41.2%, and 44.4%). Images were taken using an XL-30 SEM at 1000x (inset) and 10,000x (outset) magnification. **Electrospinning of lower concentration solutions resulted in smaller diameter (nano-scale) fibers and frequent "bead inclusions"; high concentration solutions resulted in larger fibers (micro-scale) with few or no "bead inclusions." Dextran MW was similarly correlated between fiber diameter and bead defects; 160k dextran resulted in larger fibers with little to no bead defects, while 40k dextran resulted in smaller fibers with rampant bead defects.**

As a result, there is a trade-off between achieving nano-scale fiber diameters that are also defect-free when electrospinning pure dextran or pure PAA solutions.

Effect of dex:PAA mer ratio. Figure 2.4 shows the average diameter of fibers electrospun using solutions comprised of blends of 70k dextran and PAA. Like pure PAA and pure dextran solutions, electrospun 70k dex-PAA blends displayed a relatively linear correlation between fiber diameter and solution concentration.

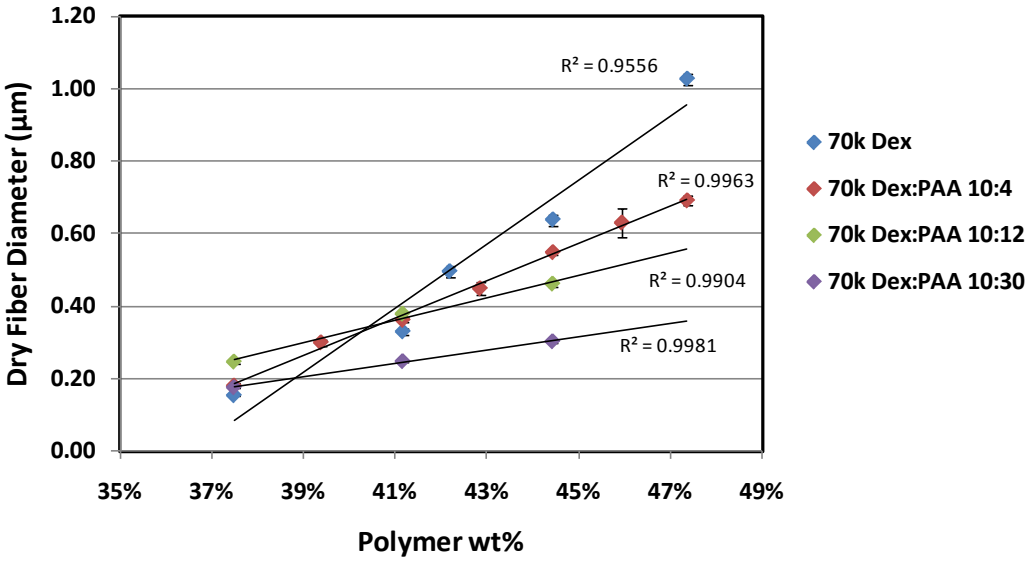

FIGURE 2.4. Dry fiber diameter vs. polymer wt% – 70k dex-PAA blend solutions. Average dry diameter of fibers electrospun using solutions of 70k dextran and 70k dex-PAA blends, and varying in solution concentration (polymer wt%). **In general, incorporating PAA reduced fiber diameter, an effect more pronounced at higher solution concentrations.** Error bars: standard error.

As more PAA was incorporated into dextran-based electrospinning solutions, the general trend was a decrease in overall fiber diameter (for a given solution concentration, or polymer wt%). For instance, as shown in Figure 2.4, at

44.4 polymer wt%, fiber diameter decreases as the relative amount of PAA mers to dextran mers increases (e.g. dex:PAA mer ratio from 1:0 to 10:4 to 10:12 to 10:30). This effect is also seen in Figure 2.5, which shows the average fiber diameter as mer% PAA is increased in the electrospinning solution. For each solution concentration, fiber diameter begins decreasing once the relative number of PAA mers exceeds that of dextran mers (PAA mer% > 50%). This trend in fiber diameter did not occur at PAA mer% < 50%.

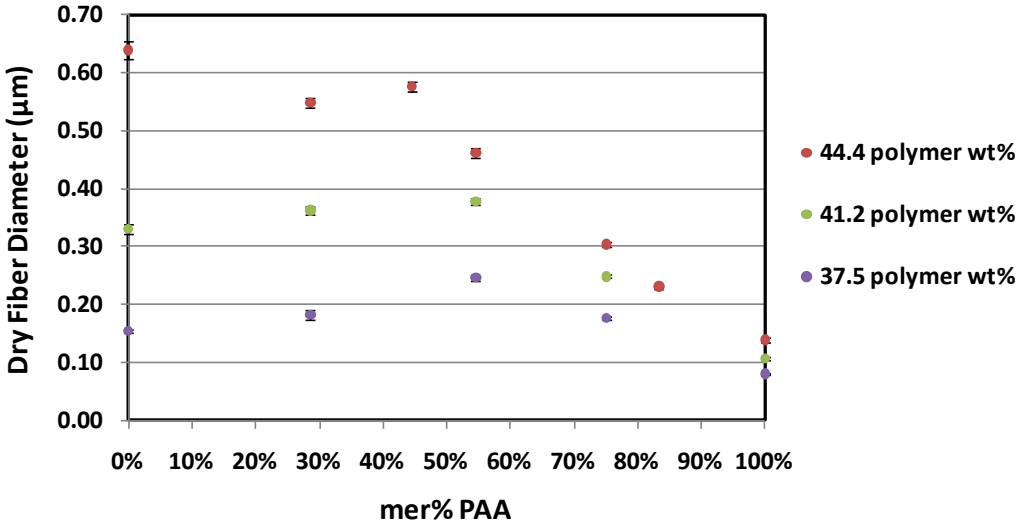

FIGURE 2.5. Dry fiber diameter vs. mer% PAA – 70k dex-PAA blend solutions. Average dry diameter of fibers electrospun using solutions of 70k dextran, 90k PAA, and 70k dex-PAA blends **As more PAA is incorporated into the electrospinning solution, fiber diameter begins decreasing once the relative number of PAA mers exceeds that of dextran mers (PAA mer% > 50%).** Error bars: standard error.

In terms of fiber morphology, incorporating any amount of PAA consistently resulted in a reduction or elimination of bead defects. This effect is easily observed in the SEM images in Figure 2.6 of fibers electrospun using 70k dextran and 70k dex-PAA blends. In the left column, frequency of bead defects

decreases as PAA in solution is increased (for 37.5 wt% concentration). In the middle column (41.2 wt% concentration), 70k dextran shows many bead defects; these defects are eliminated at a 10:4 dex:PAA ratio (mer% PAA - 28.6%) and all higher amounts of incorporated PAA.

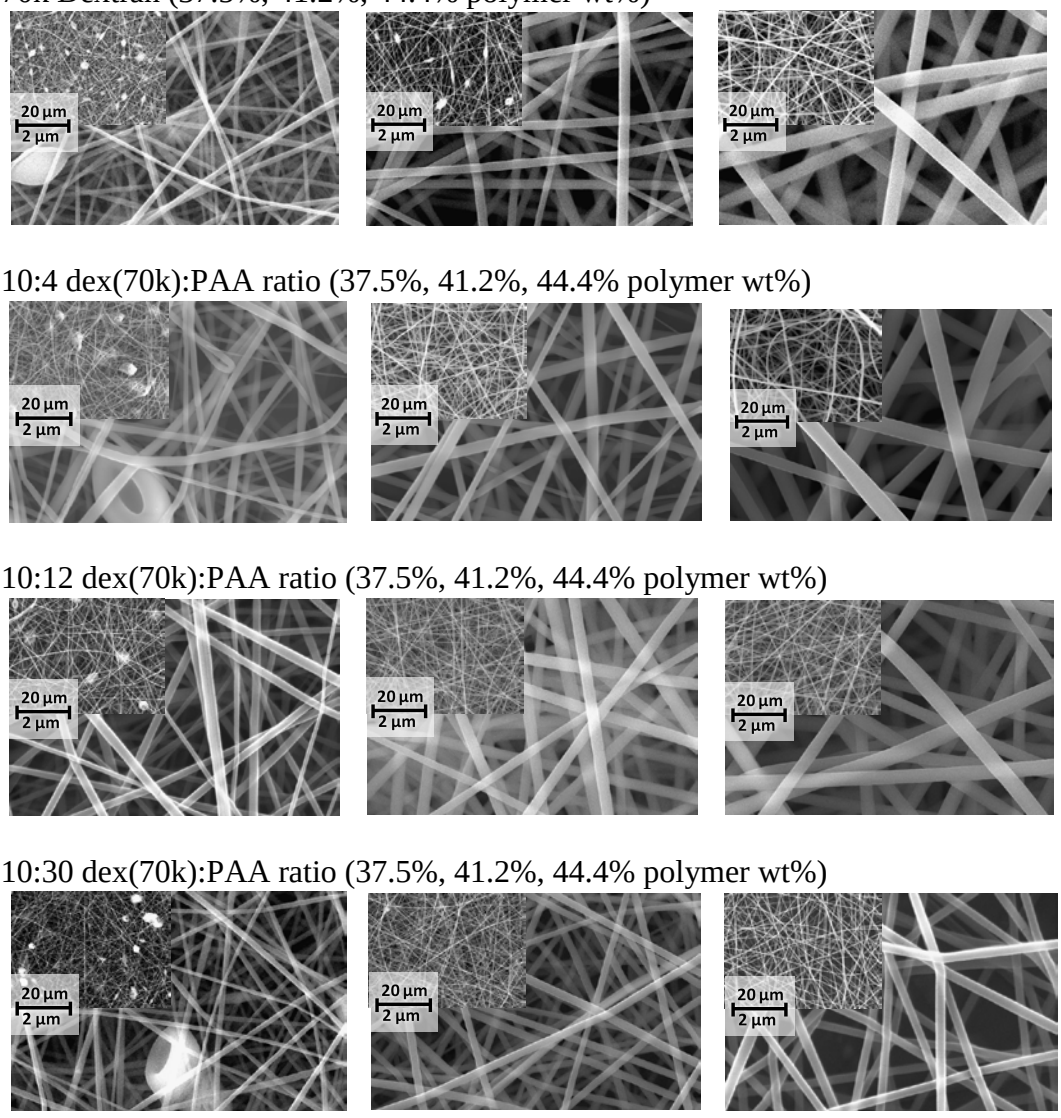

FIGURE 2.6. SEM of 70k dex-PAA dry fibers. SEM images are shown of gold sputtered dex-PAA fibers (70k dex, 90k PAA) electrospun using different solution concentrations (polymer wt%: 37.5%, 41.2%, and 44.4%). Images were taken using an XL-30 SEM at 1000x (inset) and 10,000x (outset) magnification**. For a given dex-PAA solution concentration (polymer wt%), incorporating**

increased amount of PAA decreased fiber diameter and reduced or eliminated bead defects.

The decrease in fiber diameter and bead defects observed for 70k dex-PAA blends was also assessed for dex-PAA blends using 40k and 160k dextran. For these, samples that had previously contained bead defects were electrospun with increasing amounts of PAA incorporated.

As discussed previously, all electrospun samples of pure 40k dextran contained bead defects. After incorporating PAA at 10:12 dex(40k):PAA ratio, bead defects were eliminated at the highest solution concentration (44.4 wt%), but only reduced at lower solution concentrations (41.2 and 37.5 wt%). For the lowest solution concentration (37.5 wt%), further increasing the amount of PAA (to 10:30 dex(40k):PAA ratio) reduced the size and frequency of bead defects, but still did not totally eliminate them. These morphological changes are clearly shown in the SEM images of Figure 2.7 and Figure 2.3.

10:12 Dex(40k):PAA ratio (37.5%, 41.2%, 44.4% wt%)

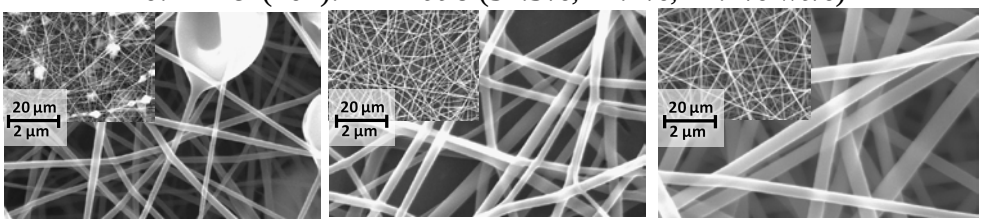

10:30 Dex(40k):PAA ratio (37.5 wt%) 10:12 Dex(160k):PAA ratio (37.5 wt%)

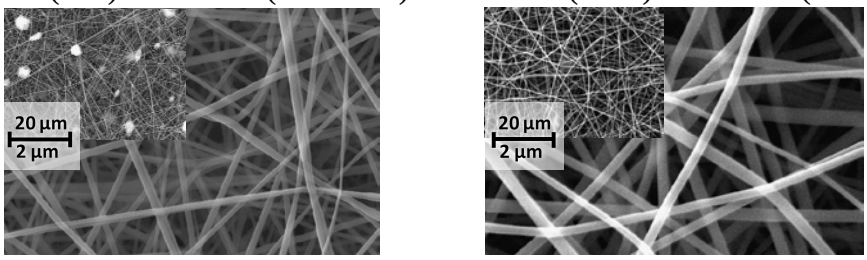

FIGURE 2.7. SEM of electrospun 40k dex-PAA and 160k dex-PAA dry fibers. SEM images are shown of gold sputtered dex-PAA fibers (40k or 160k dextran, 90k PAA) electrospun using different solution concentrations (polymer wt%: 37.5%, 41.2%, and 44.4%). Images were taken using an XL-30 SEM at 1000x (inset) and 10,000x (outset) magnification**. For a given dex-PAA solution concentration, incorporating increased amount of PAA decreased fiber diameter and reduced or eliminated bead defects.**

Figure 2.7 also shows the morphological result of incorporating PAA into 160k dextran electrospinning solution. At 37.5 wt% concentration, pure 160k dextran has bead defects (see Figure 2.3); incorporating PAA at a 10:12 160k dex:PAA mer ratio eliminated beads (see Figure 2.7).

Figure 2.8 shows the effects on fiber diameter of incorporating PAA into 40k and 160 dex-PAA blend solutions. In terms of fiber diameter, incorporating PAA resulted in slightly larger fiber diameters for 40k dex-PAA blends. However, this increase in diameter was also associated with reduced / eliminated bead defects.

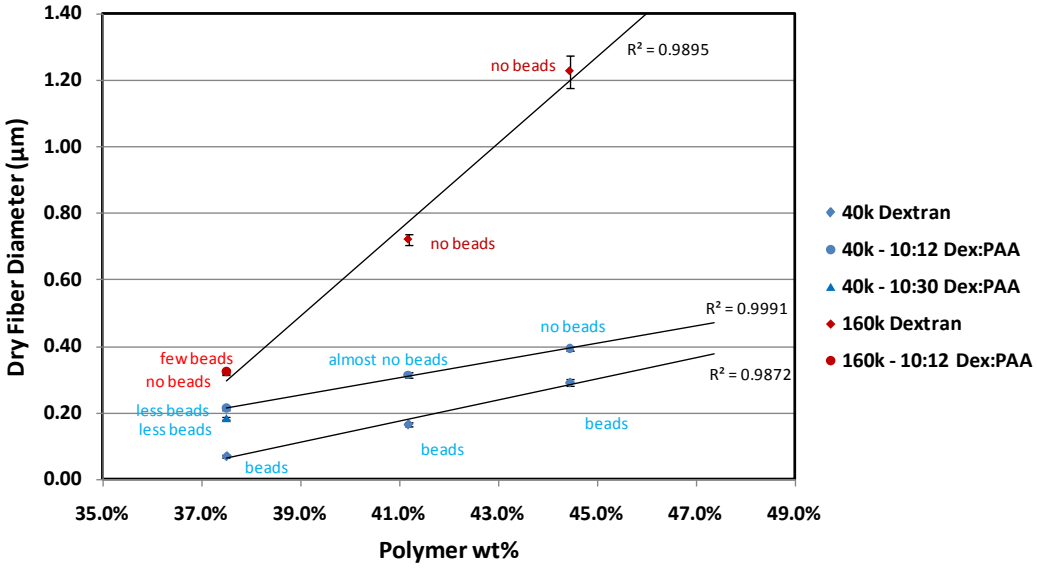

FIGURE 2.8. Dry fiber diameter vs. polymer wt% – 40k and 160k dex-PAA blend solutions. Average dry diameter of fibers electrospun using solutions of 40k dextran and 40k dex-PAA blends, and varying in solution concentration (wt% polymer). **While 40k dex fibers all have bead defects, when PAA is incorporated → bead defects minimized, although average fiber diameter is slightly larger. For 160k dextran, bead defects were eliminated at 10:12 dex:PAA mer ratio and 37.5 wt%.** Error bars: standard error.

In summary, incorporating PAA into dextran-based electrospinning solutions changes fiber morphology to result in a reduction / elimination of bead defects. In terms of fiber diameter, increase or decrease in diameter depends on whether the initial solution and composition resulted in bead defects. For solutions that electrospun into defect-free fibers, fiber diameter decreased with more PAA. For solutions that electrospun into bead-defective fibers, fiber diameter either stayed the same or increased with additional PAA.

These results indicate that interaction between dextran and PAA polymers is changing solution properties to influence overall electrospinnability. Previous studies have shown that electrospinnability and fiber diameter are strongly

correlated with solution viscosity and chain entanglement, which govern the stability of the whipping fiber jet during electrospinning. For this reason, viscosity, G' and G'' measurements were taken on electrospinning solutions to correlate with fiber diameter and electrospinnability.

3.1.2 Rheology of electrospinning solutions

Calculation of electrospinning shear rate vs. angular frequency. At the "range of interest", dextran, PAA and dex-PAA blends behave as Newtonian fluids (viscosity does not change with shear rate). In a typical electrospinning experiment, solutions are flowed through a metal capillary immediately prior to exiting the capillary tip and elongating into a fiber due to the applied electric field. To model rheological solution properties just before electrospinning, and to show that the rheological measurements taken are applicable to the electrospun fluid solution, the formula for calculating the shear rate at the inner wall within a pipe (e.g. electrospinning capillary) is:

Equation 2.1: $$\dot{\gamma} = \frac{8v}{d}$$

where:

- $\dot{\gamma}$ = shear rate (1/s)
- υ = linear fluid velocity
- d = inside diameter of pipe

The linear fluid velocity, υ, is related to the volumetric flow rate *Q* by:

Equation 2.2: $$v = \frac{Q}{A}$$

where:

- A = cross-sectional area of pipe = πr^2
- υ = linear fluid velocity
- *Q* = volumetric flow rate

Combining Equation 2.1 and 2.2 gives the final equation for shear rate:

Equation 2.3: $$\dot{\gamma} = \frac{4Q}{\pi r^3}$$

In this work, electrospinning was performed using a stainless steel capillary (ID = 0.3" → radius = 381 µm), at a constant flow rate (Q = 10 µL/min). As a result, shear rate was calculated to be 13.8 / s.

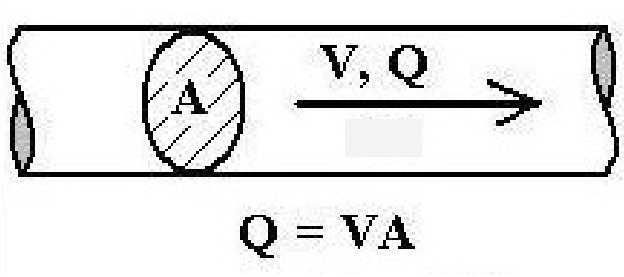

FIGURE 2.9. Schematic of fluid flow through electrospinning capillary. for calculation of *angular frequency similar to that experienced by electrospinning solution in capillary.*

To take rheological measurements, a cone-plate spindle was utilized with dimensions such that a shear rate of 13.8 / s corresponded to an angular frequency of ω = 92.2 rad/s (see Equation 2.4).

Equation 2.4: $\dot{\gamma} =$ □/□□□ □

where:

- $\dot{\gamma}$ = shear rate (1/s)
- ω = angular frequency (rad/s)
- θ = angle of truncation (=1°)

This is shown in Figure 2.10, which plots the correlation between shear rate and angular frequency exerted on a solution for the rheometer and cone-plate spindle.

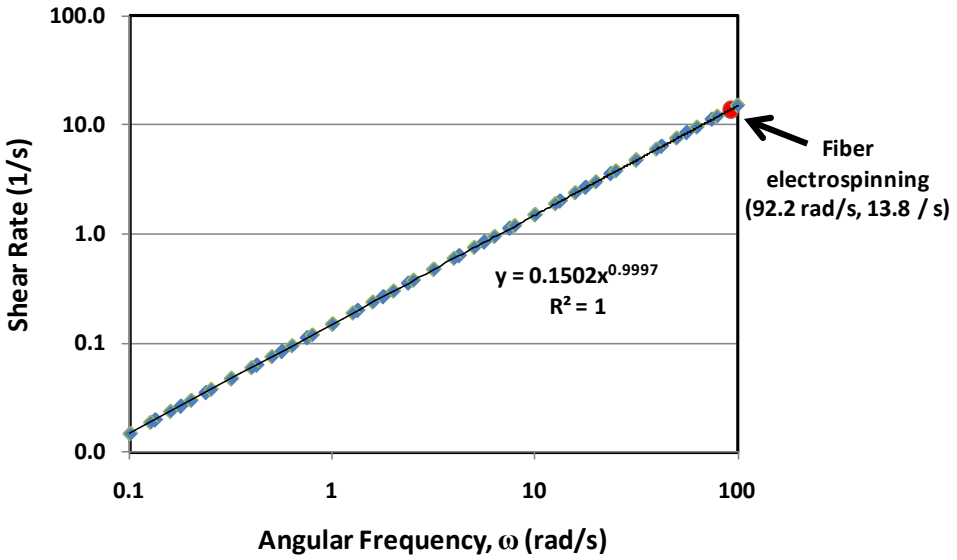

FIGURE 2.10. Angular frequency (ω) vs. shear rate. Correlation between shear rate and angular frequency to which the electrospinning solution is subjected during rheological measurement. **ω=92.2 rad/s and shear rate = 13.8/s (red dot) indicates the calculated shear rate experienced by the solution in the capillary just prior to electrospinning, and the corresponding ω by the rheometer.**

Rheological measurements. In this work, rheological measurements of electrospinning solutions were taken over an angular frequency sweep (ω) of 0.1 to 100 rad/s. This range includes the angular frequency (92.2 rad/s), corresponding to calculated shear rate (13.8/s) experienced by the solution in the electrospinning capillary, just prior to exiting the capillary tip and elongating into a fiber. By doing this, it is possible to evaluate the state of the fluid when entering into fiber elongation, which will influence ultimate electrospun fiber properties.

Numerous studies have shown correlations between rheological solution properties, such as viscosity, storage and loss modulus; these are indicative of factors that characterize what is happening at the molecular level between polymers (e.g. chain entanglement, ability to elongate) that determines how they will behave when the electric field stretches them (or fails to) into fibers. To this end, rheology was performed on solutions of 40k, 70k and 160k dextran and dex-PAA blends, which varied in solution concentration and dex:PAA mer ratio. Solution compositions were specifically selected to correspond with the previously observed differences in fiber diameter and bead defects.

G', G'' and tan δ. Figures 2.11, 2.12 and 2.13 show the storage modulus (G'), loss modulus (G'') and damping (tan δ, or G'/G'') for 70k, 40k and 160k dextran-based solutions, respectively, with varying dex:PAA mer ratios. By looking at changes in modulus over a frequency sweep, it is possible to determine the state of the solution while flowing through the electrospinning capillary, and how this influences the resulting morphology and properties of the electrospun fiber.

G', essentially a measure of the material's elasticity, for many samples begins to suddenly increase after reaching a particular frequency. G'', the ability of the material to lose energy, linearly increases for all solutions. This effect is distilled into tan δ (the ratio between these), an indicator of how efficiently a material loses energy due to such factors as molecular rearrangements or internal friction.

For dextran, PAA, and dex-PAA solutions, peaks (max) in tan δ indicate the transition point at which the solution's elastic properties dominate versus loss. This is important for electrospinnability, since solution elasticity is necessary for the polymer to elongate into a fiber and not break into beads when subjected to the electric field.

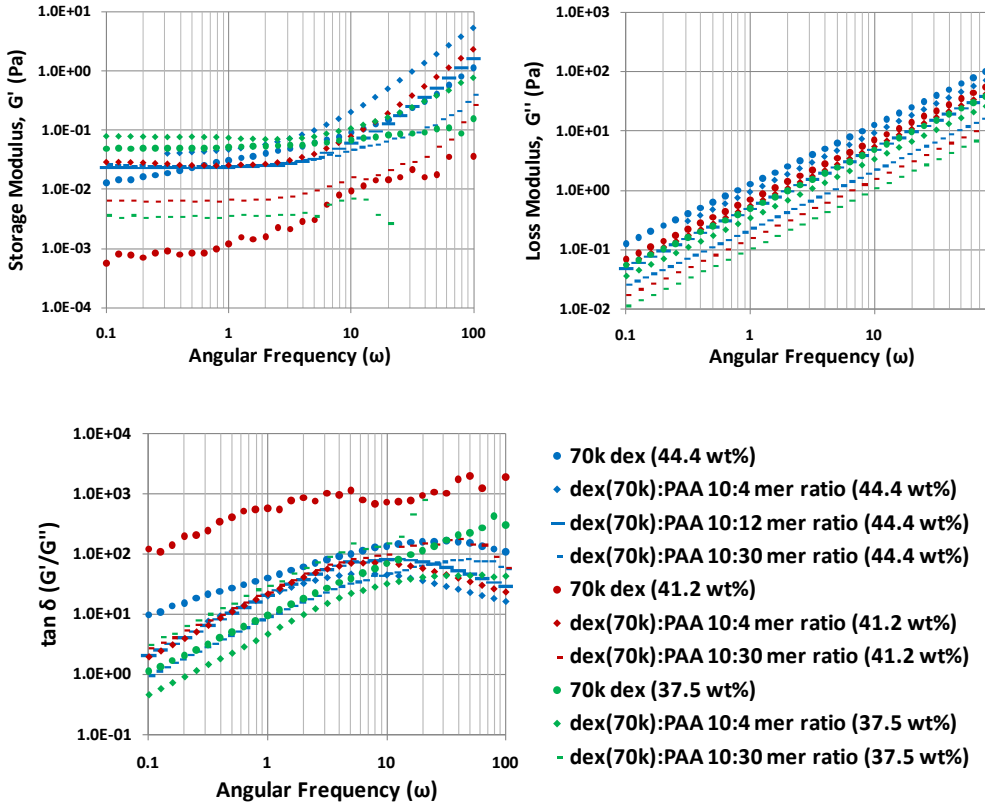

FIGURE 2.11. G', G'' and tan δ vs. ω – 70k dex and 70k dex-PAA blends. The only fiber compositions without bead defects resulted from solution compositions that showed obvious tan δ max, which occurred prior to 92.2 rad/s. For 44.4 wt% solutions (blue), which were already defect-free w/o PAA, incorporating PAA shifted tan δ max to a lower frequency. 41.2 wt% solutions (red) contained bead defects w/o PAA, and tan δ reached had a max. With PAA incorporation, it had maxes and became defect-free. 37.5 wt% solutions (green) never became defect-free with added PAA – no tan δ max and still had beads for all dex:PAA ratios.

From Figure 2.11, solutions that electrospun poorly with many bead defects were 70k dex at 37.5 and 41.2 wt%. These particular solutions did not show a tan δ peak during the frequency sweep. However, incorporating PAA into these solutions modified both tan δ and the electrospun fiber. For 41.2 wt%, adding PAA (at 10:4 dex:PAA mer ratio) resulted in a well-defined tan δ at ~ω=8 rad/s, and concurrent with elimination of bead defects. For 37.5 wt%, adding PAA (at 10:4 or 10:30 dex:PAA mer ratio) failed to result in a well-defined tan δ peak during the frequency sweep, and although bead defects were reduced, they were not eliminated. From Figure 2.11, solutions that electrospun well, with no bead defects, included 70k dex at 44.4 wt%. These solutions all showed a well-defined tan δ peak during the frequency sweep.

As calculated previously, a frequency of 92.2 rad/s simulates via rheometer the shear rate experienced by solutions in the capillary just prior to fiber formation. All solutions that were free of bead defects showed a tan δ peak prior to 92.2 rad/s; all solutions that contained bead defects did not show a tan δ peak prior to 92.2 rad/s. This indicates that for electrospinning dextran and dex-PAA solutions, elimination of bead defects requires that the elastic forces (G') are dominant during fiber formation.

These same general observations were made with dextran of lower and higher MW (40k and 160k). In Figure 2.12, all 40k dextran solutions showed no tan δ peak. However, for 41.2 and 44.4 wt% 40kdex-PAA solutions, adding PAA resulted in a tan δ max at ~30 rad/s and ~5 rad/s, respectively, and defect-free fibers.

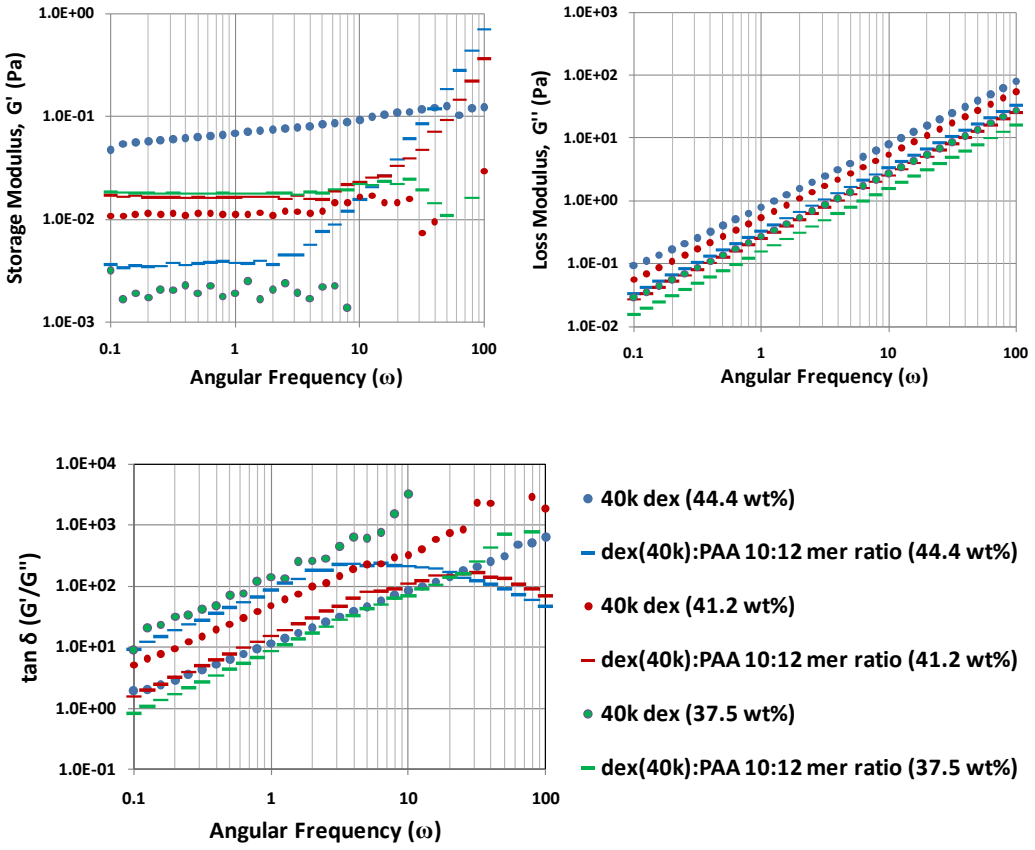

FIGURE 2.12. G', G'' and tan δ vs. ω – 40k dex and 40k dex-PAA blends. The only fiber compositions without bead defects resulted from dex:PAA 10:12 mer ratios at 41.2 and 44.4 wt%. These were the only solution compositions that showed obvious tan δ max, which occurred prior to 92.2 rad/s.

In Figure 2.13, only the 37.5 wt% 160k dex solution resulted in bead defects, although they were minimal. Unlike 40k and 70k solutions studies, this solution's tan δ peak occurred prior to 92.2 rad/s; however, it occurred very close to this particular frequency. Adding PAA (at a 10:12 dex:PAA mer ratio) shifted tan δ peak to ~5 rad/s, a much lower frequency, which had the effect of eliminating bead defects.

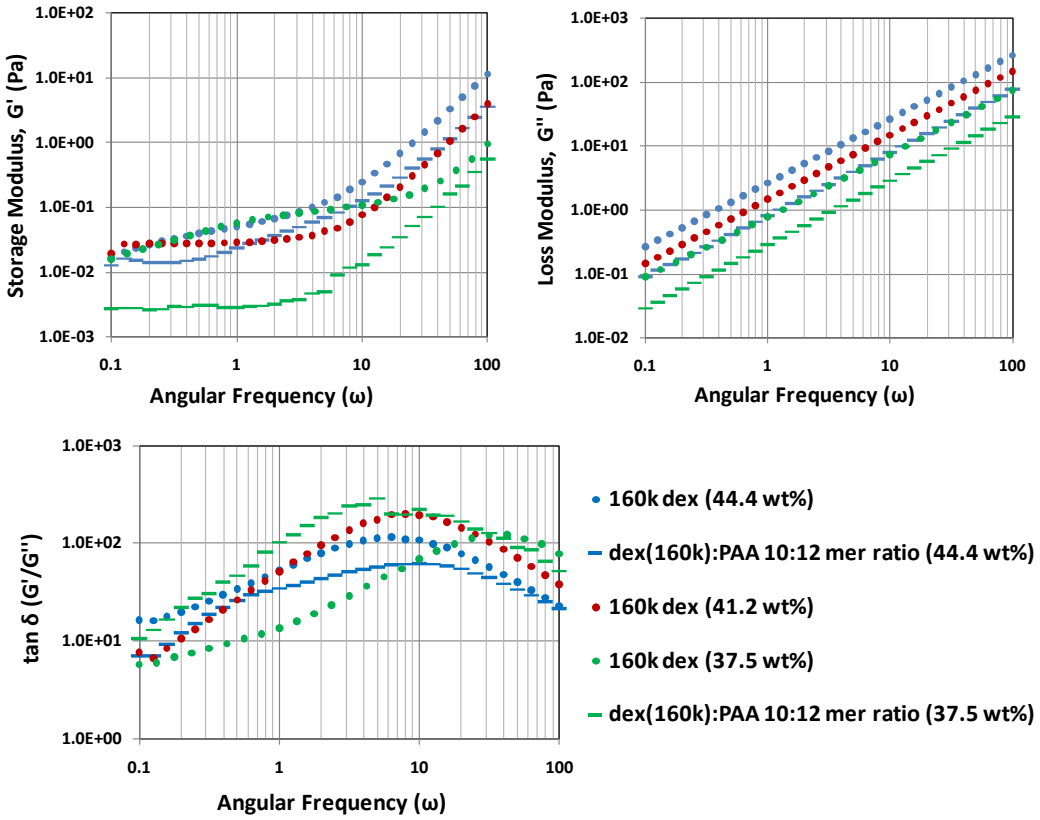

FIGURE 2.13. G', G'' and tan δ vs. ω – 160k dex and 160k dex-PAA blends. For 160k dextran, the lowest solution concentration (37.5 wt%), showed bead defects. Incorporating PAA shifted tan δ max to a lower frequency, which had the effect of eliminating bead defects.

Complex viscosity. Complex viscosity is calculated from G' and G'' measurements according to the following equations for dynamic mechanical analysis:

Equation 2.5: $G^* = G' + iG''$

Equation 2.6: $\eta^* = G^*/\omega$

' where:

- G^* = Complex modulus (Pa)
- G' = Elastic/storage modulus (Pa)
- G'' = Loss modulus (Pa)
- η^* = Complex viscosity (Pa*s)
- ω = Angular frequency (1/s)

As shown in Figure 2.14, dextran and dex-PAA blends behave as Newtonian fluids (viscosity is independent of shear rate) at the frequency range of interest (~92.2 rad/s). In Figures 2.15, 2.16 and 2.17 following, the complex viscosity measured at ω=90 rad/s is plotted for various dextran and dex-PAA solutions.

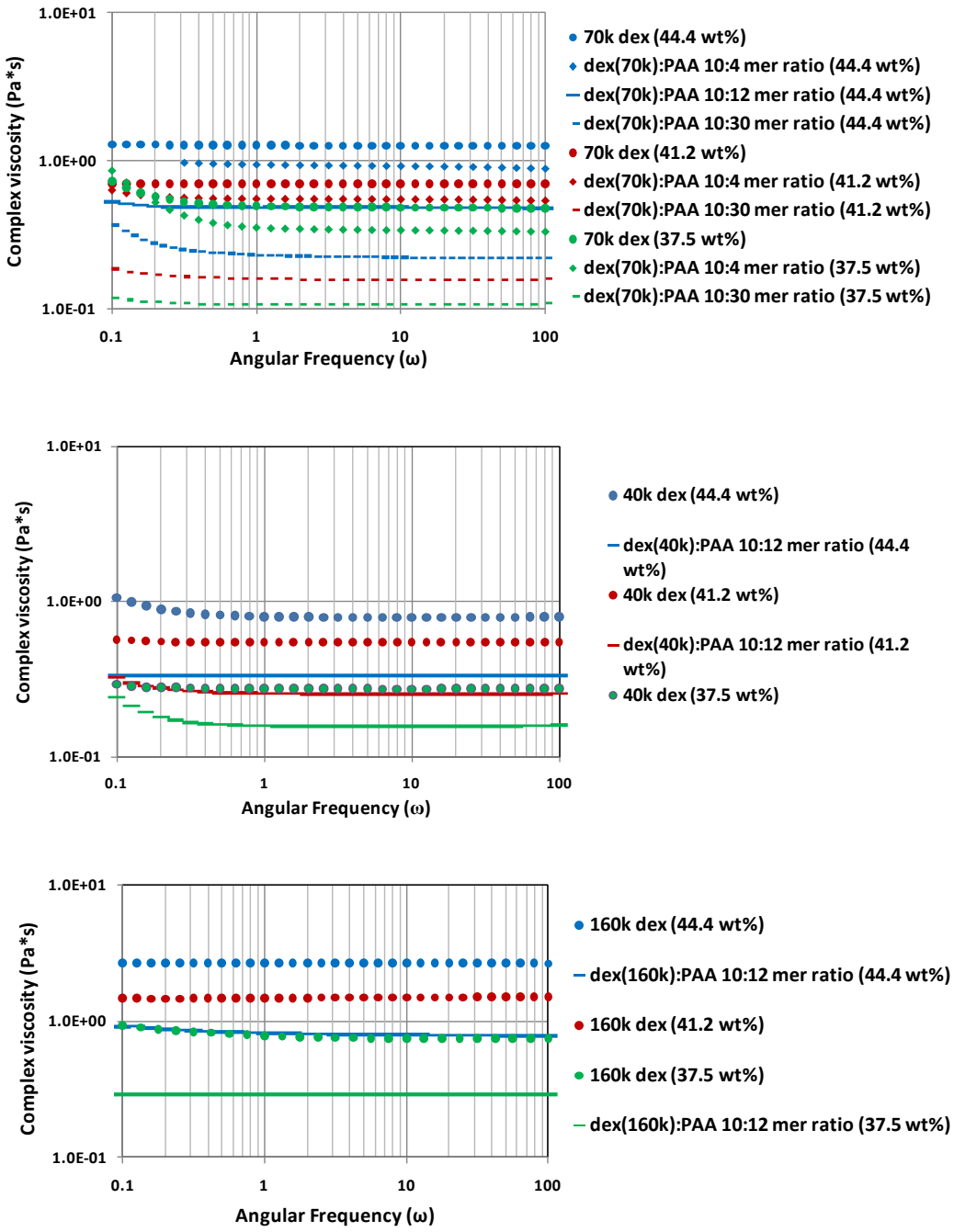

FIGURE 2.14. Complex viscosity vs. ω – 70k, 40k and 160k dex and dex-PAA blends. At the angular frequency of interest, 92.2 rad/s, dextran and dex-PAA blends exhibit Newtonian fluid behavior.

Figures 2.15 and 2.16 show the complex viscosity of 70k, 40k and 160k dextran-based solutions, respectively, with varying dex:PAA mer ratios. As

shown in Figure 2.15, viscosity decreases as increasing amounts of PAA (increasing mer% PAA) is incorporated into the electrospinning solution. However, referring back to Figure 2.5, fiber diameter only begins to decrease significantly after mer% PAA > 50%. As a result, viscosity does not correlate well with fiber diameter.

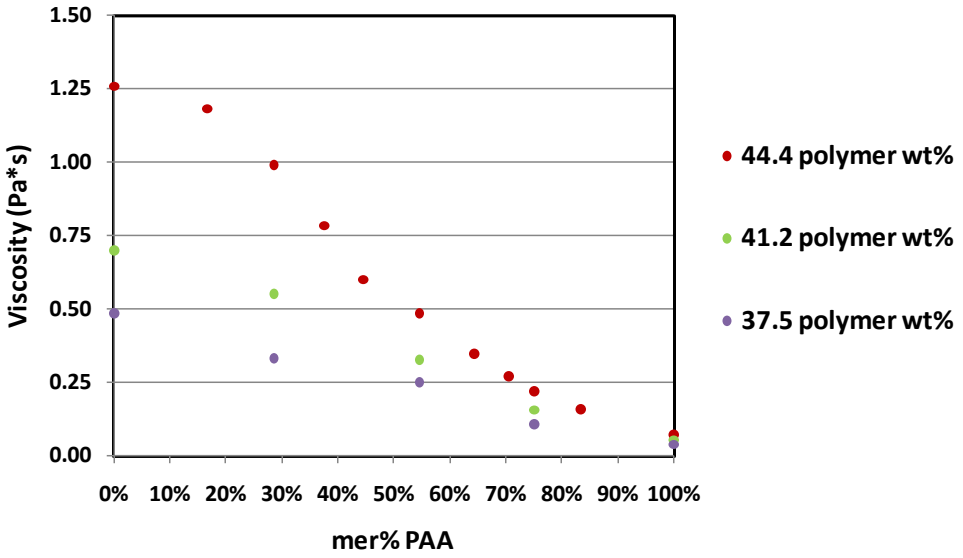

FIGURE 2.15. Mer% PAA vs. viscosity – varying polymer wt% of 70k dex-PAA blends.

As shown in Figure 2.16, viscosity decreases with decreasing solution concentration (polymer wt%). This corresponds with the general trend that fiber diameter decreases with lower solution concentration. However, at a specific viscosity, depending on the fiber composition, the diameter of the fiber varies as well as whether or not beads will appear.

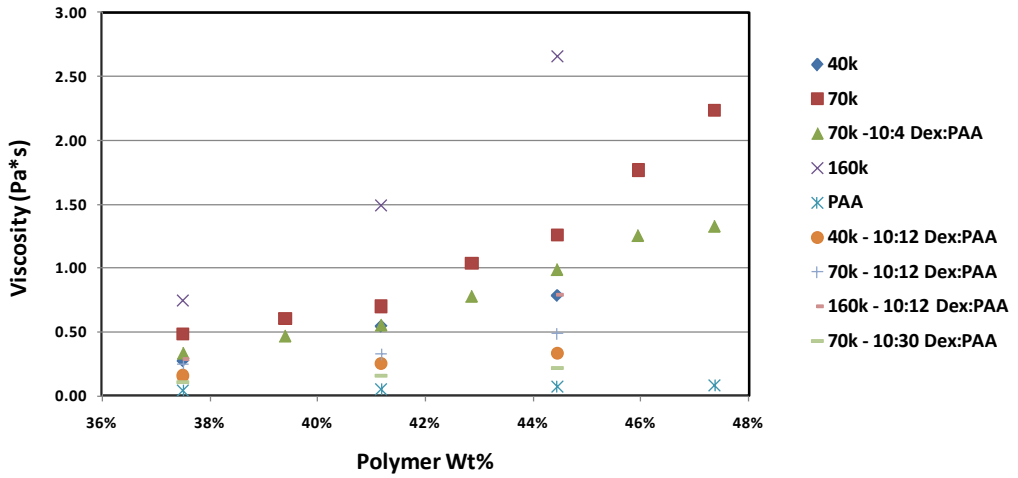

FIGURE 2.16. Polymer wt% vs. viscosity – PAA, dextran and dex-PAA blends.

In Figure 2.17, viscosity is plotted versus average fiber diameter. For each fiber composition, fiber diameter decreased with decreasing viscosity and solution concentration. The thick, segmented blue line separates solutions that resulted in bead defects (below line) versus defect-free fibers (above line).

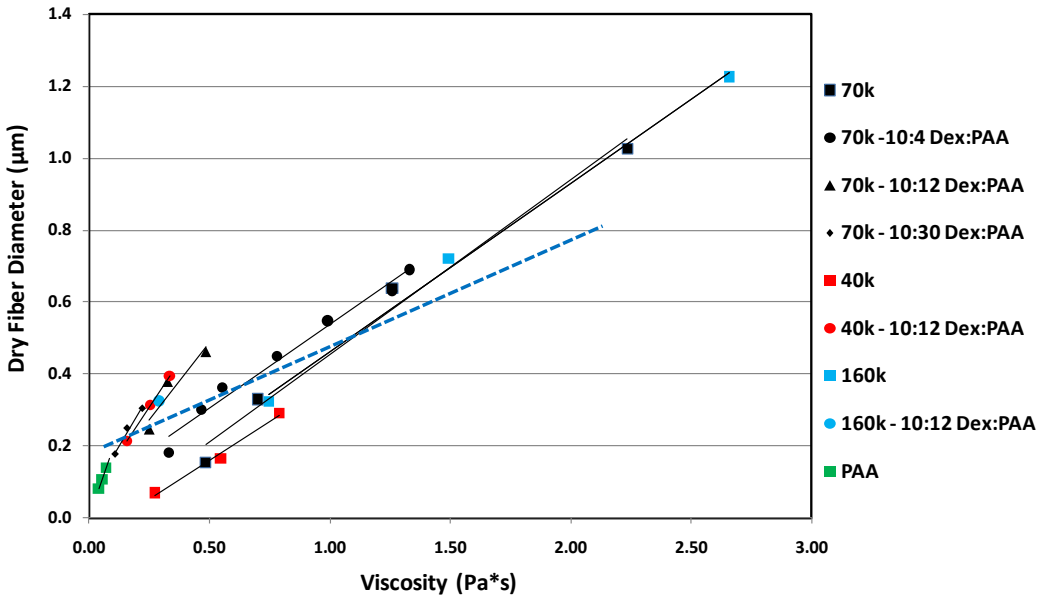

FIGURE 2.17. Viscosity vs. dry fiber diameter – dextran and dex-PAA blends. Solutions varied in terms of dextran MW (70k – black, 40k – red, 160k – blue, PAA only - green), solution concentration (min – 37.5%, max – 44.4%) and

dex:PAA ratio (1:0 – square, 10:4 – circle, 10:12 – triangle, 10:30 – diamond). **Segmented blue line separates solution properties that result in "bead defects" (below line) vs. "defect-free" (above line) fibers.** Error bars: standard error.

Correlating back to rheological properties, basically, the defect-free fibers ABOVE the blue line have tan δ peaks << 92.2 rad/sec, while BELOW the blue line, a tan δ peak was very near 92.2 rad/sec or not observed at all.

3.1.3 Empirical model to predict fiber diameter and morphology

At this point, it becomes important to be able to predict what the ultimate fiber diameter and morphology of the electrospun dex-PAA fiber will be. The effect of modifying each variable (solution concentration, dex:PAA ratio, dex MW) was determined such that an empirical model could be developed to predict the fiber diameter and morphology of the final electrospun fiber.

First, viscosity is calculated for a given solution concentration and dex:PAA fiber composition (based on Figure 2.15 and 2.16). Next, fiber diameter is calculated for a given solution concentration and dex:PAA fiber composition (based on Figure 2.4, 2.5 and 2.8). From this information, dry fiber diameter vs. viscosity can be plotted for a given solution composition and range of concentrations. At the point this line crosses the segmented blue line (Figure 2.17), it is possible to calculate the electrospinning concentration and composition corresponding to (a) average fiber diameter and (2) presence of bead defects / electrospinnability.

3.2 Fiber composition and thermal cross-linking

3.2.1 Composition of as-electrospun fibers

The composition of electrospun fibers, prior to thermal cross-linking, was determined by FTIR spectrometry. Figure 2.18 shows the absorbance spectra of dry fibers electrospun using different electrospinning solutions. For pure 70k dextran [Fig 2.18, a], a broad band from 3300-3400 cm^{-1} is attributed to hydroxyl –OH stretching [i], while bands observed from 1000-1100 cm^{-1} are typical for dextran ether linkages (C-O-C ring stretching) [ii]. For pure PAA [Fig 2.18, d], a strong absorption peak near 1710 cm^{-1} is attributed to carbonyl (C=O) stretching of the polymer's characteristic carboxylic acid (-COOH) groups [iii]. FT-IR spectra of electrospun dex-PAA blends [Fig 2.18 b and c] reveal peaks in all of these absorption bands [i-iii], indicating both dextran and PAA are present in the electrospun fiber.

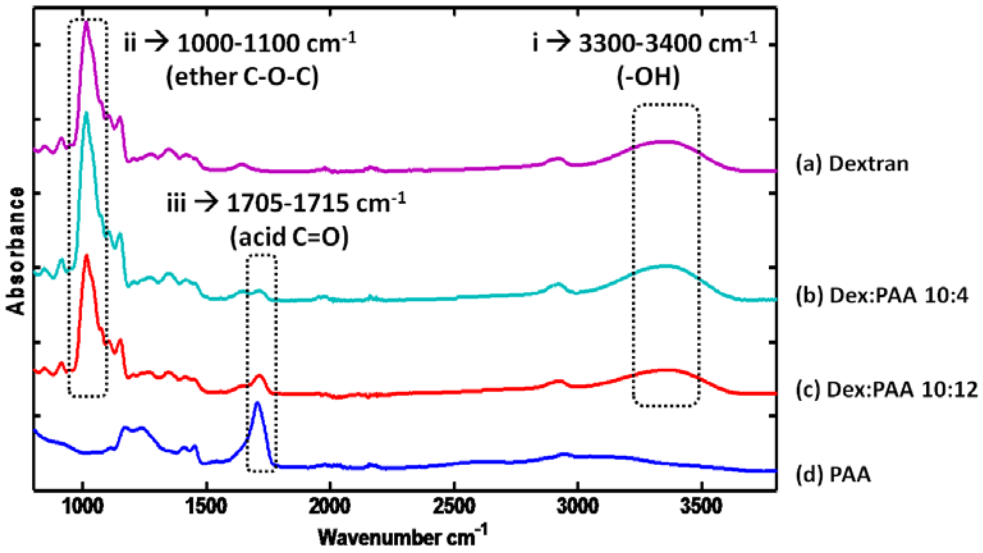

FIGURE 2.18. FTIR spectra of dry electrospun fibers *before* heat treatment: (a) 70k Dextran (b) Dex:PAA 10:4 (c) Dex:PAA 10:12 (d) PAA.

Further, the relative absorbance of dextran ether groups to PAA –COOH groups (1015/1710 cm^{-1}, or bands ii/iii) decreases as the relative amount of

dextran to PAA in the electrospinning solution decreases (Figure 2.19). These results confirm that the final fiber composition of electrospun dex-PAA fiber blends is a mixture of both dextran and PAA, and relative polymer amounts are comparable to the mer ratio of dex:PAA present in the electrospinning solution.

	Dex/PAA mers	Ether/COOH (1015/1710 cm^{-1})
Dex:PAA 10:4	2.5	14.0
Dex:PAA 10:12	0.8	6.5

FIGURE 2.19. Table of relative number of dextran and PAA mers. Relative number of dextran to PAA mers present in electrospinning solution. Ether/COOH (1015/1710 cm^{-1}): Relative peak intensities of dextran-related ether to PAA-related –COOH groups of electrospun fibers. **As the relative amount of dextran mers in electrospinning solution decreases, a corresponding decrease is seen in the relative amount of dextran-related ether peak intensities in electrospun fibers.**

3.2.2 Formation of dex-PAA hydrogel fibers via thermal cross-linking

Electrospun dextran, PAA, and dex-PAA blend fibers dissolve immediately in water. To induce water stability, fibers were incubated at 180˚C for 1 or 2 hours to thermally cross-link the –COOH and –OH groups of PAA and dextran. Following heat treatment, dex-PAA blend fibers maintained their fibrous structure when immersed in water and swelled to form stable hydrogel fibers (Figure 2.20).

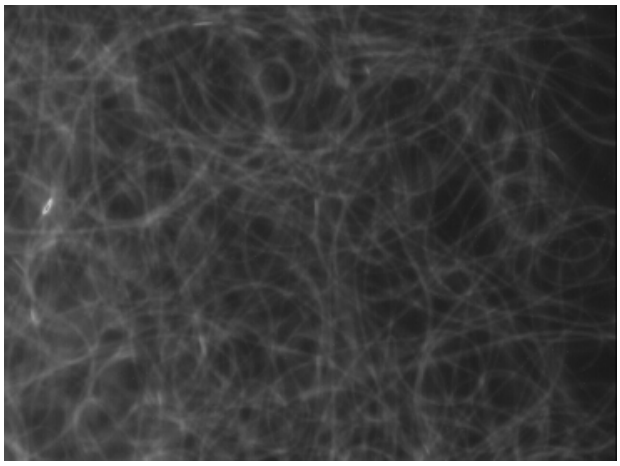

FIGURE 2.20. Epi-fluorescence image of thermally cross-linked (1 hr @ 180°C) dex-PAA fiber blend. After immersion in water, dex-PAA fibers swelled with water and maintained fibrous morphology to form hydrogel fibers.

This effect was not observed with heat-treated pure dextran or pure PAA fibers. While pure dextran fibers totally dissolved in water (data not shown), PAA appeared to "melt" (Figure 2.21) and lose fibrous structure even before immersion in water.

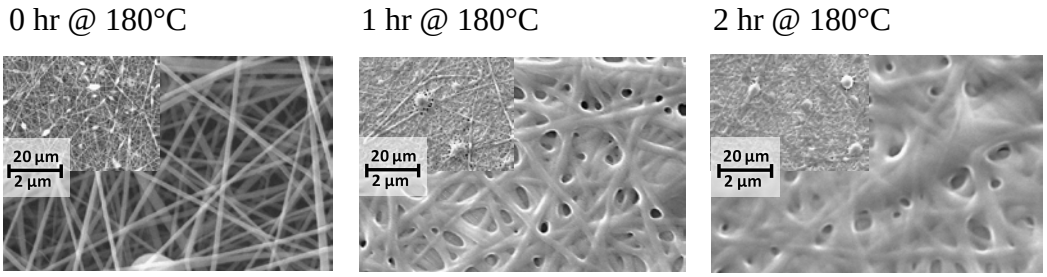

FIGURE 2.21. SEM images of thermally cross-linked PAA fibers.

3.2.3 Thermal cross-linking chemistry and composition of cross-linked fibers

Since thermally treated dex-PAA fibers were insoluble in water, this indicated that intermolecular bond formation occurred. To verify the specific type of chemical bonds forming, or cross-linking chemistry, the effect of heat

treatment was investigated using FTIR spectrometry, TGA, and quantification of –COOH groups.

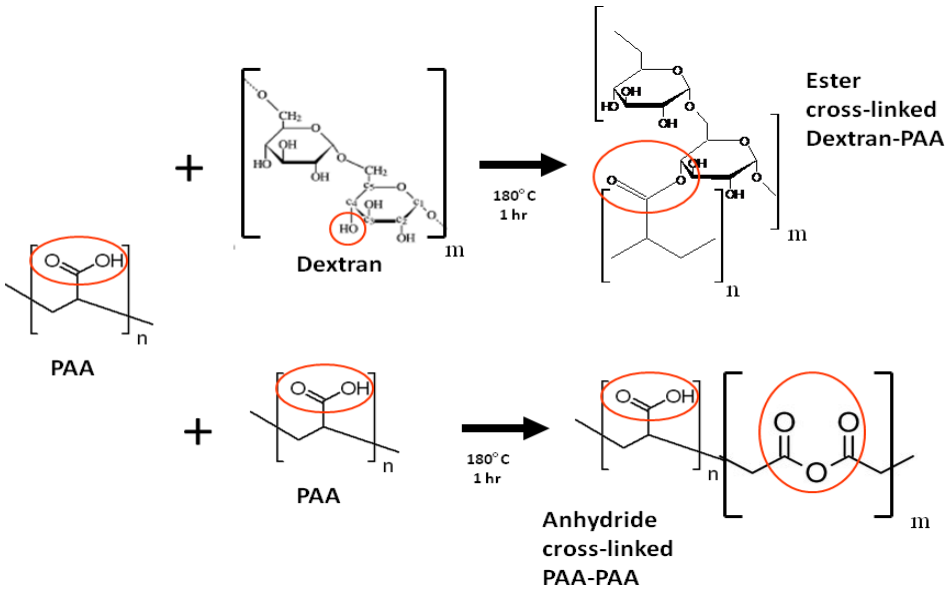

FIGURE 2.22. Schematic of thermal cross-linking reaction between dextran and PAA – anhydride and ester formation. By subjecting dry electrospun fibers of dextran and PAA to high temperature (180° C for 1-2 hrs), a dehydration reaction occurs (1) between dextran's –OH and PAA's –COOH group resulting in the formation of an ester bond, and (2) between PAA's –COOH groups resulting in formation of an anhydride. The cross-linking density is determined by the number of bonds formed. This is controlled by the mer ratio of dextran:PAA, which sets the number of PAA –COOH groups available to react with each other and dextran –OH groups.

FTIR. The composition of electrospun fibers, after thermal treatment, was determined via FTIR spectrometry. Figure 2.23 shows the IR spectra of electrospun fibers both before and after 1 and 2 hours of 180˚C heat treatment. Since anhydride formation is the dominant process in thermal cross-linking of PAA [95], peaks related specifically to anhydride cross-links are easily identified in pure PAA spectra. In Figure 2.23d, heat treatment (1 hr) resulted in the appearance of two new bands in PAA absorbance spectra between 1000-1100 cm^{-1} and at 1800 cm^{-1}. These can be attributed to new C-O-C and C=O stretching

vibrations, respectively, related to formation of new anhydrides. Both these bands increased in intensity over 2 hours as more anhydride linkages were formed. In addition, thermal treatment also resulted in a decrease of the acid adsorption band between 1680-1720 cm^{-1}, since carboxylic acids are consumed in the formation of anhydride bonds.

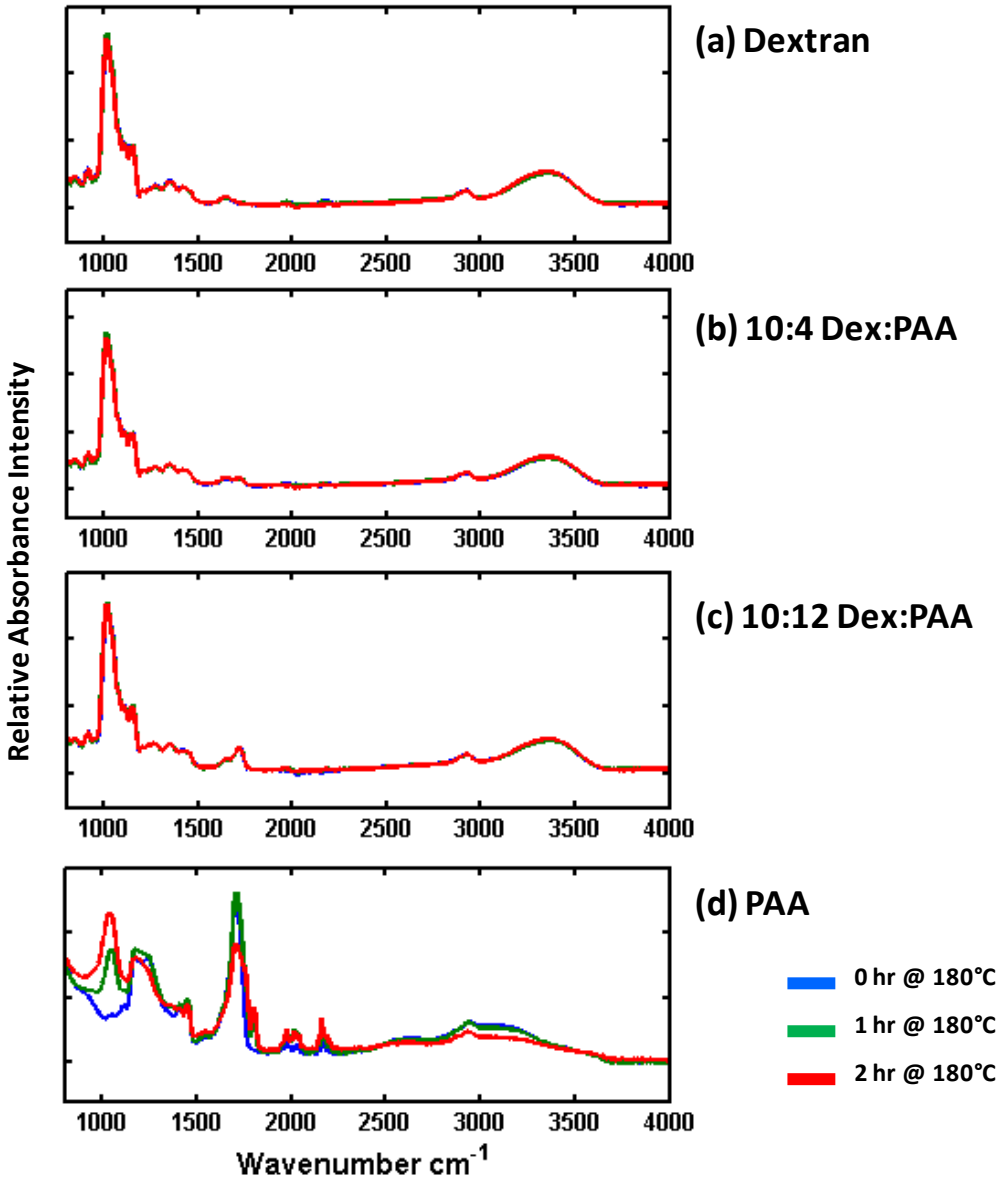

FIGURE 2.23. FTIR adsorption spectra of dry electrospun fibers *after* heat treatment: (a) 70k Dextran (b) 10:4 Dex:PAA (c) 10:12 Dex:PAA (d) PAA.

While spectra of PAA fibers showed clear differences pre- and post-thermal treatment, visual inspection of spectra from pure dextran and dex-PAA blends appear nearly identical. However, in the corresponding difference spectra, as shown in Figure 2.24, peak variation is easily discerned.

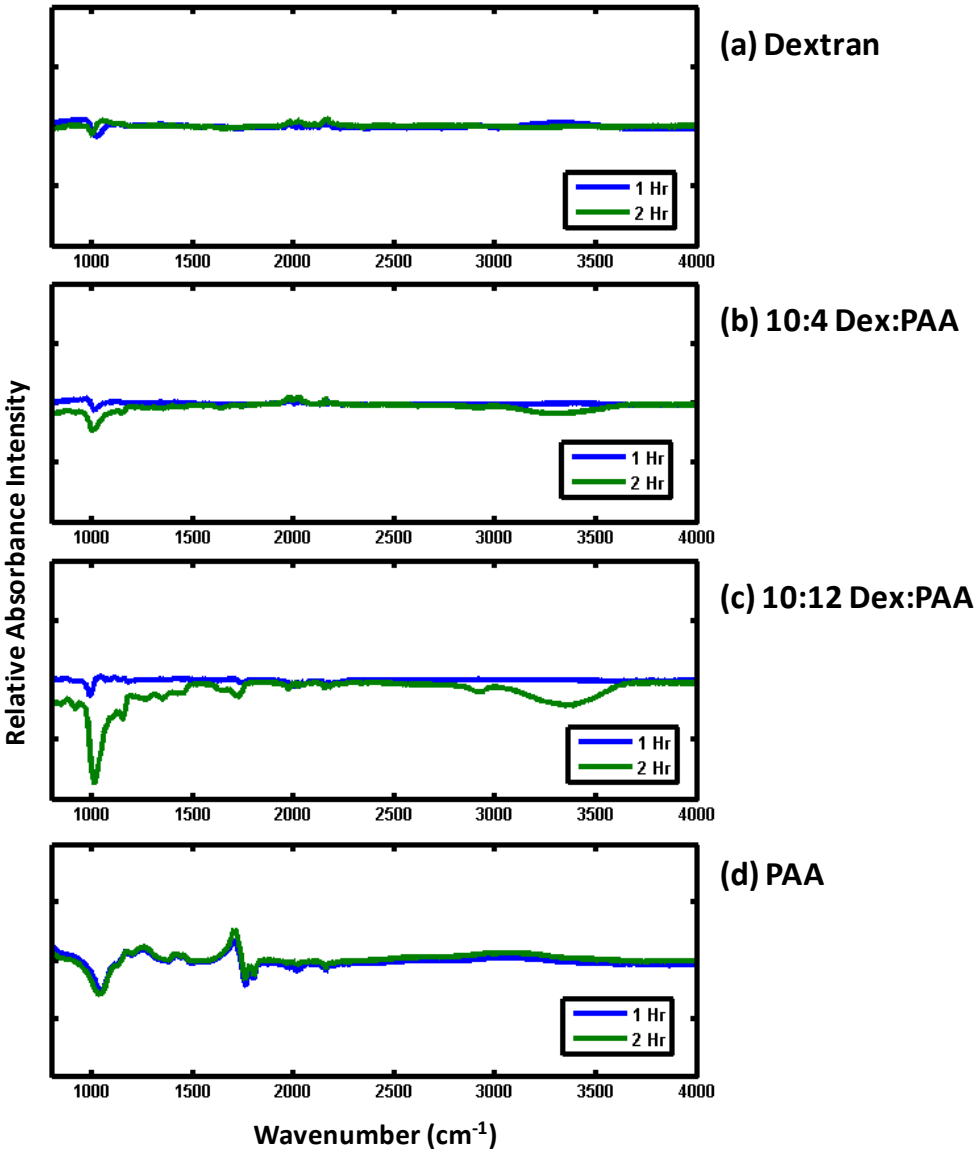

FIGURE 2.24. FTIR difference spectra of dry electrospun fibers *after* heat treatment: (a) 70k Dextran (b) 10:4 Dex:PAA (c) 10:12 Dex:PAA (d) PAA.

For thermally cross-linked PAA, peaks for PAA anhydride formation are also found in the corresponding difference spectra (Figure 2.24d). Anhydride C=O stretching resolves into two peaks increasing at 1754 cm^{-1} and 1803 cm^{-1}, while anhydride C-O-C stretching vibration resolves into a peak increase at 1032 cm^{-1}. Also, utilization of carboxylic acid groups in anhydride formation resolves into a peak decrease at 1713 cm^{-1}.

In comparing the cross-linking reaction of dex/PAA blends, Figure 2.23b and 2.23c, both these compositions lack the anhydride carbonyl peaks at 1754 cm^{-1} and 1803 cm^{-1}, although the 1032 cm^{-1} peak of C-O-C associated with anhydride formation is still present. Additionally, a peak at 1729 cm^{-1} appears (not observed in PAA cross-linking), which can be assigned to C=O ester formation. Also, since –OH groups are utilized in ester formation, there is a corresponding decrease in the –OH stretching region (3300-3400 cm^{-1}) of dextran. These results indicate that in electrospun blends of dex/PAA, both ester and anhydride cross-linking reactions are taking place during thermal treatment.

Thermo-gravimetric Analysis (TGA). DTA/TGA was performed on fibers electrospun from solutions (a) Dex:PAA 10:4, (b) Dex:PAA 10:12, (c) PAA and (d) 70k dextran. Figure 2.25 shows the amount of mass lost (wt%) as PAA and dex-PAA fibers were subjected to a 2-hr heat treatment at 180˚C. As fibers reached 180˚C, an initial weight loss (data not shown) was experienced that can be attributed to simple evaporation of water adsorbed from the environment.

After reaching 180°C, mass loss continues but at a much lower rate. The following observed mass loss over 2 hours is attributed primarily to cross-linking

reactions (ester and anhydride formation) which result in water loss associated with the dehydration reactions previously discussed. The table in Figure 2.26 quantifies the %mass loss for each fiber composition measured.

Over the course of heat treatment at 180°C, for pure dextran, a minimal amount of mass was lost (data not shown), which can be attributed to further water evaporation. For pure PAA, the greatest amount of mass was lost over time. This corresponds well to the large number of anhydride cross-links forming between –COOH groups and related water loss in the dehydration reactions. For dex-PAA blends, more mass was lost as the relative amount of PAA in the sample increased. This indicates that more cross-links are formed when more PAA is present, resulting in a higher cross-linking density for fibers comprised of higher amounts of PAA (relative to dextran).

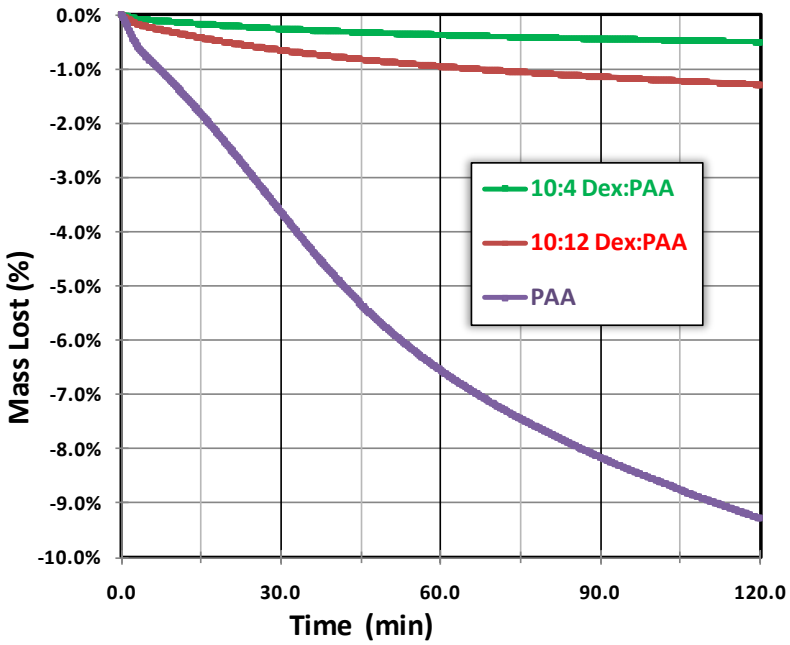

FIGURE 2.25. TGA of dex-PAA thermal cross-linking. (a) Dex:PAA 10:4 (b) Dex:PAA 10:12 (c) PAA.

In addition, for all samples, more mass loss occurs beyond the 1 hour timepoint at 180°C. This indicates that all cross-linking reactions have not completed after 1 hour, and that free –OH and –COOH groups still remain after 1-hr cross-linking time.

	1 hr	2 hr
10:4 Dex:PAA	-0.37%	-0.50%
10:12 Dex:PAA	-0.95%	-1.29%
PAA	-6.56%	-9.28%

FIGURE 2.26. Table of % mass lost with thermal dehydration cross-linking. (a) Dex:PAA 10:4 (b) Dex:PAA 10:12 (c) PAA.

Quantification of fiber –COOH groups. For all cross-linking reactions in dex-PAA fibers, a –COOH group is used in either an anhydride or ester bond. This makes quantifying the number of –COOH groups a useful indicator of the cross-linking density of a thermally treated fiber of a particular dex-PAA composition.

In this work, a TB assay (discussed in the methods section) was used to assay the amount of –COOH groups present on dex-PAA fibers after 1 hour and 2 hours of thermal treatment at 180°C. The amount of –COOH groups present on non-thermally treated fibers was calculated based upon the mer% PAA (each mer has a single –COOH group), relative to dextran, for a dex:PAA fiber composition.

In Figure 2.27, mer% PAA (in a Dex:PAA electrospun solution) is plotted versus the amount of –COOH groups on fibers (mmol –COOH / μg fiber → left y-axis) either (a) measured, after 1 or 2 hours of heat treatment, or (b) calculated,

for “as-electrospun” (non-thermally treated) fibers. Comparing “as-electrospun” to 1 hour thermally-treated fibers, not all –COOH groups are consumed. As shown on the right y-axis of Figure 2.27, only about 50% of –COOH groups are consumed in thermal cross-linking after 1 hour, independent of mer% PAA. In addition, after 2 hours of thermal treatment, remaining –COOH groups continues to decrease, indicating that further cross-linking thermal reactions are occurring. Degradation of –COOH may also be occurring, but results of this particular reaction versus anhydride formation cannot be differentiated in TGA data. FTIR studies provide information on actual reactions occurring. These observations supports the TGA data discussed previously, which showed further weight loss occurred for thermally treated fibers after 1 hour.

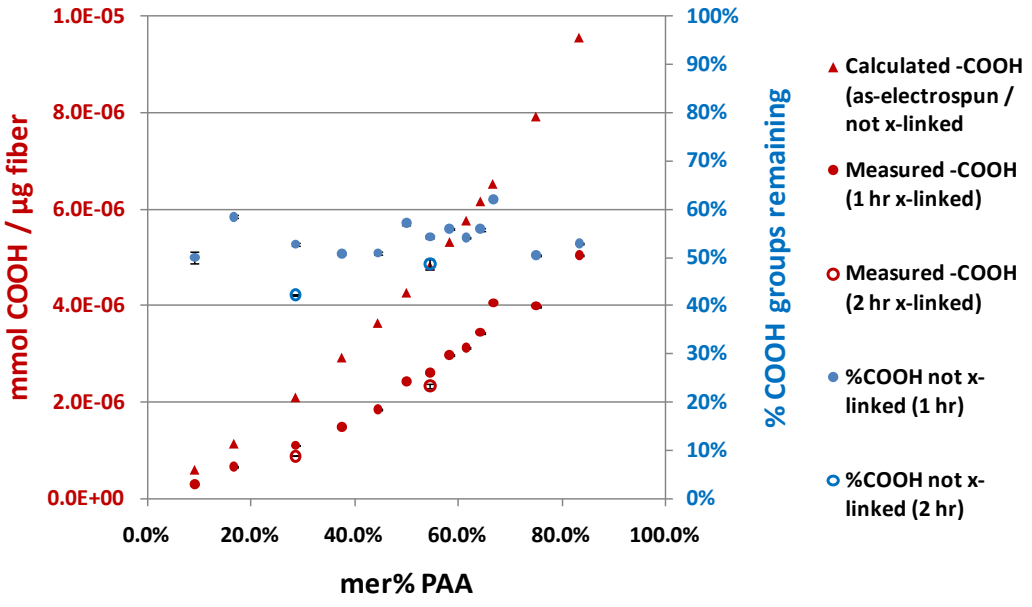

FIGURE 2.27. mer% PAA vs. mmol COOH – Quantification of –COOH groups utilized in dex-PAA thermal cross-linking.

3.3 Characterization of dex-PAA hydrogel fibers

3.3.1 Attachment of dex-PAA hydrogel fibers to surfaces

It was found that fibers would easily stick to positively charged surfaces (e.g. poly-L-lysine) in water. This is likely due to the remaining –COOH groups on fibers, as measured in the previous section, which gives them a remnant electronegative charge. This phenomenon is discussed further in Chapter 4; however, this observation is mentioned here because surface-attached fluorescent dex-PAA fibers were used to measure wet fiber diameter.

3.3.2 Swelling behavior of dex-PAA hydrogel fibers

The average wet diameter of fibers in aqueous solution (PBS, pH=7.4) was measured from epifluorescence images of fluorescent dex-PAA fibers varying in polymer wt% and dex:PAA mer ratio. Figure 2.28 shows both the dry diameter and wet diameter of dex:PAA fibers electrospun at different solution concentrations (polymer wt%), but at a constant dex:PAA composition (10:4 dex:PAA mer ratio). Similar to dry diameter, average wet diameter increased linearly with solution concentration.

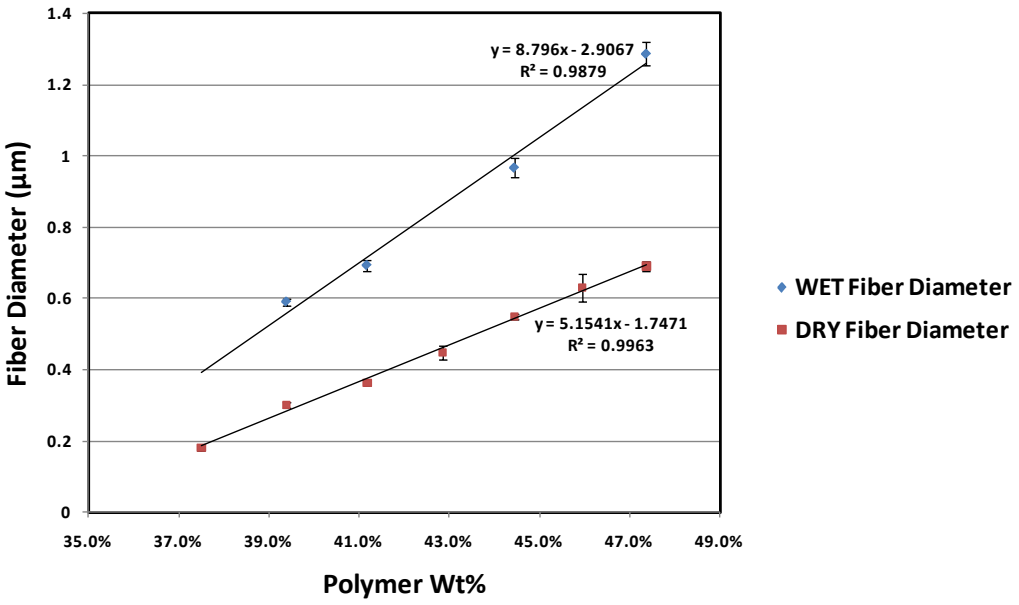

FIGURE 2.28. Wet and dry fiber diameter vs. polymer wt%. For dex-PAA blends of 10:4 dex(70k):PAA mer ratio, the same % swelling was observed across all solution concentrations. For 10:4 blends, all fibers swelled ~90% independent of solution concentration. Error bars: standard error.

Figure 2.29 shows both the dry diameter and wet diameter of dex:PAA fibers electrospun at varying dex:PAA mer ratios. In general, as the mer% PAA increases, the difference between wet and dry fiber diameter becomes less and less. Above 50 mer% PAA, swelling was so minimal and wet fiber diameter so small that epifluorescence microspcopy could not be used to measure the diameter.

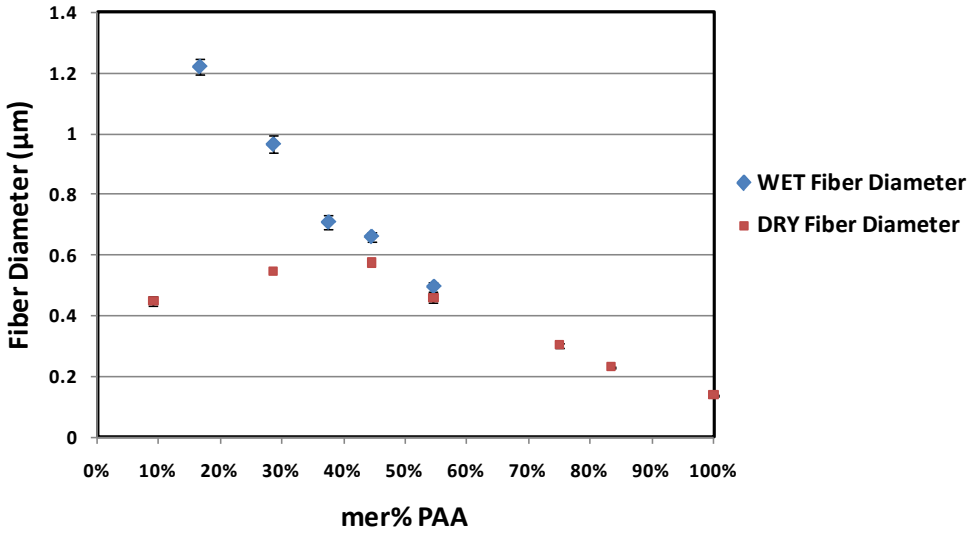

FIGURE 2.29. Wet and dry fiber diameter vs. mer% PAA. For dex-PAA blends of varying dex:PAA mer ratios (changing mer% PAA), %swelling differed. As mer% PAA increased, the %swelling decreased in a relatively predictable manner. As mer% PAA increased, higher cross-linking is expected, which would easily result in less swelling. At really high mer% PAA, %swelling was not even detectable via fluorescence microscopy. In this figure, electrospinning solution concentration used is 44.4 wt% polymer in DI water. Error bars: standard error.

3.3.3 Degradation / stability

Once immersed in water, fibers remain visually detectable in DI water for over three years. To determine degradation and stability properties, dex-PAA fibers were subjected to enzymatic degradation by incubation with dextranase enzyme (to degrade dextran). In general, compared to fibers incubated in PBS (phosphate-buffered saline, pH=7.5) or NaP (sodium phosphate, pH=7.5), dextranase significantly degraded dex-PAA fibers over 24 hours, with greater degradation occurring for higher concentrations of enzyme. These results are shown in Figure 2.30.

(A)

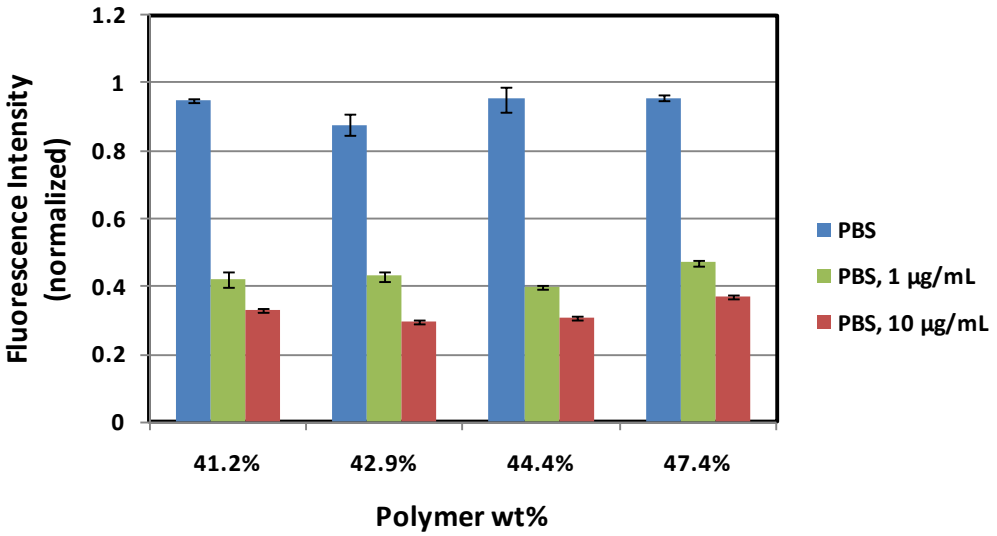

(B)

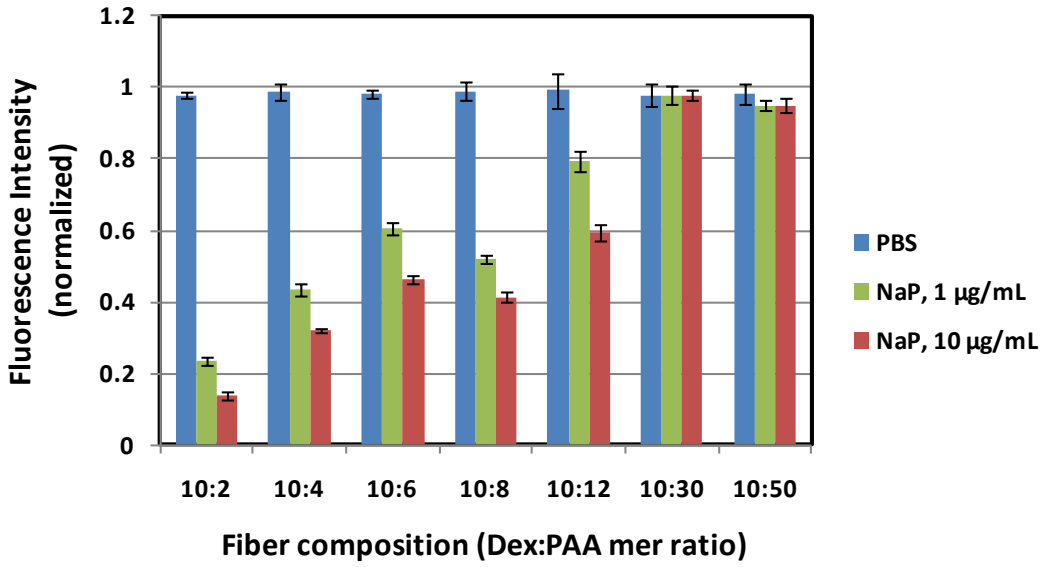

FIGURE 2.30. Enzymatic degradation of dex-PAA fibers. Fibers of varying composition (dex:PAA 10:2 to 10:50) were subjected to degradation via dextranase. Compared to dex-PAA fibers incubated in PBS or NaP at pH=7.5 @ 37°C, 10 µg or 1 µg / mL of dextranase significantly degraded fibers over 24 hours, with more degradation occurring for the higher dextranase concentration. This indicates that fibers are subject to degradation via dextran-degrading enzymes, such as dextranase. Error bars: standard error.

3.4 Live-dead assay

Dex-PAA fibers were designed with the intention of being utilized in physiological settings. To this end, fibers were attached to surfaces and the amount of live and dead cells were measured after 24 hours to determine whether fibers are cytotoxic to cells. As shown in Figure 2.31, the live/dead assay shows that independent of fiber morphology, there is minimal detectable cell death. Also, cell number (measured after 24 hours) on several fiber-coated surfaces exceeds the number on the control, PLL surface. These observations indicate fibers are compatible and non-toxic to cells.

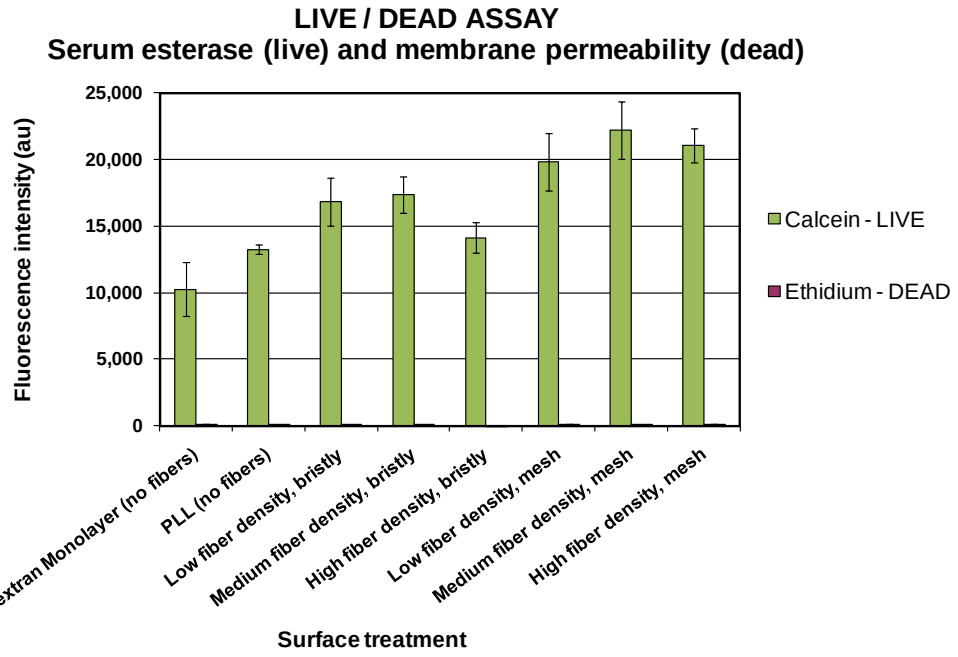

FIGURE 2.31. Live-dead cell assay on dex-PAA fiber-coated surfaces. Cell culture was performed on surfaces with dex-PAA fiber coatings of different densities (low, medium or high) and different morphologies (bristly or mesh). After 24 hours, the # of dead and live cells was measured. Compared to live cells, the # of dead cells is not even discernable from 0, indicating fibers are biocompatible and not cytotoxic to cells.

3.5 Preliminary in vitro cell culture

Since dex-PAA fibers were designed with the intention of being utilized in physiological settings, preliminary cell culture experiments were performed on fiber-coated surfaces with a variety of cell types. Imaging of cells growing with fibers are shown in Figure 2.32.

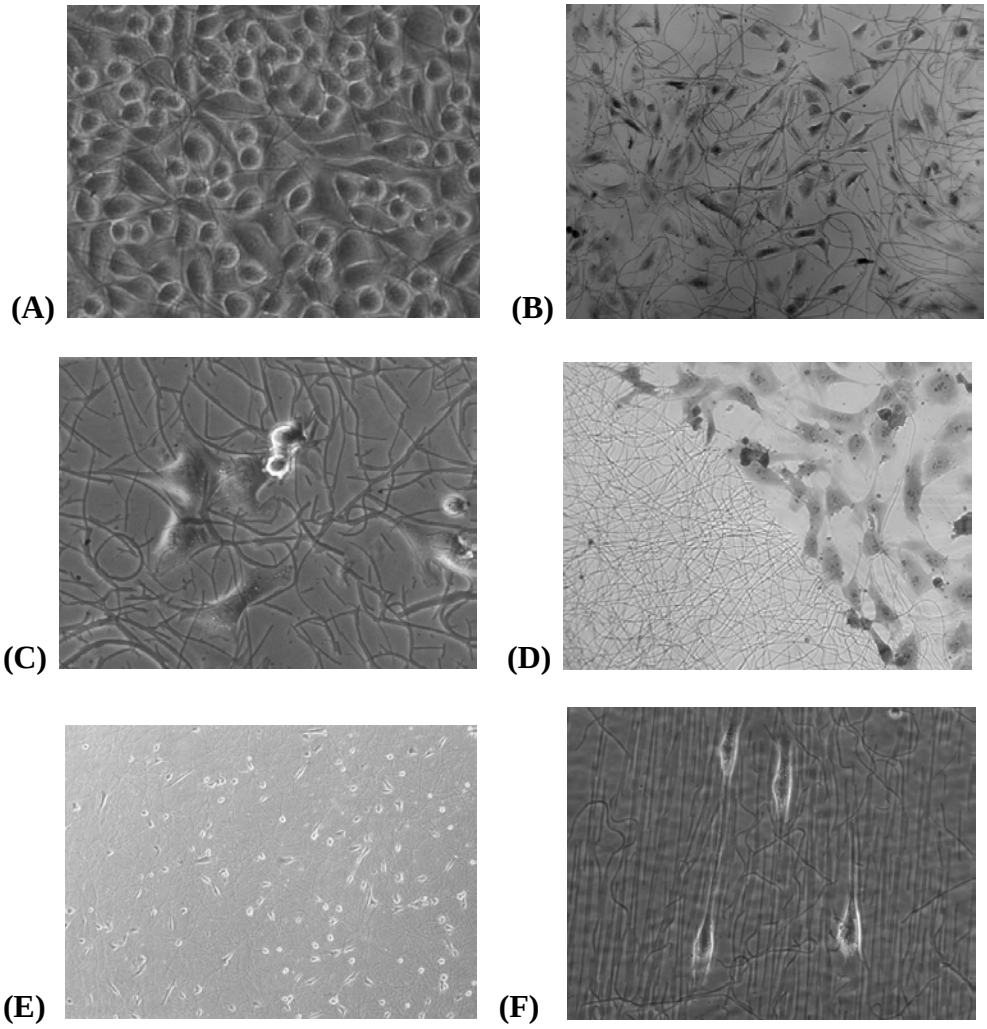

FIGURE 2.32. Preliminary cell culture on dex-PAA fiber-coated surfaces. A variety of cell types have been successfully cultured on dex-PAA fibrous surfaces, indicating good biocompatibility of the fibers. Phase-contrast microscopy. (A) L929 fibroblasts, 40x (B) CRL1444 smooth muscle cells (SMCs), 20x (C) Bovine aortic endothelial cells (BAECs), 40x (D) BAECs, 20x (E) Smooth muscle progenitor cells (SPCs), 10x (F) SPCs, 20x – appear aligned with fibers.

In vitro cell culture experiments utilizing endothelial cells (ECs), smooth muscle cells (SMCs), smooth muscle progenitor cells (SPCs) and fibroblasts showed all investigated cell types to be compatible with the fibers (Figure 2.32). Bovine aortic endothelial cells (BAECs) proliferated on nanofibrous surface coatings, crawling over and between the fibers, extending protruding processes throughout the fibrous network (Figure 2.32-C). SMCs and fibroblasts displayed a similar response (Figure 2.32 – A,B). Images are representative of BAECs, SMCs, SPCs and fibroblasts cultured on fiber-coated surfaces. As a result, *in vitro* cell culture demonstrated biocompatibility of fibrous surfaces.

4. Conclusions

Dex-PAA fibers are relatively easy to make, and toxic solvents are not required for the electrospinning process. A wide variety of fiber morphologies can be created, in terms of fiber diameter and bead defects, merely by changing solution concentration and dex:PAA compositional ratio. Further, cross-linking can be easily performed in the dry state, resulting in biocompatible fibers morphologically similar to ECM.

CHAPTER 3

Constructing nano- and micro-fibrous surface topographies

Abstract

In this work, a variety of methods were explored to determine how to generate surface coatings with unique nano- and micro- fibrous topographies using dex-PAA hydrogel fibers. It was found that dex-PAA fibers adhere easily to positively charged substrates, such as poly-L-lysine, which could be attributed to fibers' electronegative state after cross-linking. To attach fibers to surfaces, three primary methods were identified: (1) settling over time (2) drying or (3) adhering under flow. Fibers could be attached either in the "as-electrospun" state, forming a dense "slab" onto a surface, or as fragmented fibers ("bristles"), which could be processed into an even wider range of surface topographies.

To fragment fibers into "bristles," dex-PAA hydrogel fibers were subjected to high shearing forces via sonication. Fragment size was found to be dependent upon sonication time and initial hydrogel fiber properties (e.g. diameter, degree of cross-linking, or dex:PAA ratio). Less cross-linked fibers fragmented more easily and into shorter pieces. In general, fiber fragments allowed to "settle over time" tended to attach in either a "flat" or "bristly" morphology (protruding upwards from the surface). Further air-drying of bristly surfaces, however, resulted in a more "mesh" morphology as upright, end-attached fibers lay down and adhered flat onto the surface. Fiber bristles attached by adhering under flow resulted in an "aligned" morphology.

In addition to a (1) bristly, (2) mesh or (3) aligned morphology, topography could be further modified by varying (a) fiber surface density, by changing the fiber concentration in solution used for adhesion and (b) fiber surface roughness, by changing the diameter of fibers used for adhesion. Ultimately, fabrication of unique fibrous surface topographies that varied in slab-like, aligned, bristly or mesh-like morphology resulted, with differential surface roughness and surface density possible.

1. Introduction

For materials implanted within the body, eliciting an immune response and consequent rejection is one of the least desirable outcomes. For whatever the intended purpose, it is important for the body to accept the material and potentially integrate the material into normal physiology and structure (e.g. cellular scaffold for tissue regeneration). Therefore, it is important to implant a material with properties designed to elicit a specific, desirable cellular response.

A major factor that determines how the body will respond to a material is the specific topographical properties to which the immune system, proteins and cells will encounter and interact. Topographical features at the nano- and micro-scale have been shown to enhance a material's resistance to cell adhesion and proliferation, or promote some cell types versus others. For instance, studies have shown than while surfaces with planar or <10nm feature size experience similar cell adhesion properties, 50nm features sizes are non-adhesive to fibroblasts [38 45]. In contrast, endothelial cell and smooth muscle cell adhesion has been shown to

be enhanced on a nanostructured surfaces (50-100nm), versus submicron or microstructured, while fibroblast adhesion is decreased on the same nanostructured surface. A study by Kunzler et al showed that osteoblasts increased proliferation as micro-scale surface roughness increased (R_a = 1-6μm), while fibroblast proliferation decreased with increasing roughness [43]. These examples are just a small sample of the extensive literature examining the cellular response to micro- and nano- topography, and thorough reviews are available on the subject [45] [44] [46].

In this regard, topographies may be designed to either function as a (1) ***barrier***, effectively acting as a shield against protein adsorption and cell adhesion, and therefore inflammatory response or (2) ***bridge***, inducing the body's cells to interact in a specific, desirable manner and result in seamless integration of the material within the body. Topography is controlled by feature size, morphology (pillars vs. grooves vs. fibers vs. particles, etc) and surface density / surface coverage, which further determine corresponding surface roughness and surface area. Cell adhesion and proliferation may occur readily on some of these surface topographies, but not on others; the result is highly dependent upon cell type and specific responses to topography.

In this work, a fabrication method is developed for dextran/PAA surface coatings that demonstrate easily tunable topographical properties. The coatings are comprised of short hydrogel fibers, or "bristles," or as-electrospun fiber mats. The fibers can be attached as a surface coating to virtually any material carrying a positive charge. Topography is varied by changing fiber diameter (nanometers to

microns), fibrous surface density, and attachment in a slab, bristly or mesh morphology.

2. Experimental

2.1 Materials

Dextran from *Leuconostoc mesenteroides* (M_w 64k-76k) was purchased from Sigma (St. Louis, MO). Poly(acrylic acid) (M_w ~90k, 25% aqueous solution) was purchased from Polysciences, Inc. (Warrington, PA). Fluorescein dextran (FITC-dex, 70k MW, anionic) was purchased from Invitrogen (Carlsbad, CA).

2.2 Preparation of electrospinning solutions

Solutions were prepared for electrospinning by dissolving dextran and/or poly(acrylic acid) polymer in DI water and stirring overnight. Dex-PAA solutions were prepared varying in concentration between 37.5 to 47.4 wt% polymer, comprised of dex:PAA solutions with mer ratio varying between 10:1 (10%) and 3:10 (300%), using ~70k dextran and ~90k PAA.

2.3 Electrospinning and cross-linking of dex-PAA hydrogel fibers

Electrospinning was performed following the general procedure of Zong et al [91]. Briefly, a polymer solution was prepared by dissolving dextran and PAA in DI water and stirring overnight for thorough mixing. The polymer solution was loaded into a syringe and delivered out a stainless steel capillary with an inner diameter of 0.03" using a programmable syringe pump (Harvard Apparatus PHD 2000) at a constant flow rate of 10 µL/min. A voltage of 25kV was applied to the capillary tip and electrospinning solution using a high-voltage power supply

(Glassman High Voltage, Inc). Electrospun fibers were collected on a grounded aluminum foil target located 15 cm from the tip. Room humidity was maintained between 14-17%. After electrospinning, fibers were dried under vacuum overnight. To make fluorescent dex-PAA fibers, electrospinning solutions were modified by substituting ~0.4 wt% dextran polymer with 70k FITC-dex.

Dex-PAA fibers were cross-linked using a thermal dehydration reaction based on the general procedure of Chen and Hsieh [92], in which dry electrospun fibers are incubated in a vacuum oven for 1 hour at 180°C. Thermal cross-linking was performed on electrospun fibers comprised of varying dex:PAA mer ratios.

2.4 Fragmentation of dex-PAA hydrogel fibers into "bristles"

Hydrogel dex-PAA fibers were fragmented into short fiber "bristles" via sonication. In this procedure, electrospun and thermally cross-linked dex-PAA fiber mats were immersed in DI water and swelled to form long hydrogel fibers. A sonicator probe was applied to the fiber solution at a setting of 4 (using a Misonix Ultrasonic Cell Disruptor), thereby subjecting the fibers to high shearing forces and fragmenting them into short hydrogel "bristles." Sonication fragmentation was performed on dex-PAA fibers electrospun over a range of dex:PAA mer ratios (10:1 to 10:30) and solution concentrations (37.5 to 47.4 polymer wt%) for varying lengths of time (10, 20 or 30 seconds).

Solutions of specific bristle concentration (mg/mL) were prepared by immersing a measured weight of fiber mat into a given volume of DI water prior to sonication. This fibrous solution was then diluted down to specific concentrations, which is the "fiber seeding density" used for fiber bristle attachment to surfaces.

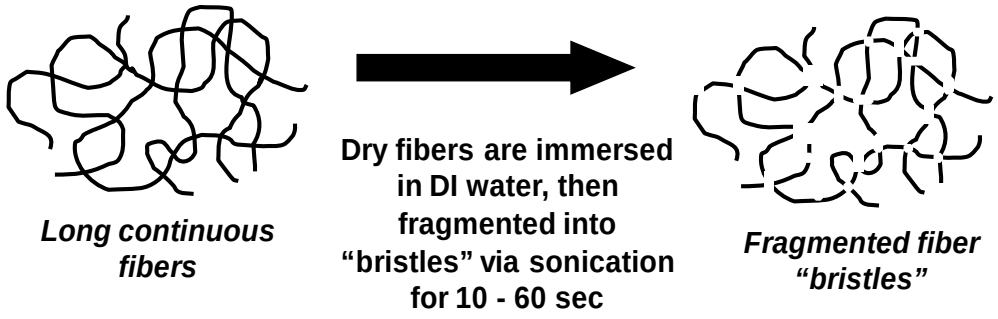

FIGURE 3.1. Pictorial representation of electrospun fibers before and after fragmentation into "bristles."

2.5 Surface immobilization of dex-PAA hydrogel fibers

Electrospun dex/PAA fibers were immobilized onto positively charged surfaces by either (1) dehydration → drying hydrogel fibers onto a positively charged surface, (2) settling → incubating a solution of fiber bristles onto a positively charged surface, and allowing fibers to settle and attach to the bottom, or (3) flow → flowing a solution of fiber bristles across a positively charged surfaces, with fibers attaching under flow (see Figure 3.2).

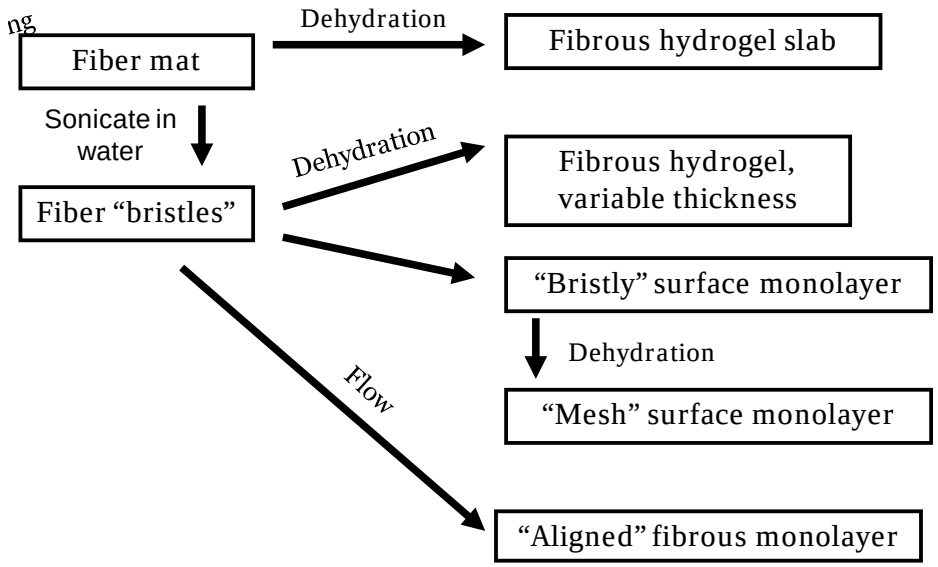

FIGURE 3.2. Schema of attachment methods: dehydration, settling and flow.

2.5.1 "Dehydration" method

Implementing the *dehydration* method differs depending on the type of fibers to be immobilized onto a surface: "bristles" or the "as-electrospun" fiber mats. **For fiber mats,** a section of the electrospun, dry cross-linked fibers are cut (while still on the aluminum foil), carefully peeled from the foil with tweezers, and then immersed in DI water. Typically, the fiber mat floats to the surface of the water. Overnight, the hydrated fiber mat is allowed to dry under vacuum. As the DI water evaporates, the fiber mat sinks to the bottom surface, dehydrates and adheres to the underlying positively-charged substrate. After rehydration, the fiber mat remains adherent; fibers retain a mat-like structure, while individual fibers adhere to each other as well as the surface, forming a dense fibrous hydrogel. **For fiber bristles**, a bristle solution is prepared at a specific concentration (mg fiber / mL DI water). Overnight, the fiber bristles are allowed to dry under vacuum. As the DI water evaporates, the bristles sink to the bottom surface, dehydrate and adhere to the underlying surface. After rehydration, the bristles remain adherent, creating a fibrous surface of which thickness depends upon the amount of bristles initially prepared in solution.

2.5.2 "Settling over time" method

In the *settling* method, a solution of fiber bristles is prepared at a specific concentration (mg fiber / mL DI water), aka "fiber seeding density". Bristles are allowed to settle (and adhere) onto a substrate for a given amount of time; subsequent rinsing removes non-adherent bristles. *The adherent bristles form a "bristly" layer of fibers on the underlying substrate.* Representative images of

"bristly" surface coatings are shown in Figure 3.6. [Note: Attempting to apply this method to fiber mats typically results in a sparse coverage of long fibers (most likely those constituting the lower/bottom surface of the fiber mat), attached in some regions but not in others. Unlike fiber bristles, which tend to sink to the bottom surface over time, fiber mats tend to float.]

Once a "bristly" surface is made, the surface can be converted into a "mesh" surface by drying the surface under vacuum overnight. During this post-attachment dehydration, bristly fibers lie down and attach to the underlying surface. When the surface is re-hydrated with water, fiber bristles stay attached to the bottom surface in a "mesh"-like morphology, as shown in Figure 3.8.

2.5.3 Flow method

In the flow method, an aqueous solution of fiber bristles is flowed over a positively-charged surface using a flow cell. Fibers attach in an aligned manner, with more fibers attaching with increasing flow time.

2.6 Variation of surface topography

Topography of dex-PAA fibrous surfaces is varied by first modifying the (1) initial state fibers are attached → whole membrane or fragmented fiber "bristles," and then the (2) method of attachment → dehydration, settling or flow. These factors change the overall morphology, including aligned vs. random or bristly vs. mesh morphology (discussed in the previous section).

Further refinement of surface topography is achieved by either varying the actual fiber composition (diameter, Dex:PAA mer ratio) and conditions used during surface attachment (fiber seeding concentration). Variation of these

factors changes how much actual fiber will attach to the surface, which changes not only fibrous surface density (surface area covered by fiber), but also the feature size / surface roughness of the overall surface.

In this work, fibrous surfaces were made using both fiber mats and fiber bristles, using all three attachment methods (dehydration, settling over time and flow). Fiber bristle attachment, via settling over time, was further investigated by varying seeding concentration and fiber composition. For these surfaces, bristly and mesh topographies were made and characterized in terms of surface density and surface roughness / feature size.

2.6.1 Measure and calculation of amount of surface-attached fibers

In this work, the amount of fiber attached for a given condition was determined by TB assay and subsequent measurement of fluorescence intensity (owing to FITC-dex used in fibers) on a fluorescence plate reader.

First, the number of –COOH groups present on 1-hour cross-linked dex-PAA fibers is determined via TB assay (as described in Chapter 2). Next, fiber-coated surfaces were made over a range of fiber compositions and fiber seeding densities. For these surfaces, TB assay was performed to calculate the actual amount of fiber attached to the surface. A matching plate was made utilizing fluorescent FITC-dextran in the electrospun dex-PAA fiber bristles. Fluorescence intensity for a known fiber amount (as determined by TB assay), for each fiber composition, was calculated. This calculation allows for the measurement of amount of surface-attached fibers utilizing fluorescence.

2.6.2 Measure and calculation of surface density / % surface coverage

Surface coverage (SurfC) is calculated as the total surface area coated by fibers versus uncoated area (background), given by the equation:

EQ 3.1 $SurfC = (FA / A)*100\%$

where: $FA = Fiber\ Area\ (cm^2)$

$A = Total\ Surface\ Area\ (cm^2)$

To vary surface coverage, dex-PAA fiber bristles were seeded onto surfaces at varying seeding concentrations, in either a mesh or bristly morphology. Fibers varied in terms of dex:PAA composition and fiber diameter. For each fiber-coated surface, a fluorescence image was taken and the surface area covered by fibers was taken and SurfC calculated.

2.6.2 Measure and calculation of surface roughness

Surface roughness is an indeterminate measurement that can be quantified in a number of different ways, and value depends on how this measurement is calculated. In this work, surface roughness (SR) is calculated based on two elements: (1) fibrous surface coverage (SurfC) and (2) fiber diameter. These two elements take into account feature size (fiber diameter) and relative frequency of occurrence (SurfC). While this calculation leaves out a lot of more specific info, this puts a number on the relative amount of fiber coverage and fiber size – it shows when a cell interacts with the surface, what it may encounter.

2.7 Microscopy – SEM and epiflouorescence imaging

To measure surface coverage and visualize fiber topographies, fluorescence imaging was performed using an inverted microscope (Leica Microsystems) on fluorescent wet fibers or inverted confocal microscope. SEM

imaging was performed using an FEI XL-30 EFSEM on dry fibers sputter-coated with Au.

3. Results and Discussion

3.1 Fiber processing used to construct surface topographies

3.1.1 As-electrospun fiber mat

For the as-electrospun fiber mat, fibers were attached via dehydration. In brief, fiber mats dried onto a surface adhered not only to the surface but also with each other. This created interesting surface topographies – depending on the fiber size, primarily, different topographies dried and were observed to have visually different surface roughness. More cross-linked fibers (less swollen fibers) showed little change in overall morphological structure (Figure 3.3, B); in contrast, less cross-linked fibers (more swollen) appeared to meld together (Figure 3.3, D) after drying.

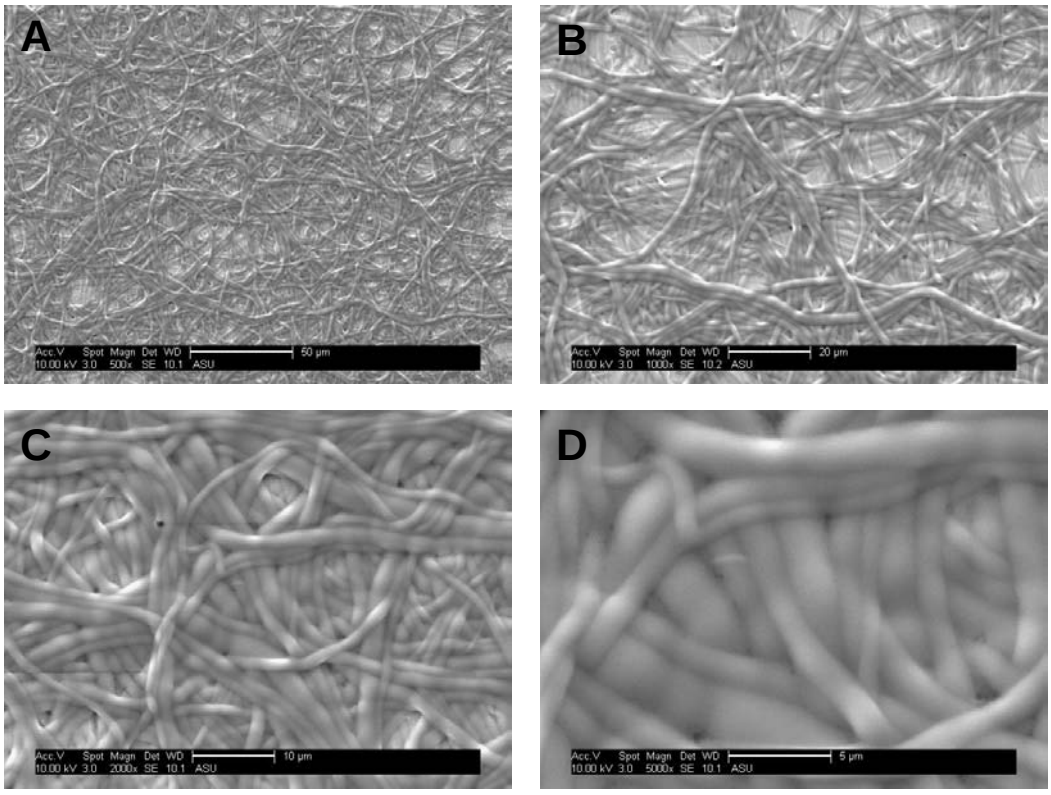

FIGURE 3.3. SEM of cross-linked, dex-PAA fiber mats, attached via dehydration.

3.1.2 Fragmented "bristles"

In this work, fiber bristles, of varying compositions, were sonicated for different amounts of time. SEM images of fragmented fibers are shown in Figure 3.4. With increasing time, fibers fragmented into much smaller fragments. This observation is easily seen in Figure 3.4, in which fragment size is much smaller with increasing sonication time. Also, fragment sizes are much longer in the more highly cross-linked fibers (dex:PAA mer ratio decreases, but mer% PAA increases), indicating that their mechanical strength is much higher and therefore resisting the shear-induced fragmentation effect.

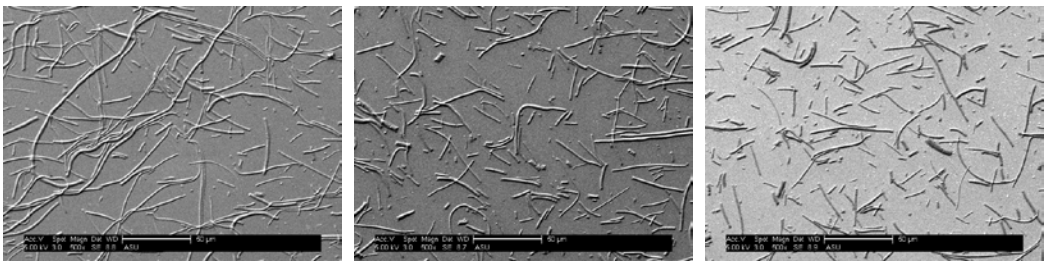

70k dex-PAA, 44.4 polymer wt%, 10:4 dex:PAA (500x, 10, 20 and 30 sec sonication)

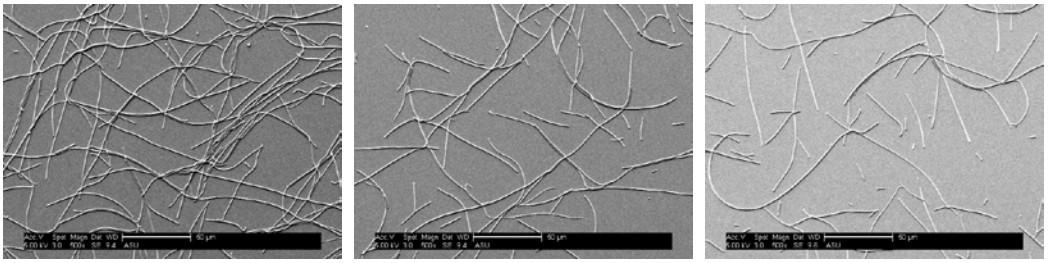

70k dex-PAA, 44.4 polymer wt%, 10:8 dex:PAA (500x, 10, 20 and 30 sec sonication)

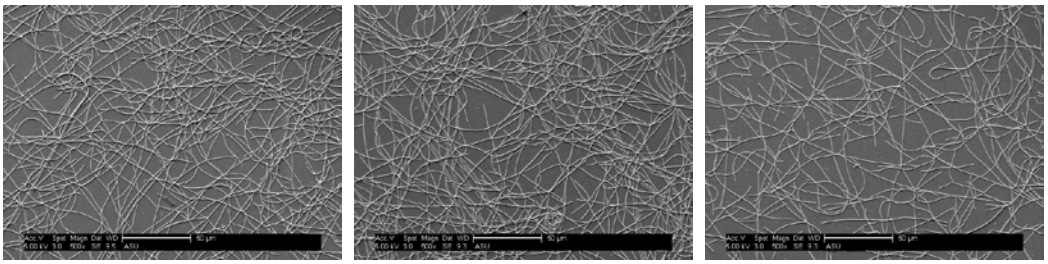

70k dex-PAA, 44.4 polymer wt%, 10:30 dex:PAA (500x, 40, 50 and 60 sec sonication)

FIGURE 3.4. SEM of fragmented fibers – varying dex:PAA mer ratio and sonication time.

It was also found that for a given fiber composition (with similar cross-linking), fragmentation was much more pronounced (smaller sizes) for the smaller diameter fibers. This effect can be observed in the SEM images of fragmented dex-PAA fibers in Figure 3.5.

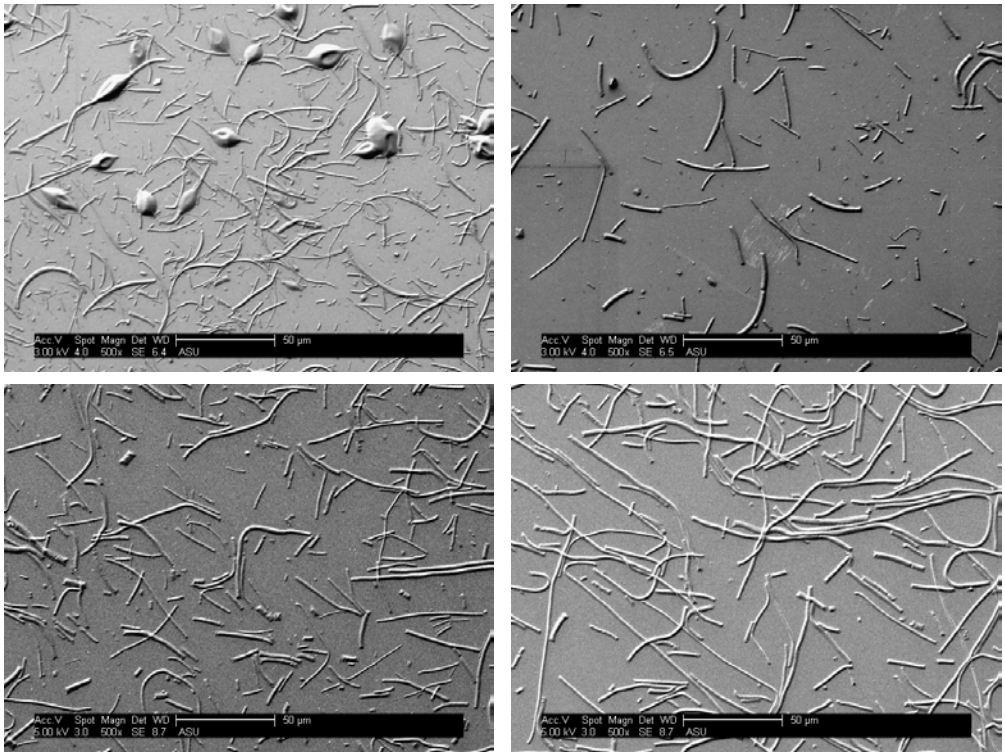

FIGURE 3.5. SEM of fragmented fibers – varying polymer wt%. Top left: 39.4 wt%, 10:4 dex(70k):PAA, 20 sec, Top right: 42.9 wt%, 10:4 dex(70k):PAA, 20 sec, Bottom left: 44.4 wt%, 10:4 dex(70k):PAA, 20 sec, Bottom right: 47.4 wt%, 10:4 dex(70k):PAA, 20 sec. All fibers are comprised of the same dex:PAA composition, to keep cross-linking density similar for all fibers, but a range of diameters was attained by varying solution concentration. After 20 seconds of sonication, smaller diameter fibers fragmented into much smaller pieces.

3.2 Surface topographies resulting from attachment methods of fiber "bristles"

For the dehydration method, attachment of fiber mats has already been shown. At this point, only attachment variations related to fiber bristles are relevant. Therefore, fiber bristles are shown attaching in the 3 different ways.

3.2.1 Settling over time

As discussed in the methods section, allowing fiber bristles to settle overnight onto a positively charged substrate results in a "bristly" morphology. Side-view (z-profile) images of "bristly" topographies, taken with a fluorescence

confocal microscope, are shown in Figure 3.6. Depending on the properties of the electrospun fiber, in terms of bead defects and fiber diameter, bristly morphology can be significantly varied. Further perspective views of the "bristly" morphology are shown in Figure 3.7.

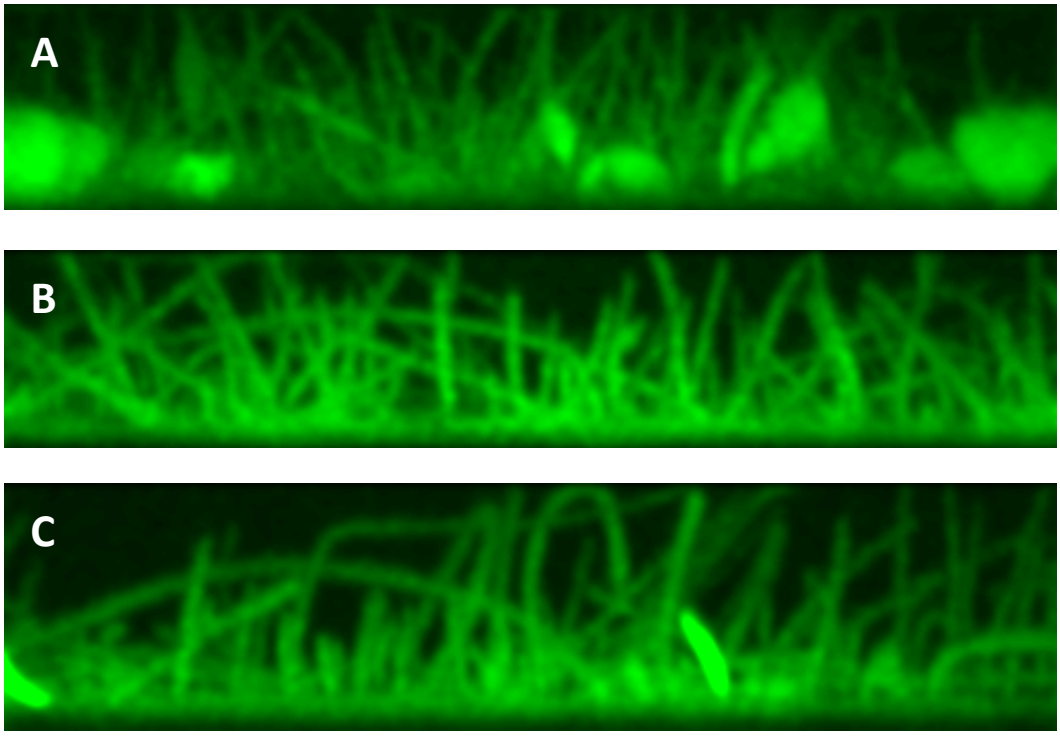

FIGURE 3.6. Fiber attachment in a "bristly" morphology. Z-profile of fibers immobilized in a "bristly" morphology. Images were generated from a maximum intensity projection in the axial direction using fluorescence confocal image-stacks of fibers immobilized using a low concentration of 30 µg/500µL, using electrospun dex-PAA solutions of: (A) 37.5 wt% (B) 41.2 wt% (C) 45.9 wt%. Images are 100 µm x 30 µm (WxH).

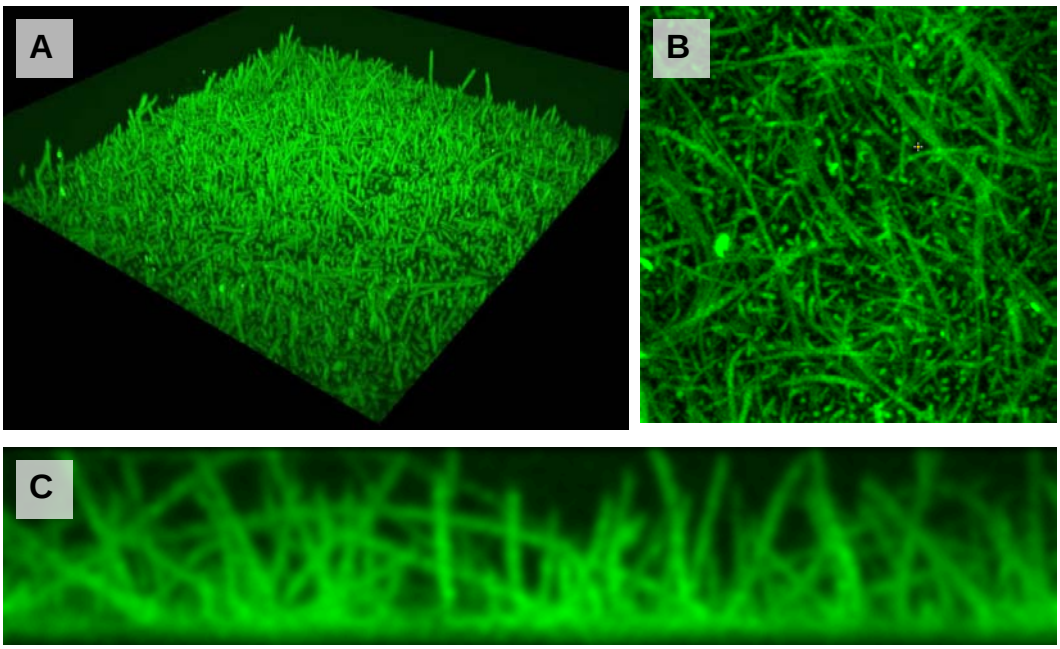

FIGURE 3.7. Fiber attachment in a "bristly" morphology, perspective views. (A) Perspective 3-D view (B) Top-view, 100µm x 100µm (C) Side-view, z-profile, 100µm x 30µm. Images were generated from a maximum intensity projections using fluorescence confocal image-stacks of fibers immobilized using a low concentration of 30 µg/500µL, 45.9 wt% solution of 10:4 dex:PAA mer ratio.

3.2.2 Dehydration

Mesh coatings were created by air- or vacuum-drying bristly fiber surfaces, causing all fibers to lie flat and attach to the underlying surface. Figure 3.8 shows fluorescent images of fibers attached in "mesh" morphology.

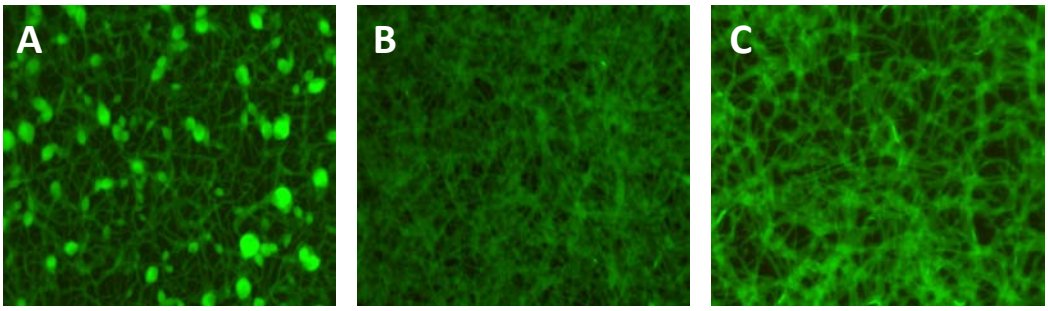

FIGURE 3.8. Fiber attachment in a "mesh" morphology. Images were generated from fluorescence confocal image-stacks of fibers immobilized using a low concentration of 30 µg/500µL, using electrospun dex/PAA solutions of: (A) 37.5 wt% (B) 41.2 wt% and (C) 45.9 wt%. All images 100µm x 100µm.

3.3 Variation and characterization of surface topography

In addition to the overall morphology (mesh vs. bristly vs. aligned), further topographical variation could be achieved by varying fiber diameter, fiber density and post-attachment treatment. As shown in Figure 3.9, using higher or lower seeding concentrations results in a more sparse or densely coated surface, respectively, for either bristly and mesh morphologies.

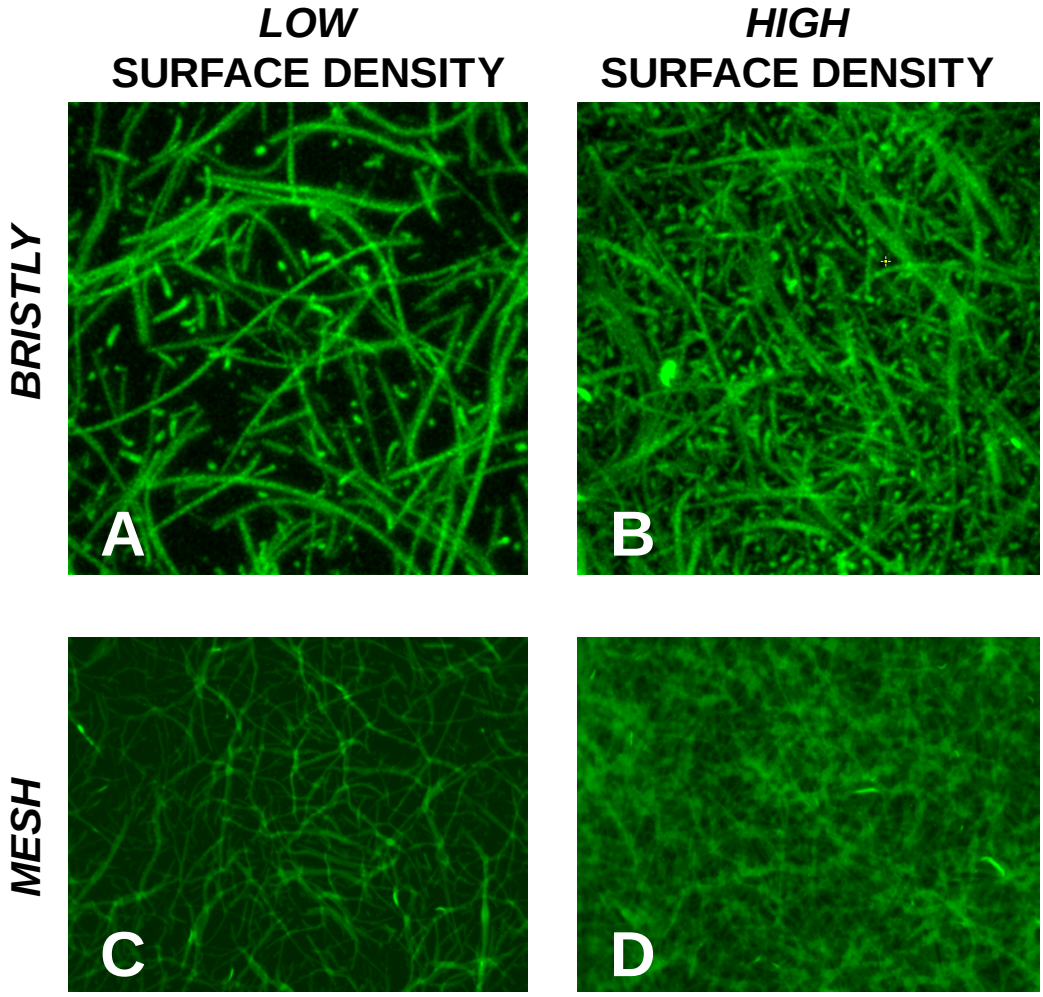

FIGURE 3.9. Fiber attachment in a "bristly" or "mesh" morphology at "low" and "high" surface density. Fluorescence images of fibers immobilized at low (15 μg/cm^2) or high (50 μg/cm^2) seeding concentrations, resulting in low (A, C) or high (B, D) surface densities. Fibers were electrospun using a 41.2 wt% solution of 10:4 dex:PAA mer ratio.

Once it was qualitatively determined that fiber seeding concentration could be used to modify surface density, the relationship between these two factors was further explored quantitatively. Figure 3.10 is a plot of how much fiber attached to a surface at increasing seeding concentrations. Supporting the imaging data, more fibers attached, creating a greater surface density, as higher seeding concentrations were utilized.

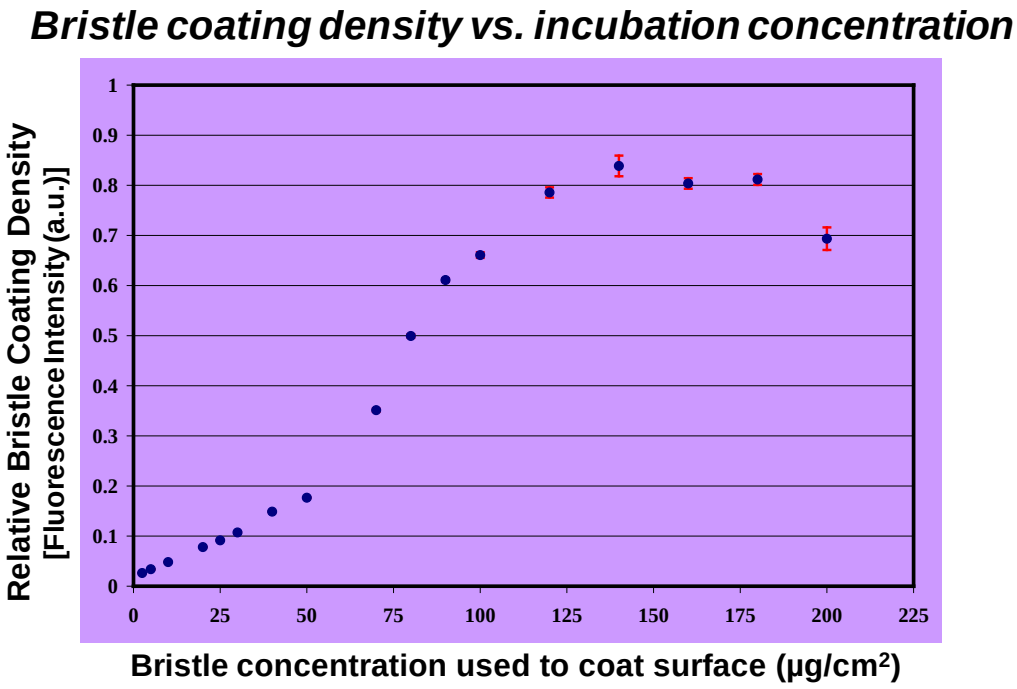

FIGURE 3.10. Attached fiber vs. fiber seeding concentration. An increasing amount of FITC-labeled fiber bristles were added for immobilization to poly-L-lysine (PLL) coated wells of a 24-well plate (2 cm^2 surface area/well). For immobilization, fiber solutions were made in DI water in concentrations ranging from 5 to 400 µg per mL. 1 mL of fiber solution was added per well, incubated overnight, then rinsed 3x with water. Fluorescence was measured at ex/em wavelengths of 485/535nm, then normalized to give "relative" coating densities.

The amount of immobilized fiber increases relatively linearly from 0µg to approximately 50µg, then suddenly increases to a saturation point. This may be

explained by the differing modes in which fibers attach to the surface. In general, fibers attach either sticking up (bristly) or relatively flat. The ratio between these morphologies depends on the packing density at each fiber concentration. As concentration increases, the amount of "end-on" fiber increases (see Figure 3.11). The total immobilized amount increases up to a saturation point at which fibers may be sterically hindering other fibers from reaching the surface (Figure 3.10, at 200 μg/cm^2).

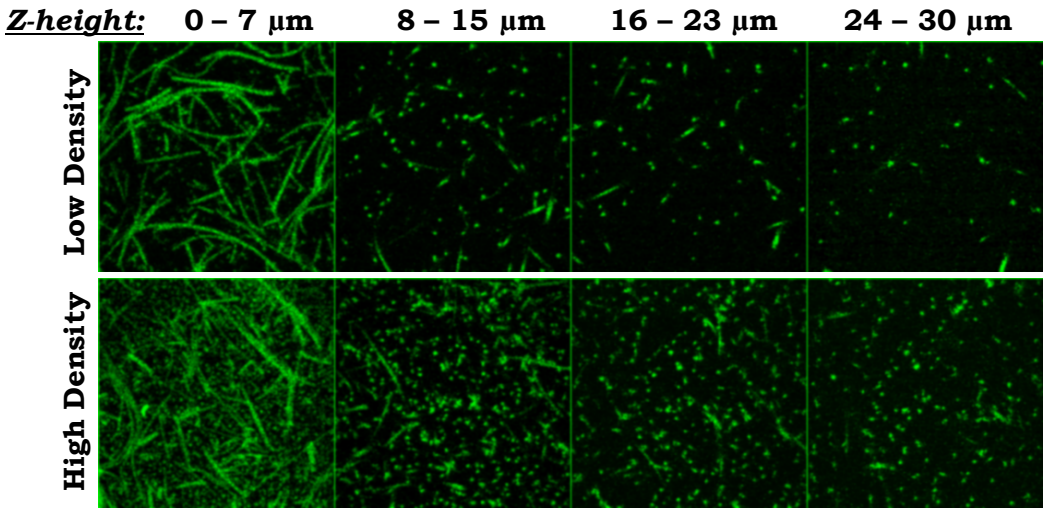

Figure 3.11. Images of fiber bristles seeded at LOW vs. HIGH concentration, showing fiber density at increasing distances (z-height) from the surface. For these images, bristles with diameters ranging from 690nm – 2.7μm were used. At the surface (column 1), many fibers attach flat, while upright end-attached fibers appear as round "dots." No flat-attached fibers appear in the higher z-height images (8-30μm), since these show areas higher than the largest fiber diameter. Further from the surface, more end-attached fibers fill the spatial volume at high-density seeding concentration (bottom row) versus low-density (top row). [Maximum intensity projections (vertical) of confocal image stacks, all images 100μm x 100μm. Low density = 15 μg/cm^2, high-density = 50 μg/cm^2.]

Figure 3.12 quantifies the amount of fiber, in terms of spatial volume occupied, at increasing distance from the surface for fibers seeded at high and low concentrations. Close to the surface (between 0 – 5 μm), there is only 2x as much

fiber on the high density surface. In contrast, this ratio does not stay constant further from the surface but increases significantly. At ~10 μm from the surface, more than 3x fiber is measured for the high density surface, thereby implying that more end-attached fibers occur (versus flat) for higher fiber seeding concentrations.

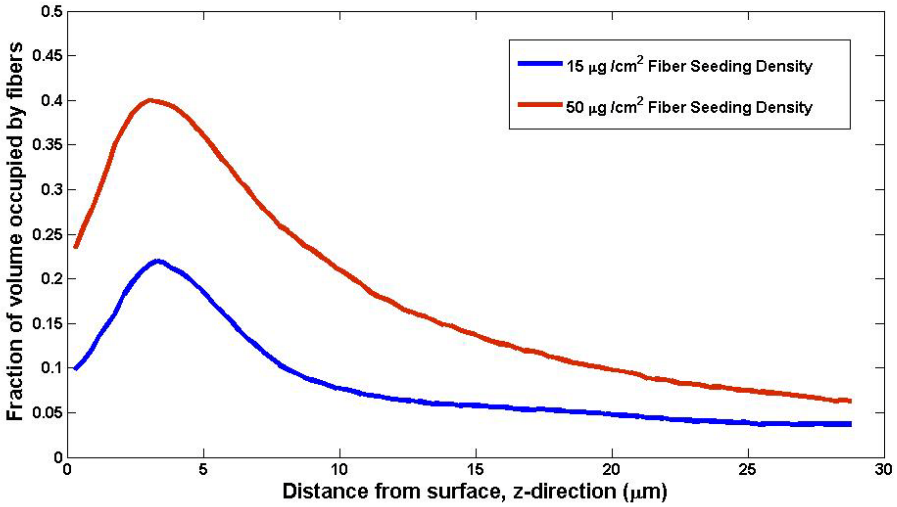

FIGURE 3.12. Spatial volume occupied by fibers vs. distance from surface. This figure shows the fraction of the spatial volume occupied by fibers (y-axis) at a given distance from the surface (x-axis). At increasing distance from the surface, a higher fractional volume occupied by end-attached fibers is seen for the surface seeded at higher concentration. Confocal image stacks of fibers seeded at low and high density were analyzed (as in Figure 3.11). The threshold was determined using the method of Otsu. The fraction is the amount of pixels in a slice greater than the Otsu threshold for the entire image stack divided by the number of pixels in a slice.

This work has shown that fiber surface density varies with fiber seeding concentration. However, depending on the fiber type (dex:PAA composition or fiber diameter), further variation in surface density and surface roughness results. As shown in Figure 3.13, the amount of attached fiber is different for fibers of different diameter or different dex:PAA composition, despite being attached at the

same seeding concentration. In general, at a low seeding concentration, a similar amount of fiber attaches independent of fiber diameter or dex:PAA composition. However, as seeding concentration increases, some surfaces significantly increase amount of attached fiber, some do not change, and some actually decrease. For instance, for 10:6 dex:PAA, a "high" seeding concentration increases surface attachment ~4.5x, while "ultra-high" decreases a little from the "high" result. For 10:2 dex:PAA, a "high" or "ultra-high" seeding concentration only increases attachment by ~1.2x.

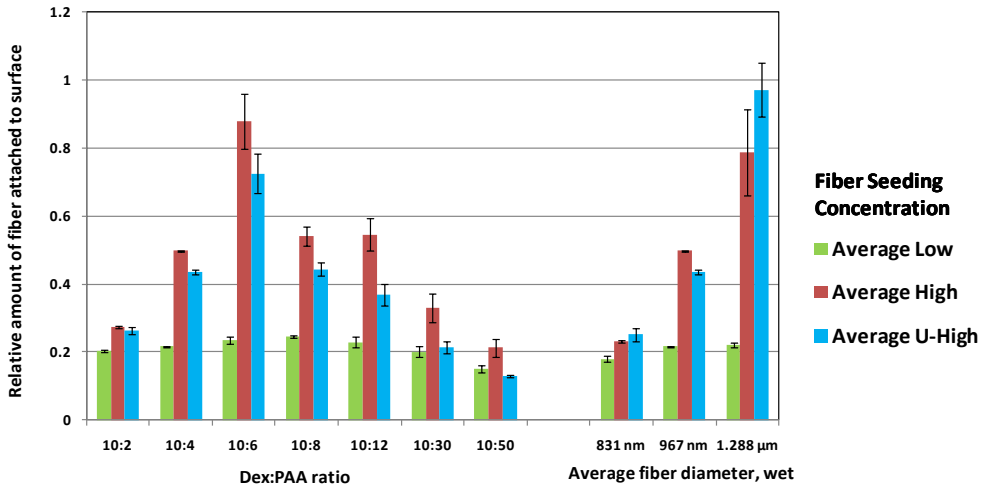

FIGURE 3.13. Attached fiber amount vs. fiber seeding density. Fluorescence intensity (%) vs. seeding concentration for varying dex:PAA compositions and fiber diameters.

4. Conclusions

A wide range of nano- and micro- fibrous surface topographies are capable of being made using dex-PAA fibers. Surface attachment methods are easy to perform: simple overnight incubation, dehydration, or flow over an adhesive positively-charged substrate. This work describes and characterizes how

to fabricate surfaces with a range of surface coverage (fibrous surface density), fibrous morphology (bristly vs. mesh) and range of feature sizes (variation in fiber diameter). These methods can be further utilized to construct surfaces with topographies to modify cell adhesion and protein adsorption for specific applications.

CHAPTER 4

Modification of dex-PAA fibrous surface chemistry

Abstract

To make surface chemistry a tunable property in fabrication of fibrous dex-PAA surface topographies, the specific modification of chemical functional groups on dex-PAA fibers was explored. For applications in which cell and protein adhesion is *not* desirable, a "passivated" surface chemistry is required. For applications in which cell and protein adhesion *is* desirable, a "bioactive" surface chemistry is required, designed to elicit a specific cellular response. In this work, fiber modification chemistries are developed to fulfill both these needs: *(1) passivation* and *(2) selective bioactivity*.

For fiber passivation, electronegative -COOH groups are converted to neutral –OH groups. For selective bioactivity, –COOH groups are functionalized via EDC/NHS chemistry, adding a small amine-containing molecule, small peptide or other protein. The degree of modification is controlled by how many –COOH groups are available for functionalizing, peptide concentration used for functionalizing, and amount of fiber (surface density) available for modification. With these methods, fibrous surface chemistry can be optimized for specific cell-interacting applications.

1. Introduction

For materials implanted within the body, eliciting an immune response and consequent rejection is one of the least desirable outcomes. For whatever the intended purpose, it is important for the body to accept the material and potentially integrate the material into normal physiology and structure (e.g. cellular scaffold for tissue regeneration). Therefore, it is important to implant a material with properties designed to elicit a specific, desirable cellular response. This work explores potential chemical modifications of fibers to make chemistry a tunable property in dex-PAA surface fabrication.

2. Experimental

2.1 Materials

Dextran from *Leuconostoc mesenteroides* (M_w 64k-76k) was purchased from Sigma (St. Louis, MO). Poly(acrylic acid) (M_w ~90k, 25% aqueous solution) was purchased from Polysciences, Inc. (Warrington, PA). Fluorescein dextran (FITC-dex, 70k MW, anionic) was purchased from Invitrogen (Carlsbad, CA). Bromoacetic acid, poly-L-lysine (PLL), N-(3-Dimethylaminopropyl)-N′-ethylcarbodiimide hydrochloride (EDC), N-hydroxysuccinimide (NHS), and 2-(*N*-morpholino)ethanesulfonic acid (MES) hydrate were purchased from Sigma.

2.2 Electrospinning, cross-linking and fragmentation of dex-PAA hydrogel fibers

Electrospinning solution preparation. Solutions were prepared for electrospinning by dissolving dextran and/or poly(acrylic acid) polymer in DI water and stirring overnight. Dex-PAA solutions were prepared varying in concentration between 37.5 to 47.4 wt% polymer, comprised of dex:PAA

solutions with mer ratio varying between 10:1 (10%) and 3:10 (300%), using ~70k dextran and ~90k PAA.

Electrospinning. Electrospinning was performed following the general procedure of Zong et al [91]. Briefly, a polymer solution was prepared by dissolving dextran and PAA in DI water and stirring overnight for thorough mixing. The polymer solution was loaded into a syringe and delivered out a stainless steel capillary with an inner diameter of 0.03" using a programmable syringe pump (Harvard Apparatus PHD 2000) at a constant flow rate of 10 µL/min. A voltage of 25kV was applied to the capillary tip and electrospinning solution using a high-voltage power supply (Glassman High Voltage, Inc). Electrospun fibers were collected on a grounded aluminum foil target located 15 cm from the tip. Room humidity was maintained between 14-17%. After electrospinning, fibers were dried under vacuum overnight. To make fluorescent dex-PAA fibers, electrospinning solutions were modified by substituting ~0.4 wt% dextran polymer with 70k FITC-dex.

Thermal cross-linking. Dex-PAA fibers were cross-linked using a thermal dehydration reaction based on the general procedure of Chen and Hsieh [92], in which dry electrospun fibers are incubated in a vacuum oven for 1 hour at 180°C. Thermal cross-linking was performed on electrospun fibers comprised of varying dex:PAA mer ratios. While untreated fibers completely dissolve in water, thermally cross-linked dex-PAA fibers maintain a fibrous structure and swell to form hydrogel fibers.

Fiber fragmentation. Hydrogel dex-PAA fibers were fragmented into

short fiber "bristles" via sonication. In this procedure, electrospun and cross-linked dex-PAA fibers were immersed in DI water and swelled to form long hydrogel fibers. A sonicator probe was applied to the fiber solution at a setting of 4 (using a Misonix Ultrasonic Cell Disruptor), thereby subjecting the fibers to high shearing forces and fragmenting them into short hydrogel "bristles." Sonication fragmentation was performed on dex-PAA fibers electrospun over a range of dex:PAA mer ratios (10:1 to 10:30) and solution concentrations (37.5 to 47.4 polymer wt%) for 30 seconds.

2.3 Preparation of fiber-coated surfaces (for chemical modification)

For chemical modification, dex-PAA fiber-coated surfaces were prepared varying in dex:PAA composition and immobilized at a constant seeding concentration. Chemical modifications were performed on fibers immobilized in either a bristly or mesh morphology.

2.4 Chemical modification of fibrous surfaces – passivation chemistry

2.4.1 Passivation chemistry (-COOH → -OH)

Ethanolamine passivation of fiber –COOH groups (converting –COOH to –OH). *Electronegative –COOH groups on fibers were converted into neutral –OH groups by the covalent attachment of ethanolamine.* To neutralize / passivate charged –COOH groups on fibers, EDC/NHS chemistry was utilized to covalently attach the amino group of ethanolamine ($NH_2CH_2CH_2OH$) to each fiber –COOH. In a typical experiment, immobilized fibers are incubated with 0.1M ethanolamine/50mM MES/30mM EDC/8mM NHS (pH=6) overnight while rocking. EDC/NHS activates –COOH groups (on fibers) to react with molecules

containing primary amines (e.g. ethanolamine), to form a covalent amide bond. The basic chemistry of this reaction is shown in Figure 4.1.

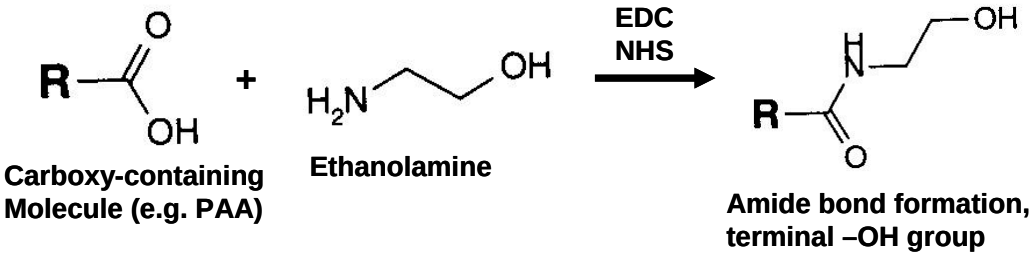

FIGURE 4.1. Chemistry to convert –COOH to –OH. Attachment of hydroxyl-terminated ethanolamine via amide bond formation to carboxyl group.

2.4.2 Chemistry for incorporating bioactive molecules

The following described chemistries were utilized for fiber carboxylation (converting fiber –OH groups into –COOH groups) and attaching molecules to fiber –COOH groups.

Fiber carboxylation (converting –OH to –COOH). Following cross-linking, fibers could be further modified to increase the number of –COOH groups for attachment of amine-containing molecules (peptides, amino acids, proteins, etc). In this carboxylation procedure, fibers are incubated in 2M NaOH/0.5M bromoacetic acid, then rinsed thoroughly with water. This converts fiber –OH groups into –COOH groups. The degree of conversion is dependent upon incubation time and concentration of bromoacetic acid. The basic chemistry of this reaction is shown in Figure 4.2.

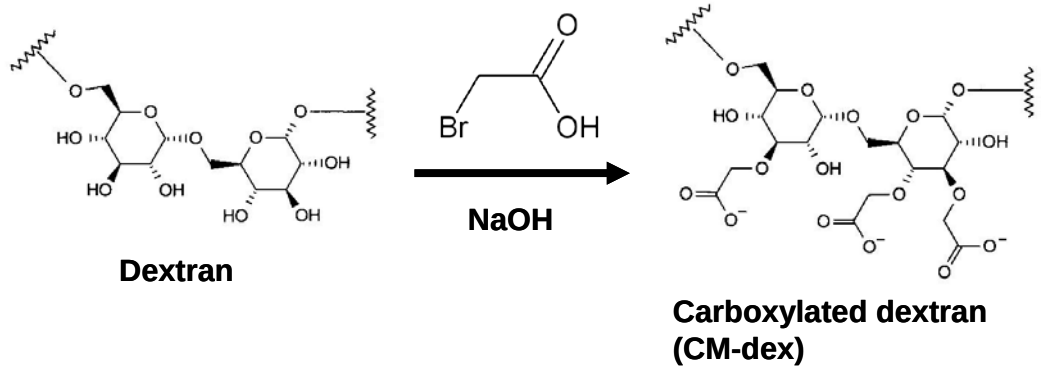

FIGURE 4.2. Chemistry to convert dextran –OH to –COOH. Carboxylation of dextran –OH groups via bromoacetic acid treatment.

Amide-attachment of bioactive molecules to –COOH groups. –COOH groups on fibers (either innate to PAA or converted from dextran –OH groups) can be modified for further bioactivity. To this end, fibers were incubated with an amine-containing molecule in 30 mM EDC/8mM NHS, forming an amide bond between –COOH and an amine group, then rinsed with DI water. Chemistry of the reaction for amide attachment to carboxy groups is shown in Figure 4.3.

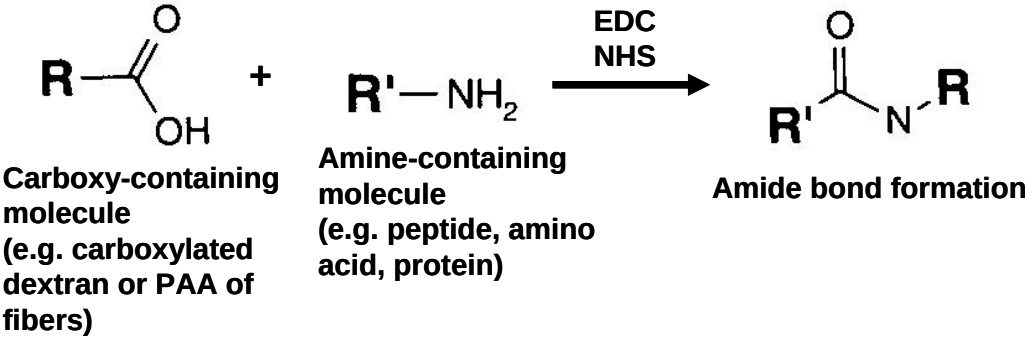

FIGURE 4.3. Attachment of amine-containing molecules to carboxyl groups.

2.5 Assay of chemical modifications

Chemical modification of fibers was measured using a TB assay for quantifying fiber –COOH groups and FTIR.

2.5.1 TB Assay (quantification of -COOH)

Quantification of fiber carboxyl groups, pre- and post- passivation, was determined following the procedure described by Nakajima and Ikada [93]. Briefly, fibers are stained with $5x10^{-4}$ M toluidene blue (TB) dye (pH=10.0) for 3 hours, then rinsed with water (pH=10.0). Bound TB is extracted from the fibers using 50 v/v% acetic acid. Concentration of extracted TB is measured using a plate reader at 633 nm absorbance. Based on the assumption that the number of bound TB dye molecules is equal to the number of carboxyl groups on the fibers, this absorbance reading is used to determine the number of fiber carboxyl groups.

2.5.2 FT-IR

To analyze chemical modification of dex-PAA fibers, fiber composition of un-modified vs. chemically modified dex-PAA fibers was performed using FT-IR analysis on representative fiber samples. FT-IR spectra of dry electrospun fibers were measured using a Thermo Nicolet Nexus 470 FT-IR spectrometer. Prior to FT-IR analysis, electrospun fibers were cross-linked for 1 hour, then (1) not chemically modified (2) carboxylated or (3) amine-attached (glycine).

3. Results and Discussion

3.1 Chemical modifications of fibers

A toluidene blue assay (described previously) for measuring relative amounts of –COOH groups was performed. Figure 4.4 shows the relative amount of –COOH groups on fibers before and after ethanolamine passivation. Absorbance readings show minimal toluidene blue is bound to fibers treated with

ethanolamine (red squares) versus untreated control fibers (red circles). After ethanolamine passivation, the amount of TB binding decreased, indicating fiber carboxy groups (-COOH) were successfully passivated, converted into hydroxyl groups (-OH), using the chemistry described here. In addition, for all dex:PAA fiber compositions, less than 10% of total –COOH groups remained after passivation (blue circles).

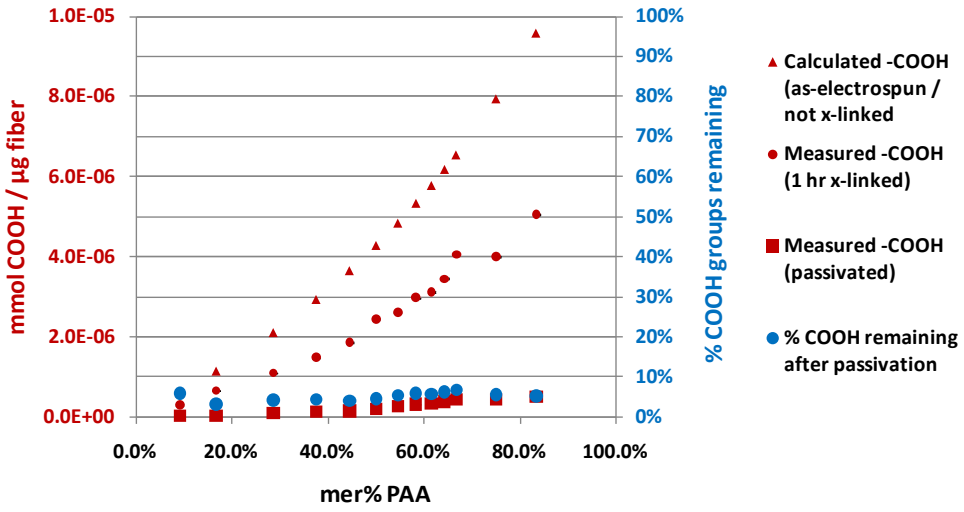

FIGURE 4.4. TB assay for –COOH conversion – passivation.

For bioactive modification, FTIR was performed on fibers modified to increase the number of –COOH groups for the attachment of amine-containing molecules. In this procedure, carboxylation was performed by incubating fibers in 2M NaOH/0.5M bromoacetic acid for 45 minutes, then rinsing thoroughly with DI water. Amide attachment was then performed using glycine (as a representative molecule containing a single amine group). Carboxylated fibers were incubated overnight with 1M glycine in 30mM EDC/8mM NHS, then thoroughly rinsed with DI water.

FT-IR results are shown in Figure 4.5. Carboxy-modified fibers have a new peak at ~1600 and ~1450, while amine-modified fibers have an amide bond peak forming at ~1620. With increased time for modification (either for carboxylation or amide), peak intensity increased, indicating that time correlated with greater conversion of groups.

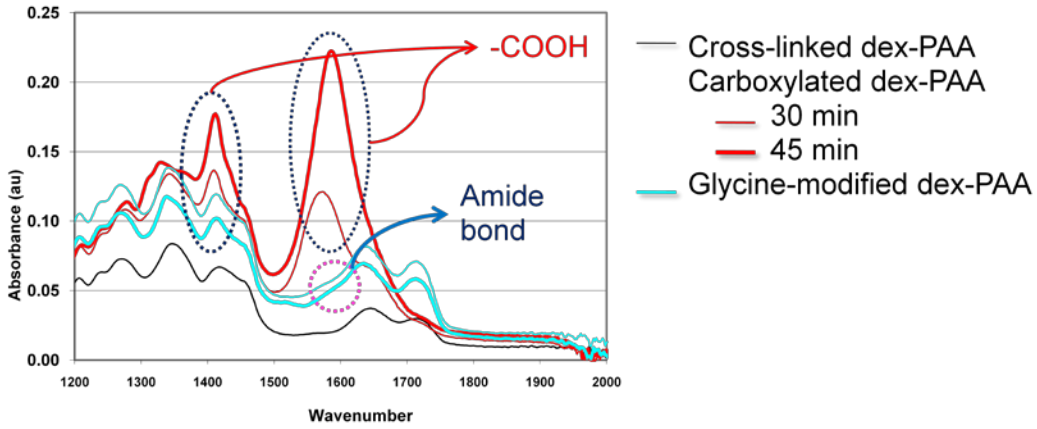

FIGURE 4.5. FTIR adsorption spectra of fiber modifications. Following cross-linking, fibers were further modified to include increase carboxylation and attach amine-containing molecules (in this figure, glycine was attached).

In summary, these results show that ethanolamine passivation successfully converts nearly 90% of fiber –COOH groups to –OH. For bioactive modification, bromoacetic acid treatment successfully converts –OH groups into an increasing number of –COOH groups. Last, molecules with primary amine groups can be attached to carboxyl groups via EDC/NHS chemistry. These results provide a basis for chemical modification of fibers for tuning fibrous surface chemistry for specific applications.

4. Conclusions

Surfaces were easily modified to be either carboxylated, passivated, or modified with attached amine-containing molecules, in a variety of morphologies and with varying fiber dex:PAA compositions. The final composition of modified fibers was verified and quantified. These results indicate that these chemical modifications can be further used to either passivate or bioactively modify fibrous surfaces for specific applications related to directing a specific cellular response.

CHAPTER 5

Low-fouling fibrous surface coatings -

Minimization of protein adsorption & cell adhesion

Abstract

The material developed in this work is designed with the expectation of being utilized in applications requiring contact with biological components, most likely with a living system in which an inflammatory, rejection response may follow. To this end, a non-fouling surface is desirable that inhibits both protein adsorption and consequent cell adhesion. Dex-PAA hydrogel fibrous surface possess a number of features suggestive of their capability to fulfill these criteria, and even surpass the performance of alternative materials commonly used in non-fouling applications.

To assess non-fouling properties, dex-PAA fibrous surface coatings were fabricated to exhibit a range of surface topographies and chemistries. Surface topography was varied in terms of fiber density, fiber diameter, and mesh vs. bristly morphology; fiber surface chemistry was varied in terms of modifying fibers to display either –OH or -COOH functional groups. Also, the background substrate to which the fibers are attached were modified to be either adhesive or non-adhesive, differentially or equivalent to the fibers. As measures of non-fouling, protein adsorption and cell adhesion assays were performed on each prepared surface. First, adsorption levels of a biologically relevant protein, albumin, was measured. Further, the ability of surfaces to resist cell adhesion was

measured using both fibroblasts and endothelial cells. It was found that synergistic combinations of dex-PAA fibrous surface topography and surface chemistry resulted in low-fouling surfaces with minimal protein adsorption and cell adhesion.

1. Introduction

For materials implanted within the body, eliciting an immune response and consequent rejection is one of the least desirable outcomes. For whatever the intended purpose, it is important for the body to accept the material and potentially integrate the material into normal physiology and structure (e.g. cellular scaffold for tissue regeneration).

In this work, a dextran-based surface coating of dextran/PAA electrospun fibers has been created that is easily tunable in chemical, mechanical and morphological properties. The material properties are optimized for serving as a "barrier" surface coating. Native dextran –OH (hydroxyl) groups endow the fibers with an inert, low protein and low cell adhesive nature, and PAA –COOH groups are converted into –OH groups. The micro- and nano- topography is modified to minimize the available underlying surface area to which cells can adhere.

2. Experimental

2.1 Materials

Dextran from *Leuconostoc mesenteroides* (M_w 64k-76k) was purchased from Sigma (St. Louis, MO). Poly(acrylic acid) (M_w ~90k, 25% aqueous solution) was purchased from Polysciences, Inc. (Warrington, PA). Fluorescein dextran (FITC-dex, 70k MW, anionic) was purchased from Invitrogen (Carlsbad, CA).

2.2 Electrospinning, cross-linking and fragmentation of dex-PAA hydrogel fibers

Electrospinning solution preparation. Solutions were prepared for electrospinning by dissolving dextran and/or poly(acrylic acid) polymer in DI water and stirring overnight. Dex-PAA solutions were prepared varying in concentration between 37.5 to 47.4 wt% polymer, comprised of dex:PAA solutions with mer ratio varying between 10:1 (10%) and 3:10 (300%), using ~70k dextran and ~90k PAA.

Electrospinning. Electrospinning was performed following the general procedure of Zong et al [91]. Briefly, a polymer solution was prepared by dissolving dextran and PAA in DI water and stirring overnight for thorough mixing. The polymer solution was loaded into a syringe and delivered out a stainless steel capillary with an inner diameter of 0.03" using a programmable syringe pump (Harvard Apparatus PHD 2000) at a constant flow rate of 10 µL/min. A voltage of 25kV was applied to the capillary tip and electrospinning solution using a high-voltage power supply (Glassman High Voltage, Inc). Electrospun fibers were collected on a grounded aluminum foil target located 15

cm from the tip. Room humidity was maintained between 14-17%. After electrospinning, fibers were dried under vacuum overnight. To make fluorescent dex-PAA fibers, electrospinning solutions were modified by substituting ~0.4 wt% dextran polymer with 70k FITC-dex.

Thermal cross-linking. Dex-PAA fibers were cross-linked using a thermal dehydration reaction based on the general procedure of Chen and Hsieh [92], in which dry electrospun fibers are incubated in a vacuum oven for 1 hour at 180°C. Thermal cross-linking was performed on electrospun fibers comprised of varying dex:PAA mer ratios. While untreated fibers completely dissolve in water, thermally cross-linked dex-PAA fibers maintain a fibrous structure and swell to form hydrogel fibers.

Fiber fragmentation. Hydrogel dex-PAA fibers were fragmented into short fiber "bristles" via sonication. In this procedure, electrospun and thermally cross-linked dex-PAA fiber mats were immersed in DI water and swelled to form long hydrogel fibers. A sonicator probe was applied to the fiber solution at a setting of 4 (using a Misonix Ultrasonic Cell Disruptor), thereby subjecting the fibers to high shearing forces and fragmenting them into short hydrogel "bristles." Sonication fragmentation was performed on dex-PAA fibers electrospun over a range of dex:PAA mer ratios (10:1 to 10:30) and solution concentrations (37.5 to 47.4 polymer wt%) for 30 seconds.

Solutions of specific bristle concentration (mg/mL) were prepared by immersing a measured weight of fiber mat into a given volume of DI water prior to sonication. This fibrous solution was then diluted down to specific

concentrations, which is the “fiber seeding density” used for fiber bristle attachment to surfaces.

2.3 Fabrication of non-fouling surface

To assess fouling properties of dex-PAA fiber-coated surfaces, a variety of surfaces were made to exhibit a range of surface topographies and chemistries. First, topography is varied in terms of fiber density and fiber diameter, as well as mesh or bristly morphology. Surface chemistry is modified to display either –OH (passivated) or –COOH (as-electrospun, electronegative) functional groups, using fibers of varying dex:PAA compositions. In addition, the background substrate to which the fibers are attached is modified to display functional groups either differential or equivalent to the fibers.

To attach fibers to surfaces at a range of surface densities, fiber seeding concentration was varied between 75 to 400 µg/mL for each PLL-coated well, incubated overnight, and rinsed with DI water. For “bristly” topographies, surfaces were not dehydrated; for “mesh” topographies, water is removed from wells and surfaces were dehydrated under vacuum overnight, then rehydrated with DI water.

To passivate fibers (convert –COOH to –OH), surfaces were incubated with 0.1M ethanolamine, 30mM EDC and 8 mM NHS in 50 mM MES buffer overnight, then rinsed thoroughly with DI water.

In terms of modifying the background substrate, an adhesive PLL background is already present. To passivate the PLL background substrate, a coating of dextran monolayer (DM) is applied. In this chemistry, each well is

incubated with 10 mg/ml oxidized dextran (ox-dex) in 0.1M phosphate buffer overnight. Next, the ox-dex solution is removed and 0.1M $NaBH_4$ is added to each well, incubated 2 hours, then rinsed. Plates are stored in DI water until used.

2.4 Protein adsorption assays

To measure protein adsorption on constructed fibrous surfaces, surfaces were incubated with FITC-BSA in PBS overnight, then rinsed thoroughly. Amount of adsorbed BSA was then measured using a fluorescence plate reader (ex/em = 490/525 nm).

2.5 Cell adhesion assays

To measure cell adhesion on constructed fibrous surfaces, BECs and 3T3s were seeded at high density. After 24 hours, amount of cell proliferation was measured using an Invitrogen assay.

3. Results and Discussion

3.1 Protein adsorption

As a first measure of fouling, protein adsorption of BSA, a physiologically relevant protein, was performed on fibrous surfaces. Surfaces varied in surface density, fiber passivation and background modification, and compared to adhesive PLL surface and non-adhesive DM.

In terms of non-fouling, it is expected that passivated fibers on a passivated DM background will exhibit the lowest amount of protein adsorption. As shown in Figure 5.1, these particular surfaces exhibited the least amount of protein adsorption (light green), at a level comparable to that of only dextran

monolayer. In terms of surfaces with higher levels of protein adsorption, this occurred on surfaces with a PLL background (red and light red). Greatest amount of protein adsorption were measured on low density fiber surfaces (seeded at low concentrations) with PLL background.

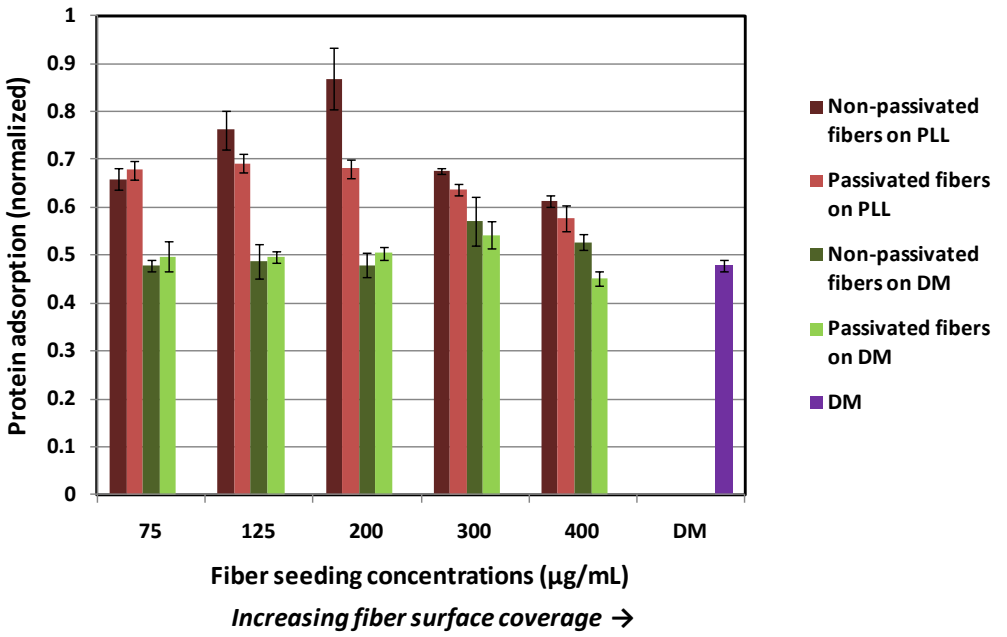

FIGURE 5.1. Protein adsorption – Passivated vs. non-passivated fiber surfaces. Surfaces were seeded at a range of concentrations (75, 120, 200, 300 or 400 µg/mL per PLL-coated well), with higher fiber density correlated with higher seeding concentration, using electrospun 41.2 wt% solutions of 10:4 dex:PAA compositions. Fibers were either passivated or unmodified (non-passivated). Background substrates were either passivated (DM monolayer attached) or unmodified (adhesive PLL). Protein adsorption was performed using FITC-BSA (concentration of 500 µg/mL in PBS - 500 µL/well). Error bars: standard error.

Comparing passivated vs. non-passivated fibers, protein adsorption levels were similar on DM background or PLL backgrounds. An exception, however, occurred at a seeding concentration of 200 µg/mL, at which more protein adsorbed to the surface with non-passivated fibers.

These results indicate that fibers do not adsorb BSA at higher levels than a typically accepted low-fouling surface (DM). In addition, protein adsorption levels correspond to the amount of "adhesive" background substrate (PLL) available for BSA adsorption.

Next, protein adsorption was measured on surfaces coated with passivated fibers of varying dex:PAA composition. Figure 5.2 shows results of protein adsorption on mesh morphology fibers with either PLL or DM background, while 5.3 shows results on a bristly morphology. As is expected, in general, in terms of background substrate, fibers attached with PLL background results in higher levels of protein adsorption vs. DM background (regardless of bristly or mesh morphology).

In terms of dex:PAA fiber composition, by looking at protein adsorption on fibers attached on DM background, the adsorption levels of the fibers themselves can be compared (since DM background is minimum). In general, all fibers had protein adsorption levels comparable to DM. However, in Figure 5.2, dex:PAA compositions from 10:1 to 10:6 shows significantly less protein adsorption than dex:PAA compositions 10:16 (and 10:50).

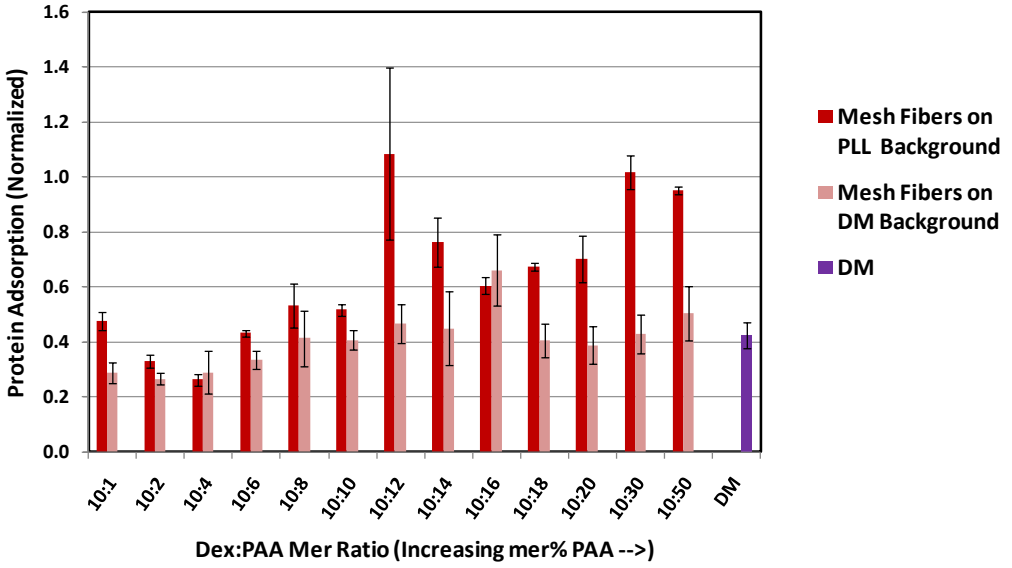

FIGURE 5.2. Protein adsorption – Passivated mesh fiber surfaces, PLL or DM background.

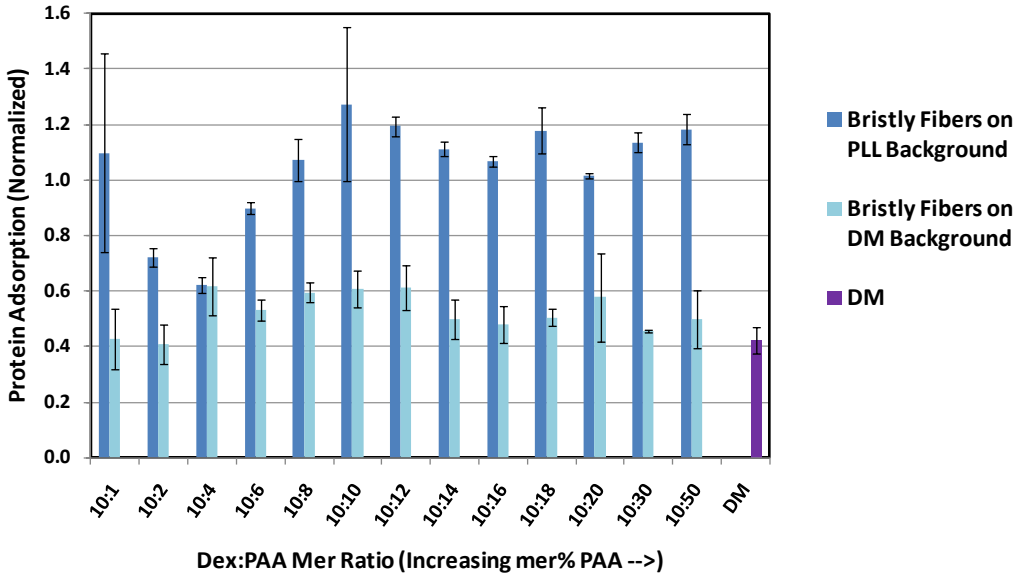

FIGURE 5.3. Protein adsorption – Passivated bristly fiber surfaces, PLL or DM background.

Next, by comparing bristly versus mesh morphologies, on an adhesive PLL background, it is possible to determine how much influence fiber surface coverage influences overall protein adsorption. It has already been established

that mesh morphology results in a higher fibrous surface density / coverage of the underlying surface (see Chapter 3). As shown in Figure 5.4, for all dex:PAA fiber compositions, all mesh surfaces have lower protein adsorption than bristly; this indicates that fibers attached to the surface prevent protein adsorption on the underlying substrate.

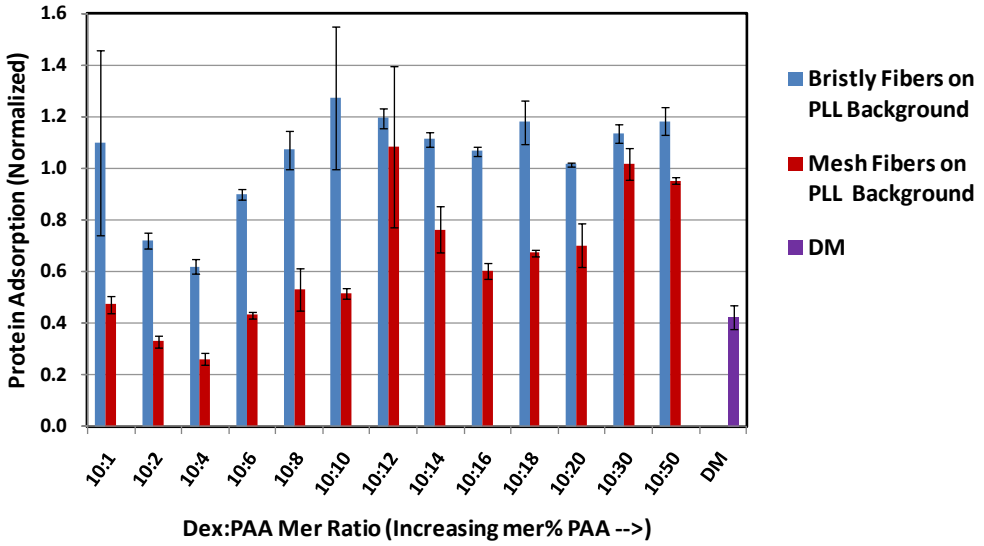

FIGURE 5.4. Protein adsorption – Bristly vs. mesh fiber surfaces, passivated.

In addition, compared to DM substrate, some fiber mesh surfaces still have higher protein adsorption. Since protein adsorption is similar between dex:PAA compositions, this indicates that at increasing mer% PAA, there is less fibrous surface coverage of the underlying substrate allowing for increased protein adsorption if the substrate is adhesive. These results indicate that a mesh-like fibrous topography effectively prevents protein adsorption.

3.2 Cell adhesion

Protein adsorption is a primary indicator of whether a surface is biologically adhesive / fouling. However, the main reason protein adsorption is

important is because if proteins adsorb, this provides a nice substrate for cells to adhere and proliferate. While low protein adsorption is a good first indicator of a cell-resistant surface, cells may still freely grow on the surface, or still be inhibited.

In this work, both fibroblasts and endothelial cells were cultured on dex-PAA fibrous surfaces to determine their adhesive nature to this different cell types. Since the mesh topography, versus bristly, resulted in lower protein adsorption, mesh topography was also utilized in cell adhesion assays. As shown in Figure 5.5, endothelial cells had a lot of trouble growing on surfaces with dex:PAA compositions between 10:2 to 10:6 mer ratios.

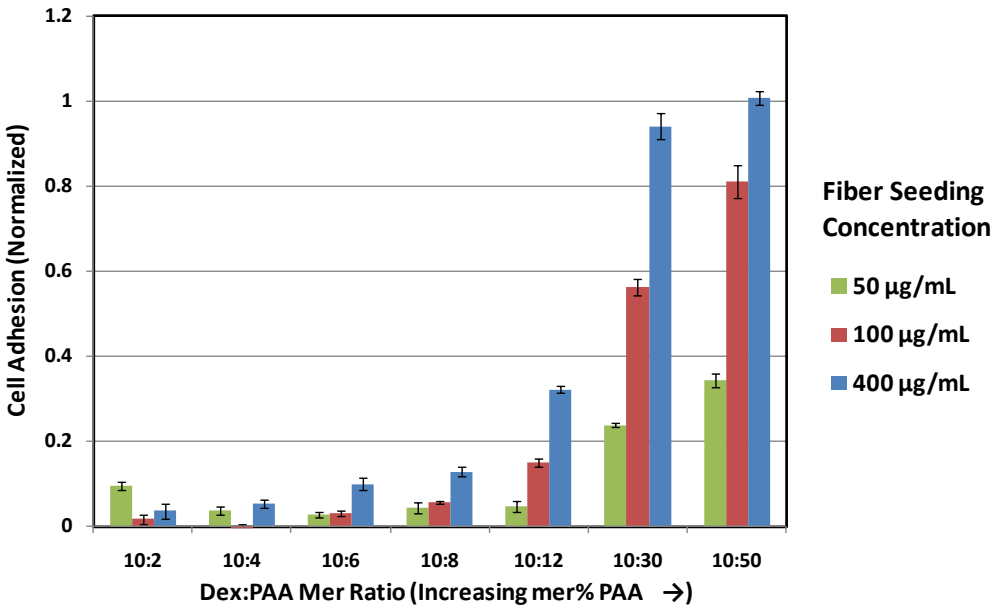

FIGURE 5.5. Cell adhesion (BECs) on "non-fouling" fiber-coated surfaces. Passivated fibers on DM background, and increasing mer% PAA.

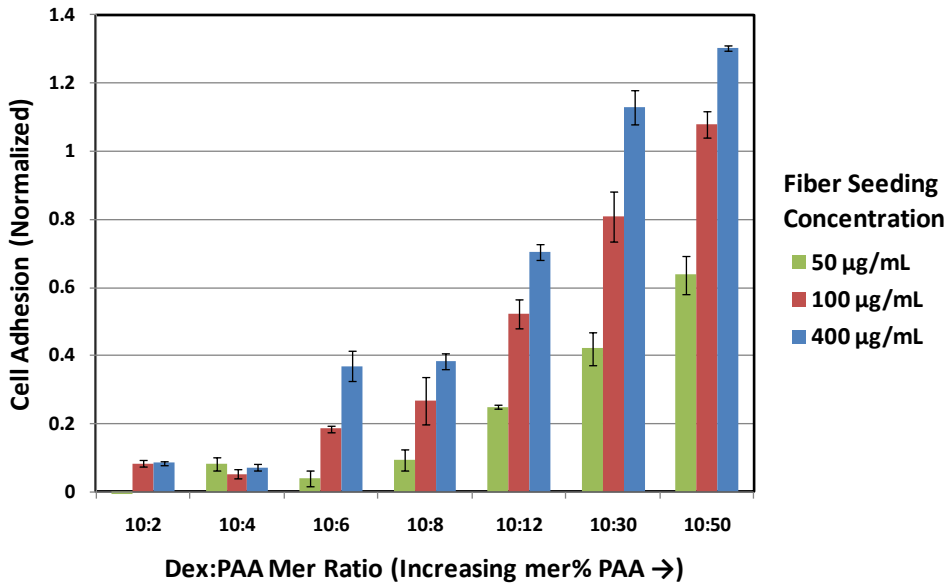

FIGURE 5.6. Cell adhesion (3T3s) on "non-fouling" fiber-coated surfaces. Passivated fibers on DM background, and increasing mer% PAA.

4. Conclusions

This work shows that dex-PAA surfaces can be created with functionality comparable to DM, an already well-accepted low-fouling surface. In addition, as shown by cell adhesion assays, these surfaces are also more cell-repellant dependant on fiber topography. Even when the background surface is protein adhesive, the overlying fibrous topography still prevents cells from proliferating by minimizing the available underlying surface area to which cells can adhere. Depending on the specific surface topography, BECs vs. fibroblasts proliferate more or less easily on a given surface. As a result, a fibrous topography is generated that effectively resists cell adhesion.

CHAPTER 6

Bioactive fibrous surface coatings –

Modified cellular interaction

Abstract

In this work, cell adhesion properties are modulated through surface topography and surface chemistry utilizing nano- and micro- fibrous coatings comprised of dextran/polyacrylic acid (dex/PAA) fibers. Since the fibrous nature of dex-PAA fibers is similar to native ECM, fibers can be modified to display bioactive peptides for cell adhesion, and dex-PAA cross-linking modulates fiber mechanical properties, the capability of these surfaces to function as an ECM-mimetic cellular scaffolding material was evaluated

The ECM-mimetic properties of dex-PAA fibrous surfaces was assessed by *in vitro* cell culture experiments, exposing physiologically relevant cells (3T3 fibroblasts, endothelial cells and smooth muscle cells) to dex-PAA fibrous surfaces with a range of topographies and surface chemistries. Fibers were either bioactively modified with the fibronectin-derived peptide –GRGDSP, or passivated to inhibit cell adhesion to fibers. Additionally, the background substrate was differentially modified from fibers to be cell-adhesive (poly-L-lysine coating) or minimally cell adhesive (dextran monolayer coating). Cellular response was characterized in terms of cell adhesion and proliferation, as well as morphology. Results are compared with cell culture experiments performed on non-fibrous (“flat”), PLL control surfaces.

1. Introduction

The ability to fine-tune and control cellular adhesion, migration, and differentiation in a predictable manner will play an important role in revolutionizing the effectiveness of biomedical devices and open the doors for the development of new applications yet to be realized. In particular, the manner in which different cell types respond to different mechanical stimuli and biochemical cues is a challenging area of biomaterials development where major advancements are needed. Here, three cell types are tested on a variety of dex-PAA fiber scaffolds. These scaffolds are designed to have morphological characteristics similar to that found in native biological structures (e.g. extracellular matric) and chemical properties tuned to differentially promote or inhibit cell adhesion.

2. Experimental

2.1 Materials

Dextran from *Leuconostoc mesenteroides* (M_w 64k-76k) was purchased from Sigma (St. Louis, MO). Poly(acrylic acid) (M_w ~90k, 25% aqueous solution) was purchased from Polysciences, Inc. (Warrington, PA). Fluorescein dextran (FITC-dex, 70k MW, anionic) was purchased from Invitrogen (Carlsbad, CA). N-(3-Dimethylaminopropyl)-N′-ethylcarbodiimide hydrochloride (EDC), N-hydroxysuccinimide (NHS), and 2-(*N*-morpholino)ethanesulfonic acid (MES) hydrate were purchased from Sigma.

2.2 Electrospinning, cross-linking and fragmentation of dex-PAA hydrogel fibers

Electrospinning solution preparation. Solutions were prepared for electrospinning by dissolving dextran and/or poly(acrylic acid) polymer in DI water and stirring overnight. Dex-PAA solutions were prepared varying in concentration between 37.5 to 47.4 wt% polymer, comprised of dex:PAA solutions with mer ratio varying between 10:1 (10%) and 3:10 (300%), using ~70k dextran and ~90k PAA.

Electrospinning. Electrospinning was performed following the general procedure of Zong et al [91]. Briefly, a polymer solution was prepared by dissolving dextran and PAA in DI water and stirring overnight for thorough mixing. The polymer solution was loaded into a syringe and delivered out a stainless steel capillary with an inner diameter of 0.03" using a programmable syringe pump (Harvard Apparatus PHD 2000) at a constant flow rate of 10 µL/min. A voltage of 25kV was applied to the capillary tip and electrospinning solution using a high-voltage power supply (Glassman High Voltage, Inc). Electrospun fibers were collected on a grounded aluminum foil target located 15 cm from the tip. Room humidity was maintained between 14-17%. After electrospinning, fibers were dried under vacuum overnight. To make fluorescent dex-PAA fibers, electrospinning solutions were modified by substituting ~0.4 wt% dextran polymer with 70k FITC-dex.

Thermal cross-linking. Dex-PAA fibers were cross-linked using a thermal dehydration reaction based on the general procedure of Chen and Hsieh [92], in which dry electrospun fibers are incubated in a vacuum oven for 1 hour at 180°C. Thermal cross-linking was performed on electrospun fibers comprised of varying

dex:PAA mer ratios. While untreated fibers completely dissolve in water, thermally cross-linked dex-PAA fibers maintain a fibrous structure and swell to form hydrogel fibers.

Fiber fragmentation. Hydrogel dex-PAA fibers were fragmented into short fiber "bristles" via sonication. In this procedure, electrospun and thermally cross-linked dex-PAA fiber mats were immersed in DI water and swelled to form long hydrogel fibers. A sonicator probe was applied to the fiber solution at a setting of 4 (using a Misonix Ultrasonic Cell Disruptor), thereby subjecting the fibers to high shearing forces and fragmenting them into short hydrogel "bristles." Sonication fragmentation was performed on dex-PAA fibers electrospun over a range of dex:PAA mer ratios (10:1 to 10:30) and solution concentrations (37.5 to 47.4 polymer wt%) for 30 seconds.

Solutions of specific bristle concentration (mg/mL) were prepared by immersing a measured weight of fiber mat into a given volume of DI water prior to sonication. This fibrous solution was then diluted down to specific concentrations, which is the "fiber seeding density" used for fiber bristle attachment to surfaces.

2.3 Fabrication of bioactive surfaces

To assess cellular interaction with dex-PAA fiber-coated surfaces, a variety of surfaces were made to exhibit a wide range of surface topographies and chemistries.

Topographical variation. Topography was varied in terms of (1) surface density, (2) feature size and (3) bristly / mesh morphology. *To modify*

morphology, a solution of fragmented dex-PAA fibers was allowed to "settle over time" and adhere to PLL-coated wells, resulting in a "bristly" morphology after rinsing off excess fibers. Once a "bristly" surface was made, it could then be converted into a "mesh" morphology by drying the surface under vacuum overnight. *To modify feature size*, dex-PAA fibers of different diameter were attached to surfaces. A range of diameters were obtained by electrospinning dex-PAA solutions (10:4 dex:PAA) prepared over a range of solution concentrations (37.5 to 47.4 polymer wt%). *To modify surface density*, the amount of attached fiber was varied by using a range of fiber seeding concentrations (5, 10, 25, 50, 100, 400 $\mu g/cm^2$), resulting in either a low or high surface density of attached fibers.

Surface chemistry variation. Surface chemistry was varied such that (1) fiber chemistry was differentially modified from the (2) background substrate chemistry.

In terms of fiber chemistry, fibers were modified to display either –OH (passivated) or a cell-adhesive peptide (-RGD). In this work, –COOH groups of electrospun, cross-linked dex-PAA fibers are utilized for modification. *To passivate fibers*, electronegative -COOH groups were converted to neutral –OH groups. Briefly, fiber-coated surfaces were incubated with 0.1M ethanolamine / 30mM EDC / 8mM NHS in 50 mM MES buffer (pH=6) overnight, then rinsed thoroughly with DI water. *To functionalize fibers with –RGD peptide*, fibers were first incubated with 30mM EDC / 8mM NHS in 50mM MES buffer (pH=6) for 30 minutes, then rinsed with MES buffer. This converts fiber –COOH groups to

active NHS esters to which amine-containing molecules can attach. Next, surfaces were incubated with solutions of –RGD in 0.1M NaP buffer (pH=7.5) for 2 hours. This covalently attaches –RGD to the fibers via amide bond formation. Last, RGD-modified fiber surfaces were incubated overnight with 0.1M ethanolamine in 0.05 MES buffer (pH=6) to passivate (convert to –OH) any remaining activated esters.

In terms of background substrate chemistry, backgrounds were modified to display either adhesive poly-L-lysine (PLL) or a generally non-adhesive dextran monolayer (DM). For a PLL background, PLL is already present as the substrate for fiber attachment. For a DM background, a dextran coating is applied *after* fibers have been attached. In this chemistry, each well is incubated with 10 mg/ml oxidized dextran (ox-dex) in 0.1M phosphate buffer (pH=10) overnight. In this step, ox-dex adsorbs to PLL and forms a Schiff base. Next, the ox-dex solution is removed and 0.1M $NaBH_4$ is added to each well, incubated 2 hours, then rinsed 3x with DI water. In this step, the Schiff base is reduced to a covalent amide bond to form a homogeneous dextran monolayer. Plates were stored in DI water until used.

2.4 RGD-modified fibrous surfaces

–RGD density on a fiber-coated surface was modified by either: (1) varying the local -RGD density on fibers or (2) varying the total –RGD surface density on fiber-coated surfaces. To modify the amount of –RGD attached to fibers, a range of –RGD concentrations (1, 10, 50, 100, 250 and 500 μg/mL) was used to functionalize a fiber-coated surface. To modify the overall –RGD surface

density, -RGD was attached to surfaces made over a range of fiber seeding concentrations (5, 10, 25, 50, 100, 400 μg/cm^2), using fibers electrospun over a range of electrospinning solution concentrations (37.5 to 47.4 polymer wt%, @ 10:4 dex:PAA mer ratio) to vary fiber diameter. The peptide –RADSP, rather than –RGD, was also attached to fiber-coated surfaces (@ 500 μg/mL) to serve as a non-specific control peptide.

For all RGD-functionalized fibrous surfaces, the background substrate was modified with a passivated DM to isolate observations of the cellular interaction with RGD-modified fibers.

2.5 Cell proliferation

To determine amount of cell proliferation on fiber-coated surfaces, a cell proliferation assay was performed using a CyQUANT NF Cell Proliferation Assay Kit (Invitrogen, C35006). This assay is based on measuring cellular DNA content via fluorescent dye binding, which is closely proportionate to actual cell number.

2.6 Microscopy – Epiflouorescence imaging

Fluorescence imaging was performed using an inverted fluorescence microscope (Leica Microsystems) on fiber-coated surfaces cultured with 3T3, BEC or SMC cells. Fibers were fluorescently labeled using FITC-dextran in the electrospinning solution, while the actin cytoskeleton and cell nucleus of cells was fluorescently stained using rhodamine-phalloidin (AlexaFluor568 from Invitrogen) and DAPI (4',6-diamidino-2-phenylindole, dihydrochloride). While

rhodamine-phalloidin emits red fluorescence after binding F-actin, DAPI emits blue fluorescence after binding AT regions of DNA.

3. Results and Discussion

3.1 Cell culture on bristly vs. mesh topography

The influence of mesh vs. bristly morphology was explored for cellular interaction with fiber-coated surfaces. Mesh and bristly surface topographies were fabricated, which also varied in (1) range of fiber diameters / feature size and (2) surface density. An adhesive poly-L-lysine surface served as the "background" underlying immobilized fibers. These surfaces were used as culture substrates for bovine aortic endothelial cells (BAECs).

On the flat, PLL control surface (Figure 6.1), endothelial cells exhibited a well-developed actin cytoskeleton, reaching confluency and displaying a characteristic cobblestone appearance. These characteristics were disrupted on bristly and mesh fiber-coated surfaces.

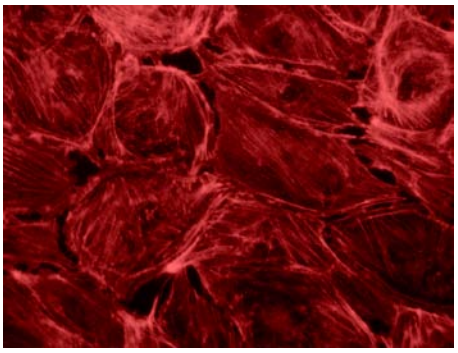

FIGURE 6.1. Endothelial cells cultured on flat PLL surface, control. Bovine aortic endothelial cells (BAECs) were cultured for 4 days on a PLL-treated surfaces. Cells were formaldehyde-fixed and actin cytoskeleton stained with phalloidin-AlexaFluor568, then wide-field epifluorescence micrographs taken using an inverted fluorescence microscope, 40x objective. Image is188µm x 141 µm (W x H).

Bristly surfaces showed a greater number of adherent cells than mesh surfaces (Figure 6.2). Since fibers are generally non-adhesive to cells, this effect can be attributed to a larger amount of adhesive (PLL) background substrate remaining accessible to cells on bristly surfaces.

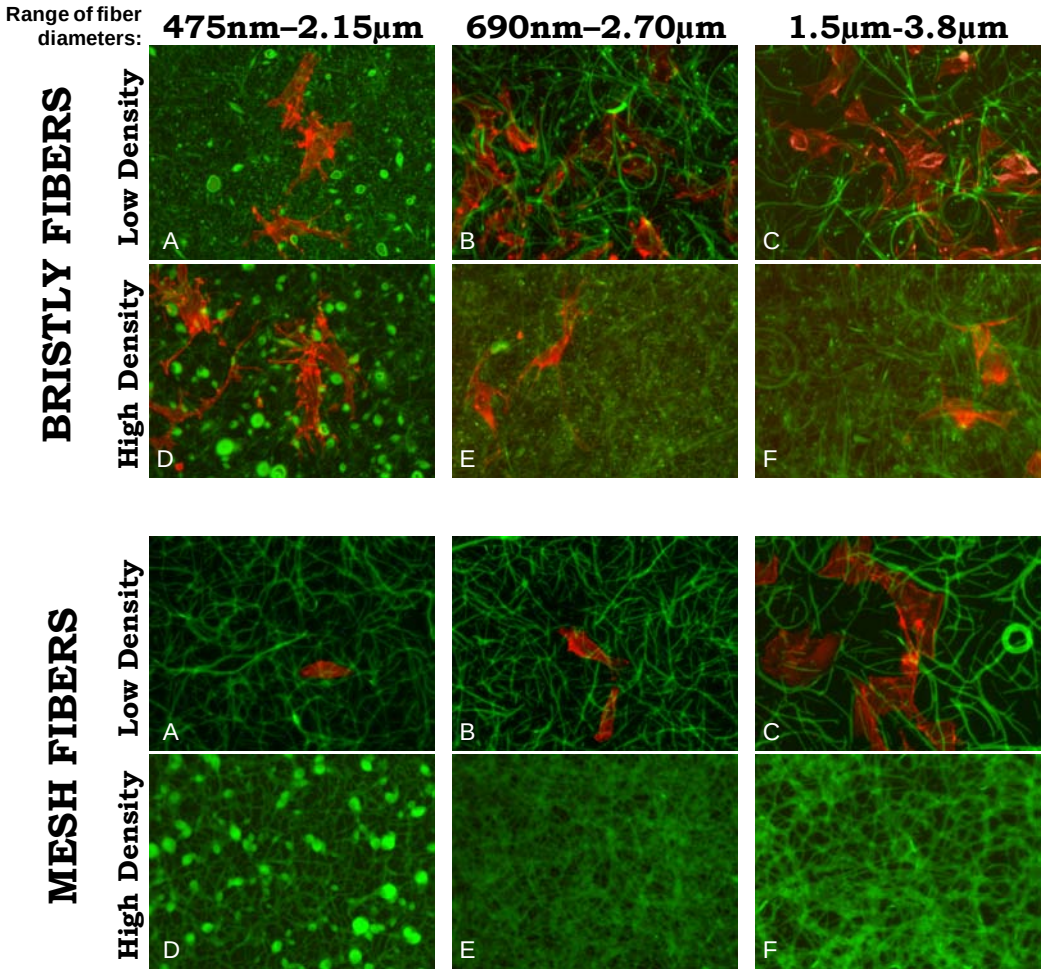

FIGURE 6.2. Endothelial cells cultured on "bristly" or "mesh" fiber-coated surfaces. Bovine aortic endothelial cells (BAECs) were cultured for 4 days on fibers immobilized on PLL-treated surfaces. Fibers were immobilized at low or high density, in either a "bristly" or "mesh" morphology, and using fibers with a range of nano- and micro- diameters [fibers generated using electrospinning polymer concentrations: 37.5 wt% (left column), 41.2 wt% (middle column) and 45.9 wt% (right column)]. Cells were formaldehyde-fixed and actin cytoskeleton stained with phalloidin-AlexaFluor568, then wide-field epi-fluorescence micrographs taken using an inverted fluorescence microscope, 40x objective. Images are 188µm x 141 µm (W x H).

Mesh surfaces, in contrast, tend to shield the background substrate from adherent cells. In general, endothelial cell adhesion was the most restricted on high density mesh surfaces (Figure 6.2, 4th row). During microscopic imaging, no cells could be located on high density mesh surfaces. Fibers effectively prevented cells from reaching and attaching anywhere to the underlying PLL substrate.

On low density mesh surfaces, cells appeared to be able to traverse smaller diameter fibers. However, fiber interference restricted cells from becoming well-spread (Figure 6.2, 3rd row). Cells appeared unable to cross over thicker, larger diameter fibers (Figure 6.2, right column), such that the cell edge followed along the fiber path.

Bristly surfaces also modified cellular morphology. Endothelial cells on bristly surfaces did not spread evenly, but extended protruding processes throughout the fibrous network (Figure 6.2, 1st and 2nd row).

3.2 Cell culture on mesh topography

Although bristly surfaces showed interesting cellular interaction, mesh-like fiber morphology (1) more closely resembles native extracellular matrix (ECM), which is important for ECM-mimetic applications and (2) exhibited anti-cell adhesive properties, which is important for non-fouling applications.

In consideration of these factors, the influence between fiber-coated "mesh" surfaces and cells was explored for three physiologically relevant cell types: (1) endothelial cells (ECs), which line the interior surface of blood vessels (2) fibroblasts (3T3s), and (3) smooth muscle cells (SMCs), which comprise

blood vessel walls and are found in other various organs (lymphatic vessels, urinary bladder, uterus, etc).

3.2.1 Passivated (-OH) fibers w/ adhesive (PLL) background – varying fiber diameter and surface density

Mesh surface topographies were fabricated over a wide range of (1) fiber diameters / feature sizes and (2) surface densities. Surface density was varied via fiber seeding concentration (10 µg/mL to 400 µg/mL), while fiber diameter was varied by electrospinning 10:4 dex:PAA solutions over a range of concentrations (39.4 to 47.4 wt%). For surface chemistry, adhesive poly-L-lysine served as the "background" underlying immobilized fibers, while fibers were passivated (-COOH groups converted to –OH) with ethanolamine. These surfaces were used as culture substrates for 3T3s, SMCs and ECs.

Figure 6.3 shows the relative number of cells measured on each surface topography after 5 days of culture. For all cell types, cell proliferation was most inhibited on high density fibrous surfaces (seeding conc. = 400 µg/mL). As fibrous surface density decreased, cell proliferation increased for all cell types. These effects can be attributed to the relative amount of adhesive background substrate to which cells could adhere.

In terms of fiber diameter, differences in cell proliferation become apparent at lower surface densities. For example, as shown in Figure 6.3, for all cell types, at a seeding concentration of 10 µg/mL, cell proliferation is higher on surfaces coated with large diameter fibers versus small diameter fibers. However, as shown in Figure 6.5(A-C), differences in cellular interaction with fibers of

varying diameter is more clearly illustrated looking at fluorescence images of cells cultured on surfaces, and comparing them to cells cultured on a flat substrate (Figure. 6.4).

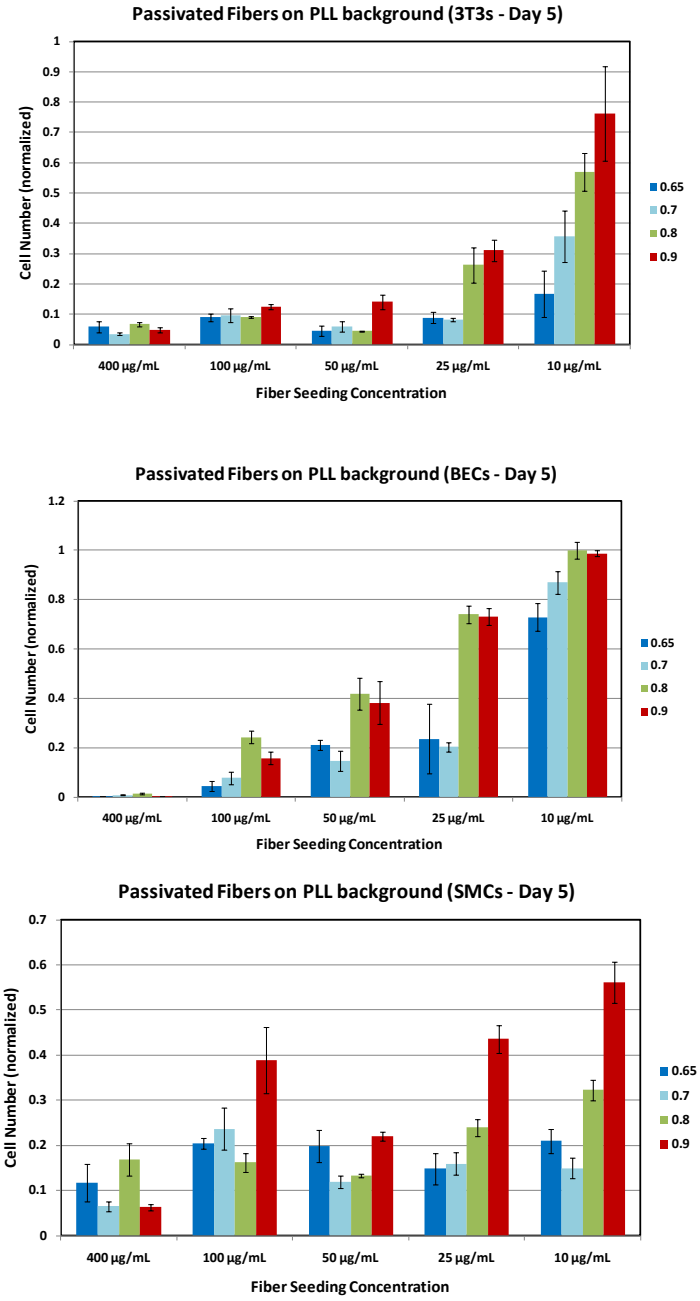

FIGURE 6.3. 3T3, BEC and SMC cell proliferation on passivated "mesh" fibers on adhesive background – varied fiber diameter and surface density. Cell number is normalized versus flat PLL surfaces. Error bars: standard error.

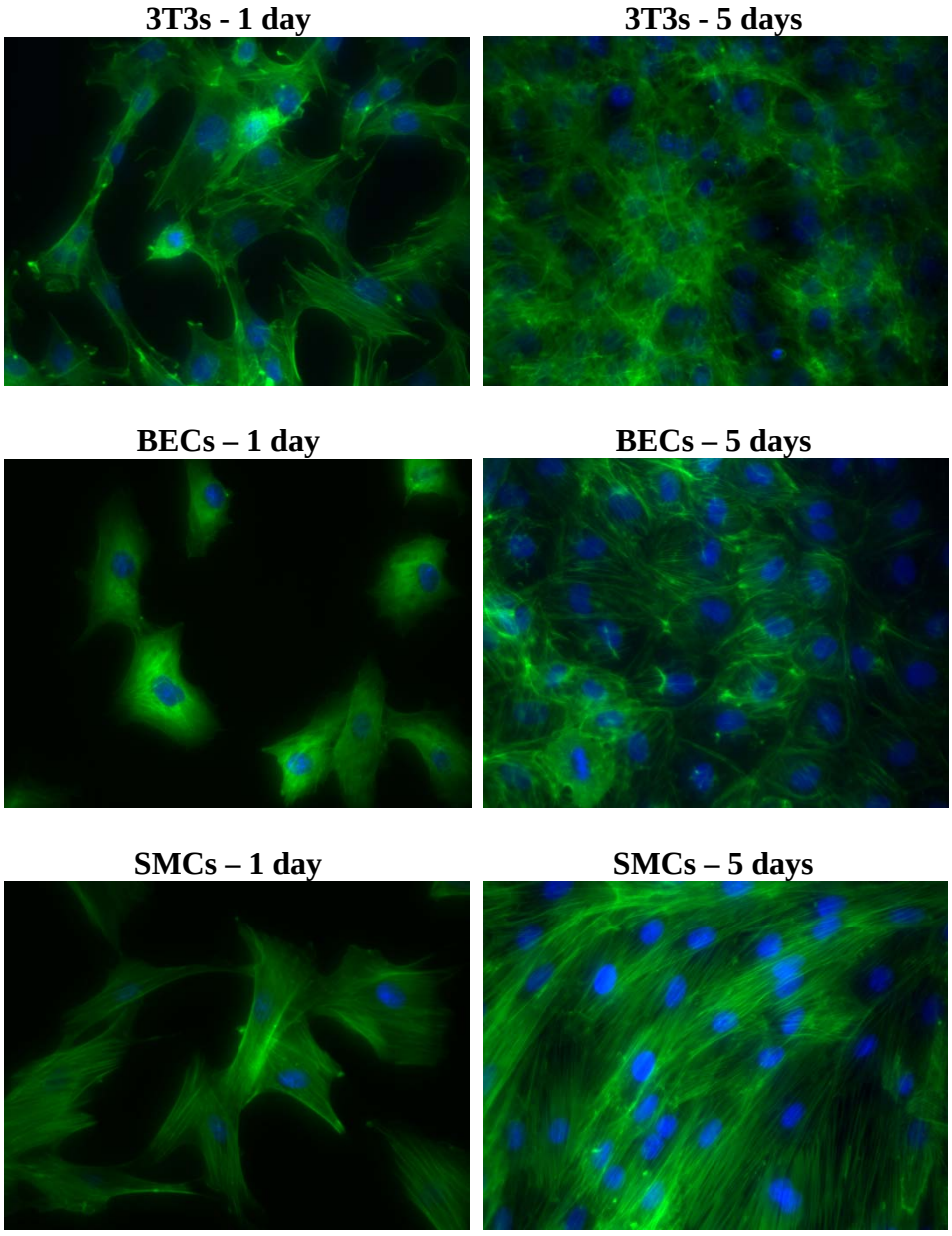

FIGURE 6.4. Imaging of 3T3, BEC and SMC cell culture on PLL-coated, flat control surfaces. Characteristic morphologies of 3T3, BECs and SMCs are displayed in the images above. Morphology associated with cell spreading is clearly seen on day 1, while morphology of confluent cells are observed on day 5. 3T3s extend long processes and crawl over each other, while BECs remain more round and form a cobblestone-like monolayer at confluency. SMCs tend to elongate unidirectionally while spreading, as shown by actin-staining, and appear relatively aligned at confluency. Actin cytoskeleton is stained with phalloidin-AlexaFluor568 and nucleus via DAPI, then wide-field epi-fluorescence micrographs taken using an inverted fluorescence microscope, 40x objective. Images are false-colored: actin – green, and nucleus – blue. Images are 188μm x 141 μm (W x H).

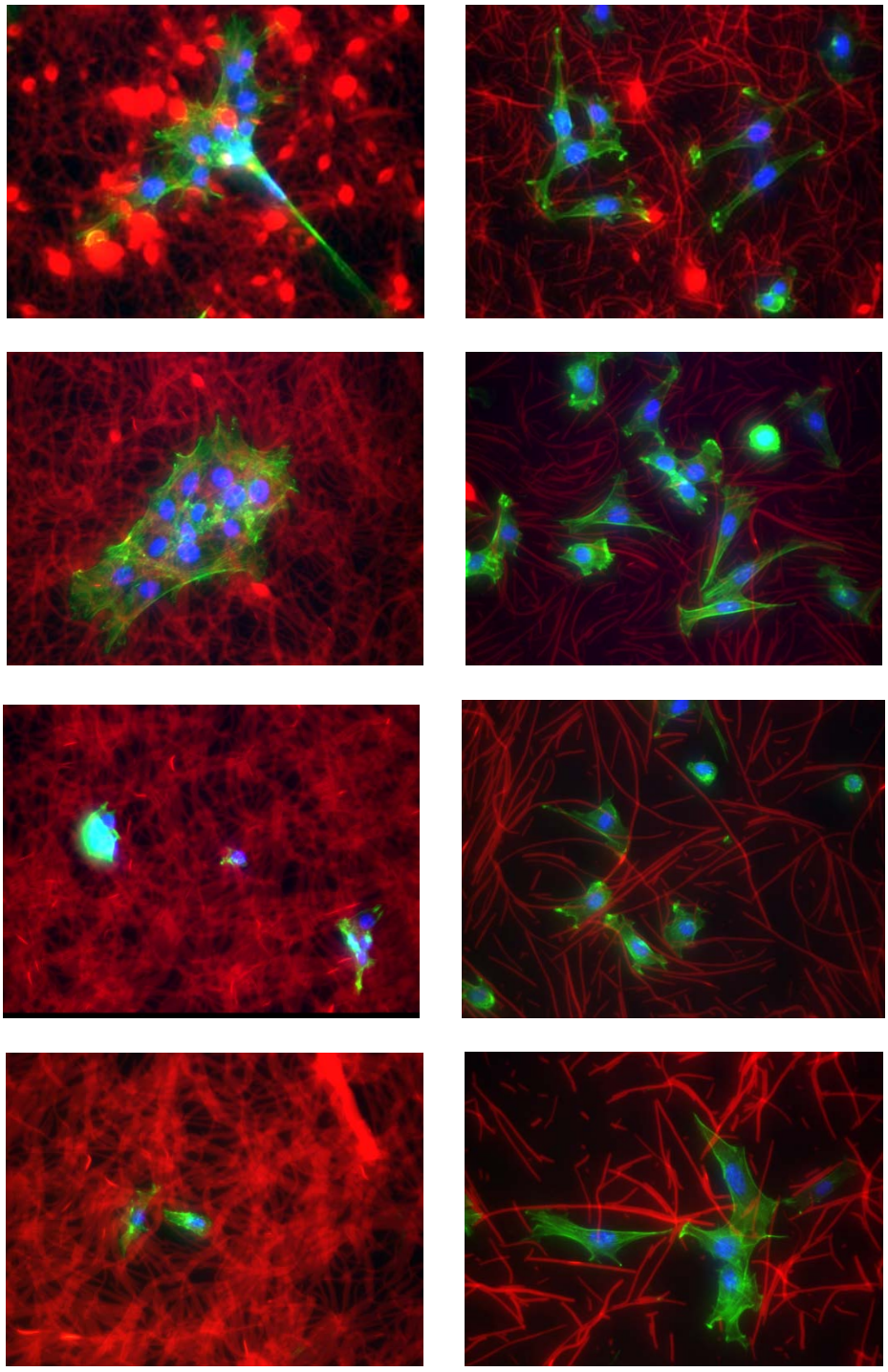

FIGURE 6.5A. 3T3s cultured on passivated "mesh" fibers on adhesive background – varied fiber diameter and surface density. 3T3s were cultured 5 days on high surface density (left column, seeded @ 400 µg/mL) or a low surface density (right column, seeded @ 25 µg/mL). Fiber diameter ranged from nano-fibrous to micro-fibrous (increasing from 1st row to 4th row). Images are false-colored: Fibers – red, actin – green, and nucleus – blue. Inverted fluorescence microscope, 40x objective. Images are 188µm x 141 µm (W x H).

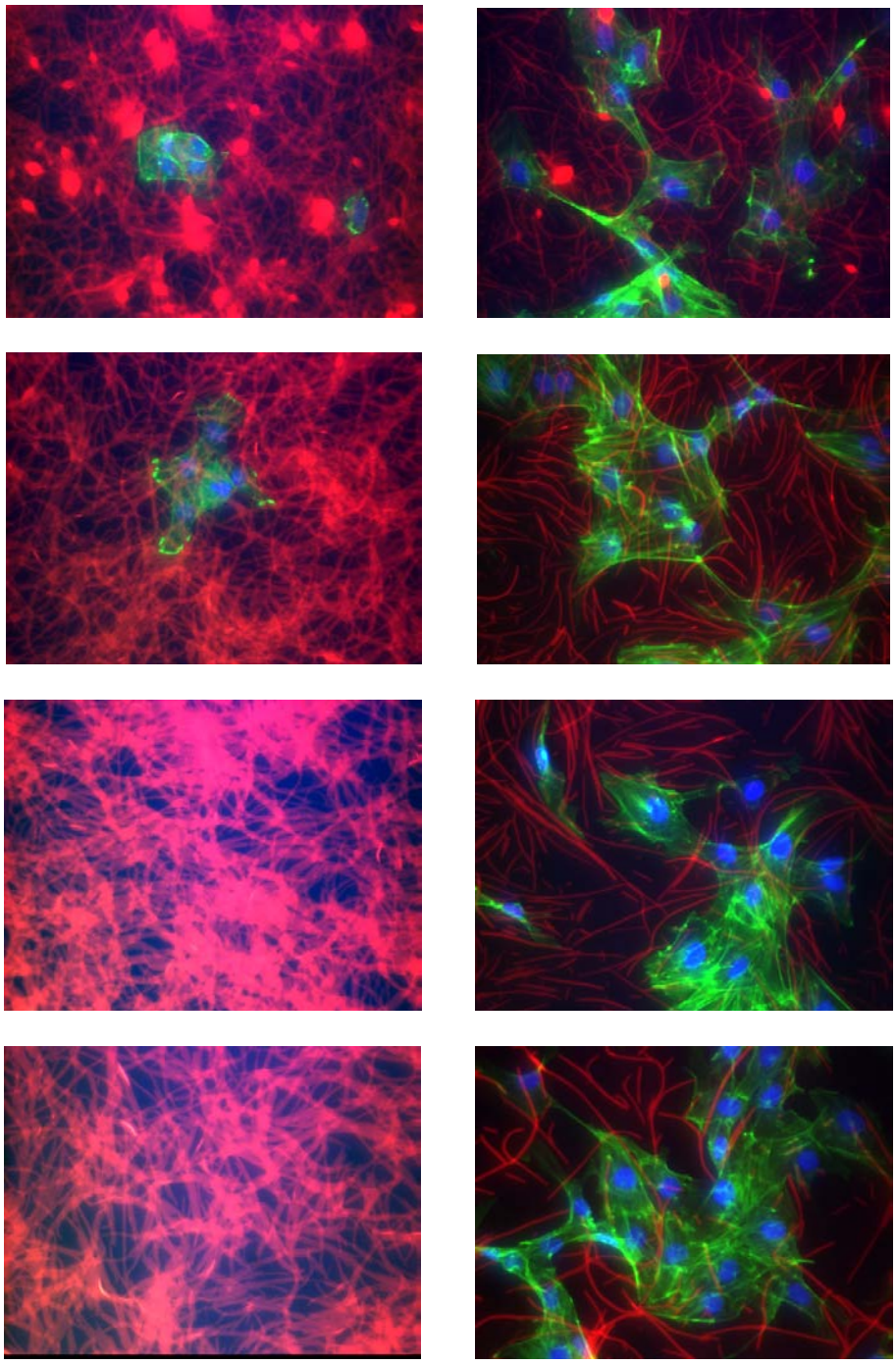

FIGURE 6.5B. BECs cultured on passivated "mesh" fibers on adhesive background – varied fiber diameter and surface density. BECs were cultured 5 days on high surface density (left column, seeded @ 400 µg/mL) or a low surface density (right column, seeded @ 25 µg/mL). Fiber diameter ranged from nano-fibrous to micro-fibrous (increasing from 1st row to 4th row). Images are false-colored: Fibers – red, actin – green, and nucleus – blue. Inverted fluorescence microscope, 40x objective. Images are 188µm x 141 µm (W x H).

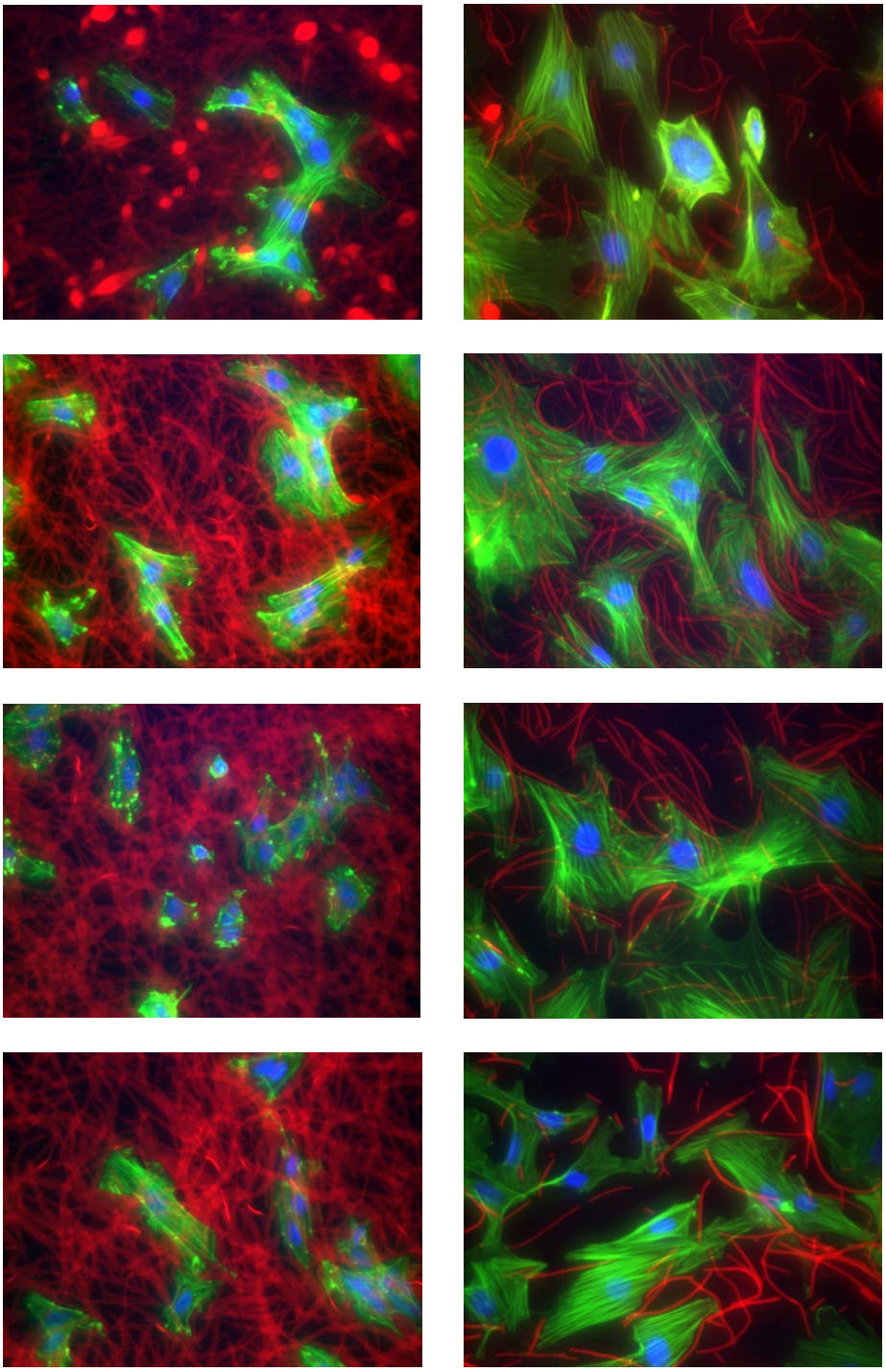

FIGURE 6.5C. SMCs cultured on passivated "mesh" fibers on adhesive background – varied fiber diameter and surface density. SMCs were cultured 5 days on high surface density (left column, seeded @ 400 µg/mL) or a low surface density (right column, seeded @ 25 µg/mL). Fiber diameter ranged from nano-fibrous to micro-fibrous (increasing from 1st row to 4th row). Images are false-colored: Fibers – red, actin – green, and nucleus – blue. Inverted fluorescence microscope, 40x objective. Images are 188µm x 141 µm (W x H).

3.2.1 Passivated (-OH) fibers w/ adhesive (PLL) background – varying fiber composition (dex:PAA ratio) and surface density

Mesh surface topographies were fabricated over a wide range of (1) fiber compositions and (2) surface densities. Surface density was varied via fiber seeding concentration (5 µg/mL to 400 µg/mL), while composition was varied by electrospinning dex:PAA solutions over a range of dex:PAA mer ratios (10:2 to 10:50). For surface chemistry, adhesive poly-L-lysine served as the "background" underlying immobilized fibers, while fibers were passivated (-COOH groups converted to –OH) with ethanolamine. These surfaces were used as culture substrates for 3T3s, SMCs and ECs.

Figures 6.6, 6.7 and 6.8 show the relative number of cells measured for each surface topography after 1 and 3 (or 4) days of culture. 4 days of cell culture was used for BECs since their growth rate is slower than either SMCs or 3T3s.

For all cell types, regardless of dex:PAA composition, cell proliferation was most inhibited on high density fibrous surfaces (seeding conc. = 400 µg/mL) by Day 3 & 4. As fibrous surface density decreased, cell proliferation increased for BECs (Figure 6.7, Day 4) and SMCs (Figure 6.8, Day 3), with BECs exemplifying this trend exceptionally well. In contrast, proliferation of 3T3s appears inhibited of fiber-coated surface independent of surface density or dex:PAA composition (Figure 6.6, Day 3), with only a few exceptions.

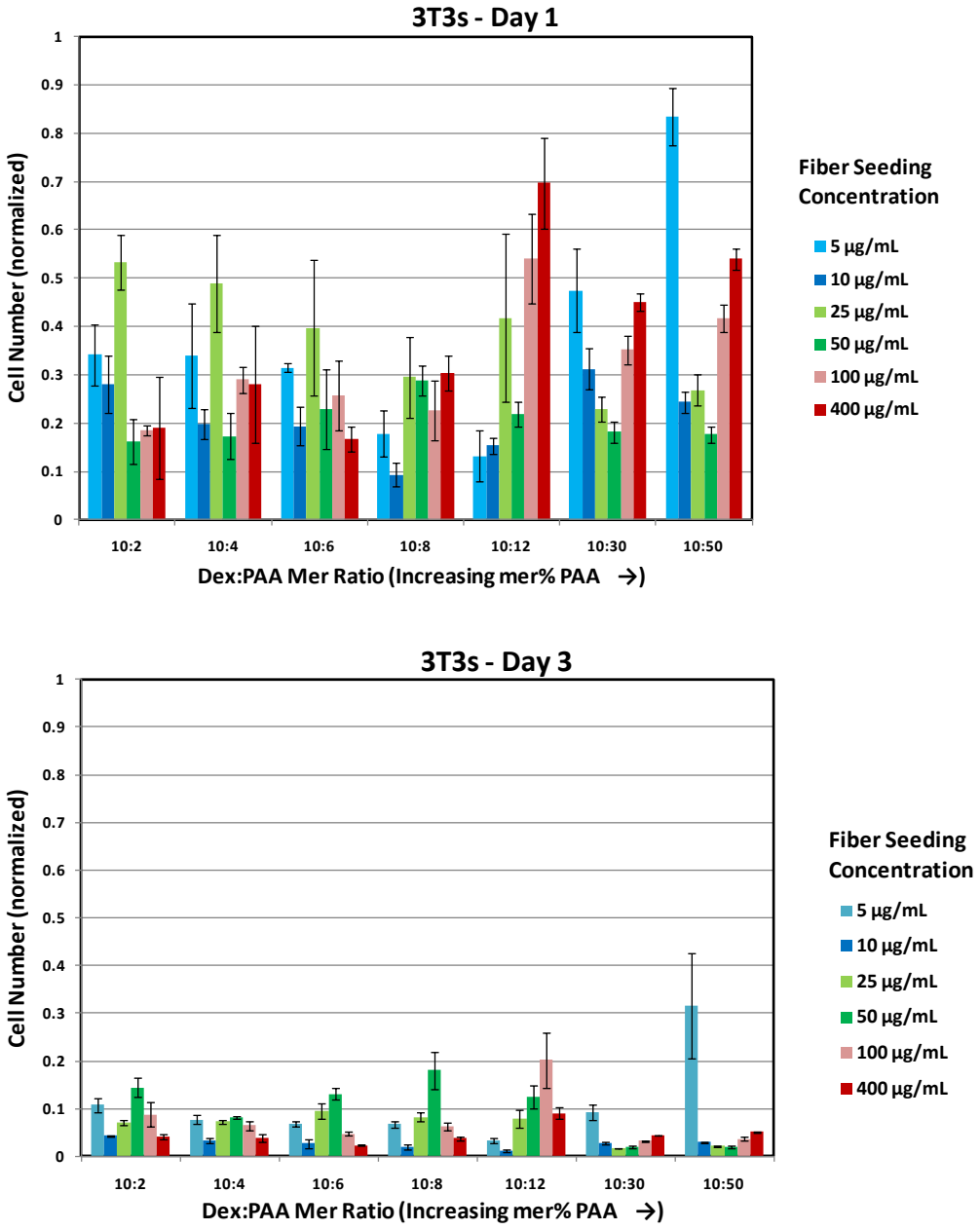

FIGURE 6.6. 3T3 cell proliferation on passivated fibers on adhesive (PLL) background, varying fiber composition (dex:PAA ratio) – 1 and 3 day. Cell number is normalized versus flat PLL surfaces. Error bars: standard error.

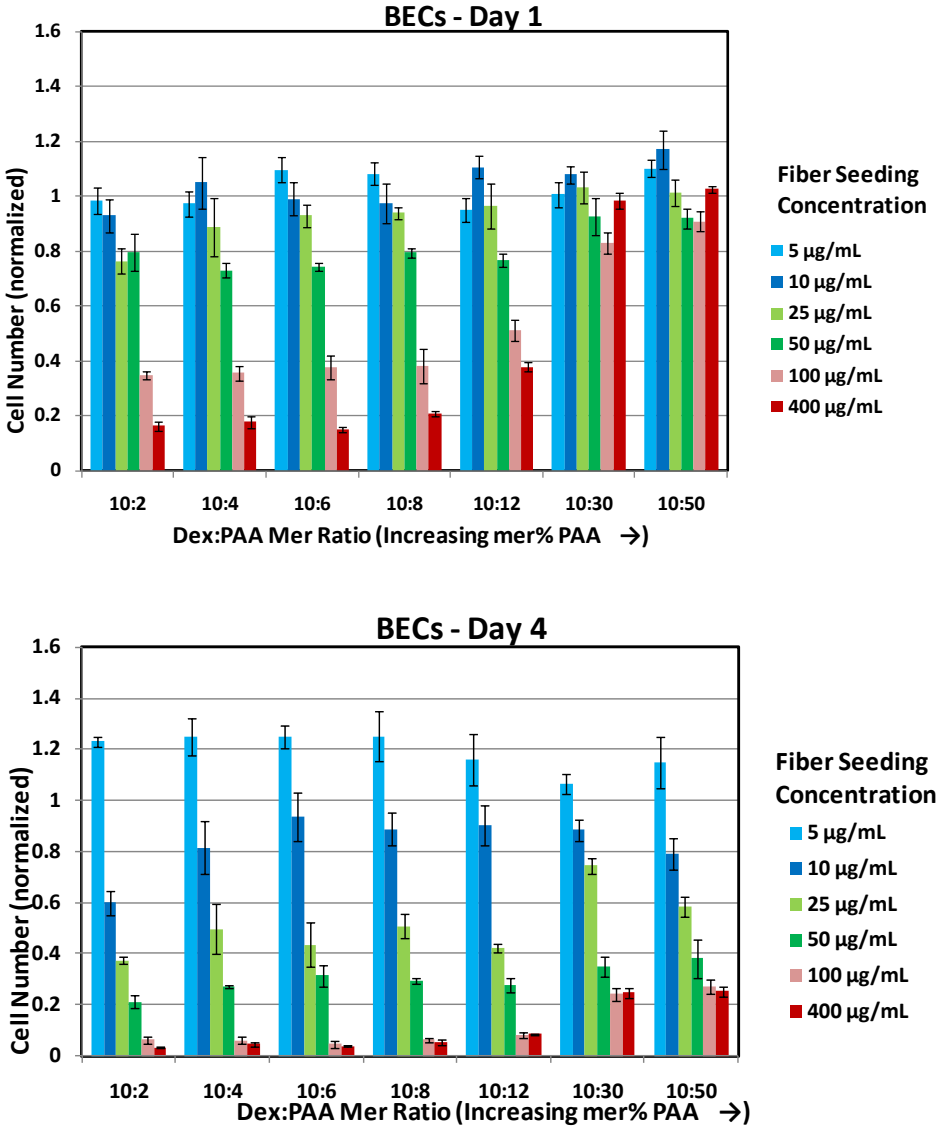

FIGURE 6.7. BEC proliferation on passivated fibers on adhesive (PLL) background, varying fiber composition (dex:PAA ratio) – 1 and 4 day. Cell number is normalized versus flat PLL surfaces. Error bars: standard error.

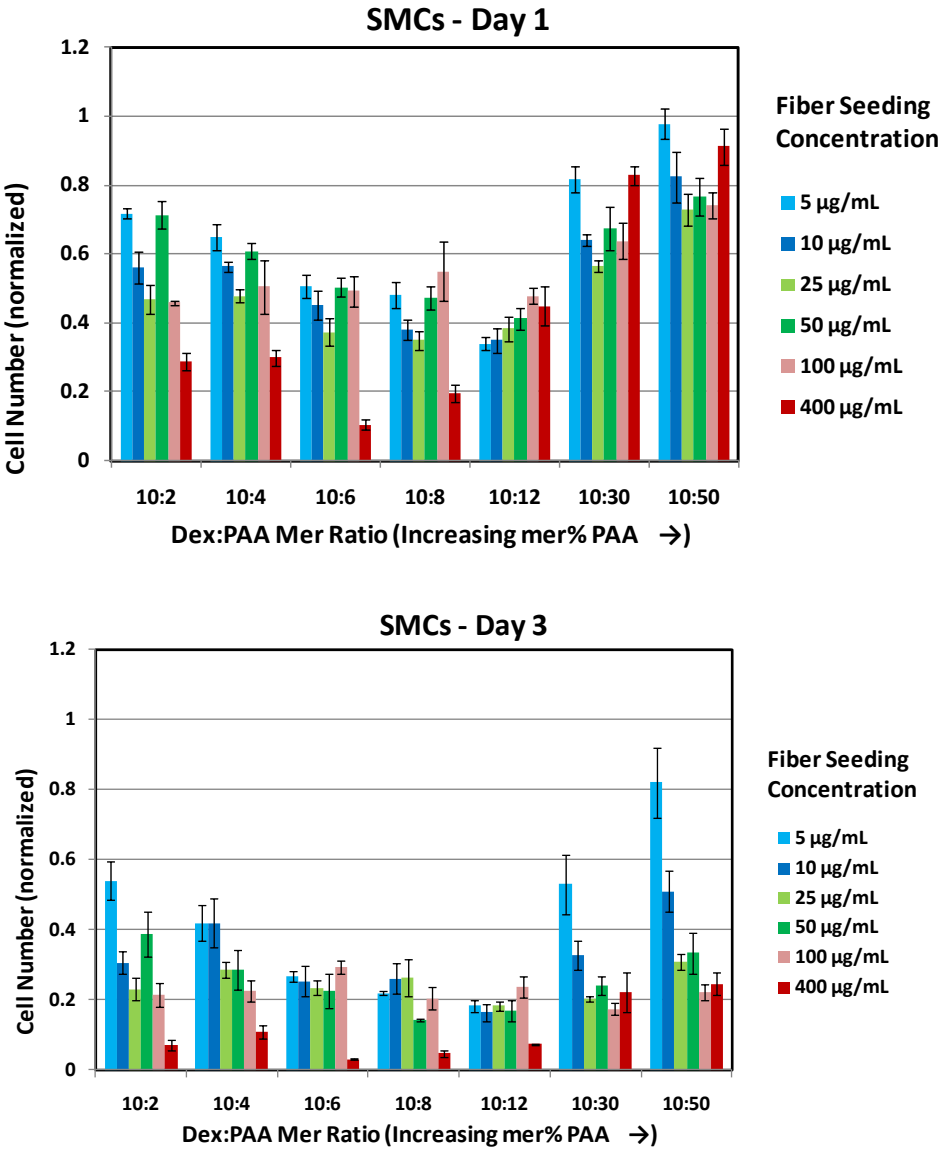

FIGURE 6.8. SMC proliferation on passivated fibers on adhesive (PLL) background, varying fiber composition (dex:PAA ratio) – 1 and 3 day. Cell number is normalized versus flat PLL surfaces. Error bars: standard error.

In terms of fiber composition, dex:PAA ratios ranging from 10:2 to 10:8 resulted in the least amount of cell proliferation at high fiber density (seeding @ 400 µg/mL). These compositions contain the least amount of PAA (relative to dextran), which is associated with lower cross-linking density as well as larger fiber diameters. Looking at the corresponding fluorescent images of SMCs

cultured for 3 days (images not shown), cells more readily traverse smaller diameter fibers (10:12, 10:30 and 10:50 dex:PAA) while larger diameter fibers (10:2, 10:4, 10:6 and 10:8) limit spreading.

3.3 Fabrication of RGD-functionalized fibers

In this work, fibers used in surface fabrication have been generally non-adhesive (un-modified or passivated via –OH), while the background has varied between being adhesive (PLL) or non-adhesive (DM). In order to assess cellular interaction with surfaces more representative of native ECM, fibers were functionalized with the fibronectin-derived peptide –RGD. To this end, surfaces were made with –RGD-functionalized fibers on a non-adhesive (DM) background substrate, with varying RGD density and fiber topographies. Surfaces were made to vary the local –RGD density on fibers, as well as the total –RGD surface density.

As shown in Figure 6.9, the amount of –RGD attached to a fibrous surface could be modified by varying–RGD concentration. For a given fibrous surface density, the total amount of attached –RGD increased as –RGD concentration used for attachment increased. In addition, when more fiber was present on a surface (higher surface density), more –RGD attached for a given –RGD solution concentration.

Further, as shown in Figure 6.10, -RGD density could be varied for fibrous surfaces made from a range of fiber diameters, seeded at a range of surface densities. For this, fibers were modified with –RGD at a constant solution concentration (250 μg/mL). Independent of fiber diameter, as seeding concentration increased (concurrent with an increase in fibrous surface density),

more –RGD attached to fibers. As a result, -RGD surface density can be controlled via –RGD concentration (used for attachment) and overall surface coverage of fibers.

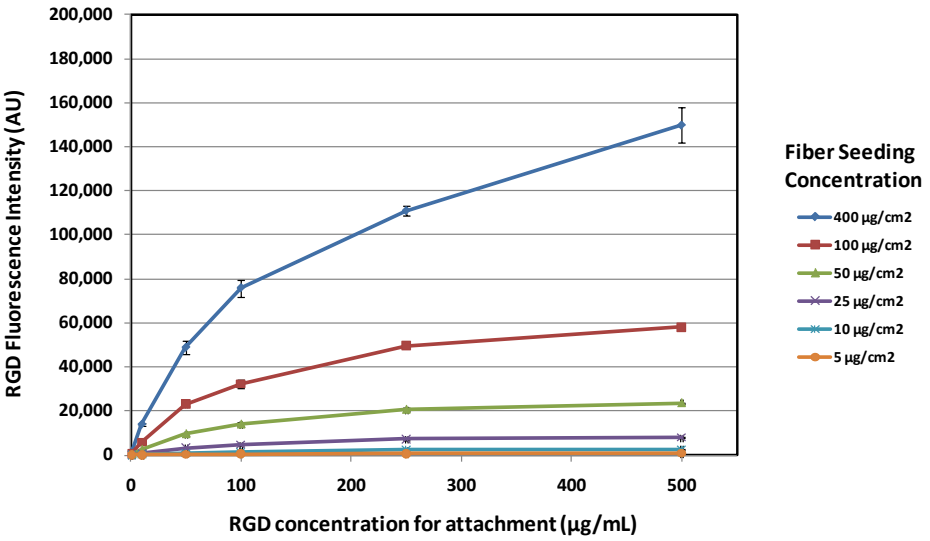

FIGURE 6.9. RGD-modified fiber surfaces – varying RGD concentration for modification and fiber surface density.

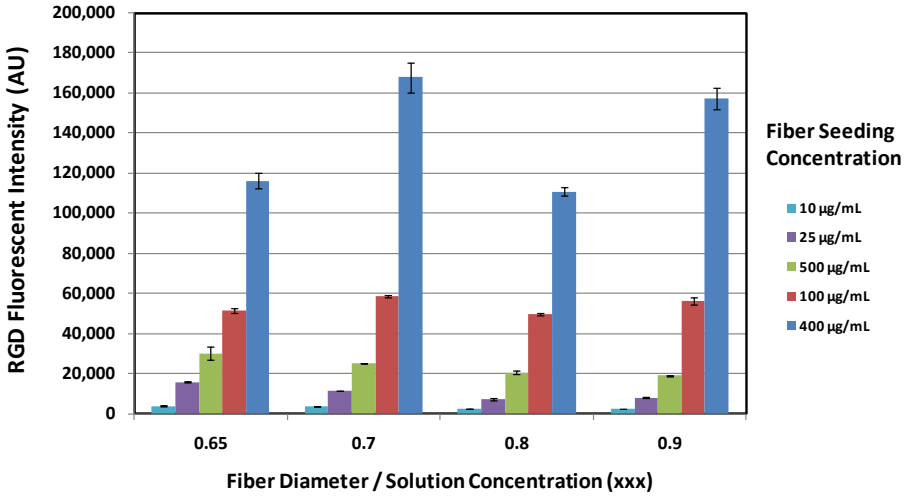

FIGURE 6.10. RGD-modified fiber surfaces – varying fiber diameter and surface density.

3.4 Cell culture on RGD-functionalized fibers

To assess cellular behavior on surfaces in which fibers, as an ECM-mimetic, are functionalized with –RGD, a variety of surface topographies were created. The influence between –RGD functionalized fibrous surfaces and cells was explored for ECs, 3T3s and SMCs.

3.4.1 Cell culture on RGD-functionalized fibers- varying RGD concentration and fibrous surface density

Mesh surface topographies were fabricated over a wide range of surface densities by varying fiber seeding concentration (5 µg/mL to 400 µg/mL). The amount of attached –RGD on a surface was varied by functionalizing surfaces over a range of –RGD concentrations (1 µg/mL to 500 µg/mL –GRGDSP). As a control peptide, for non-specific cell adhesion, surfaces were also functionalized with 500 µg /mL mixed –GRADSP peptide. Background substrate was passivated with a dextran monolayer.

Figures 6.11, 6.12 and 6.13 show the relative number of 3T3, BEC, and SMC cells measured for each surface after 1 and 5 days of culture, while figures 6.15A, 6.15B and 6.15C show corresponding fluorescence images of cells after 1 day of culture.

On day 1, both 3T3s and BECs showed the general trend of increased amount of cell adhesion as RGD-fiber density increased; additionally, at higher concentrations of attached RGD, greater cell adhesion was also observed.

In contrast, day 5 cell proliferation did not show the same day 1 trends. For 3T3s, the highest amount of cell proliferation was measured on high fibrous density, high RGD density surfaces (500 µg/mL GRGDSP concentration, 400

μg/mL seeding concentration). Further, on all 3T3 surfaces, cell proliferation was inhibited versus control PLL surfaces, ranging between only 0.5% to 16% of control on day 1, and 0.005% to 6% on day 5 (Figure 6.11).

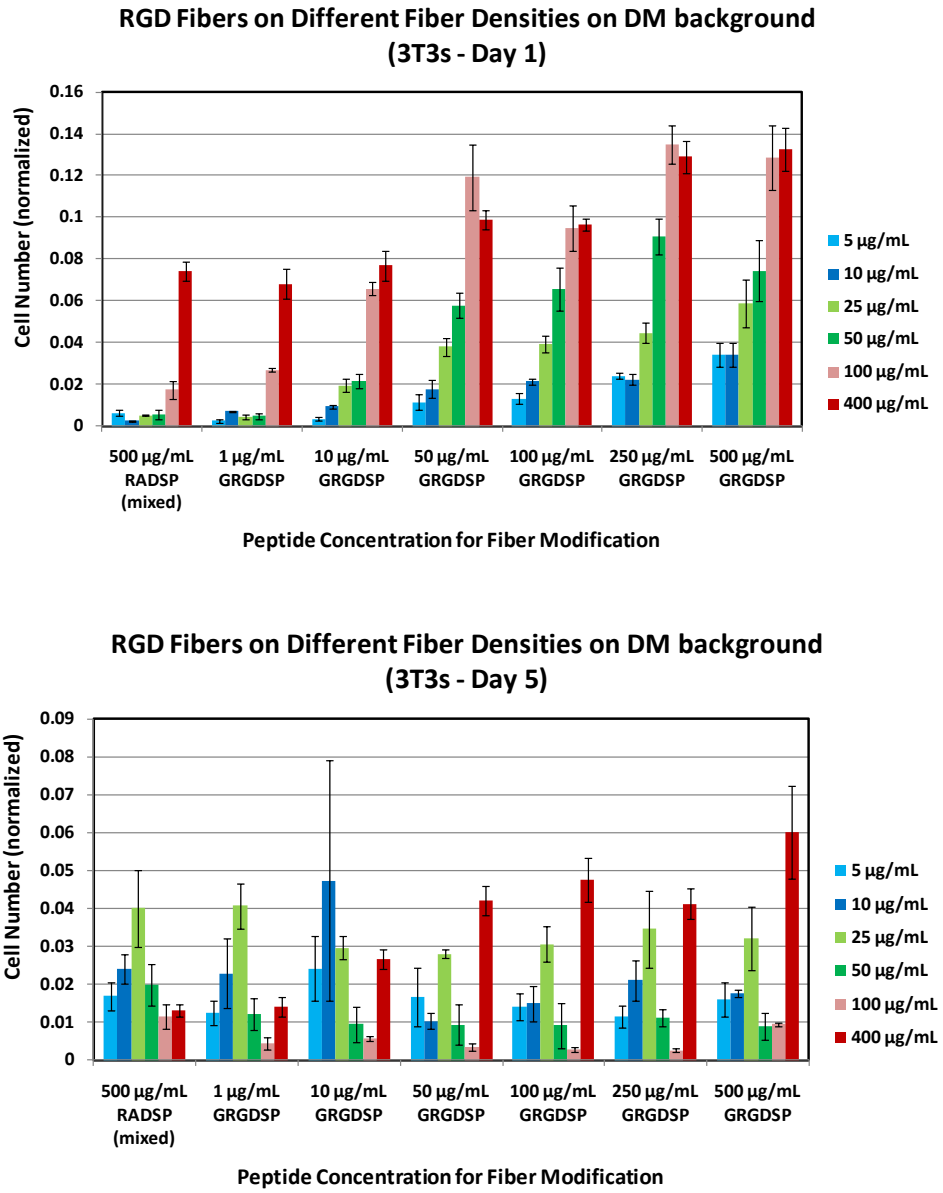

FIGURE 6.11. 3T3 cell proliferation on RGD-functionalized fibers on passivated (DM) background, varying RGD density and fiber surface density – 1 and 5 day. Cell number is normalized versus flat PLL surfaces. Error bars: standard error.

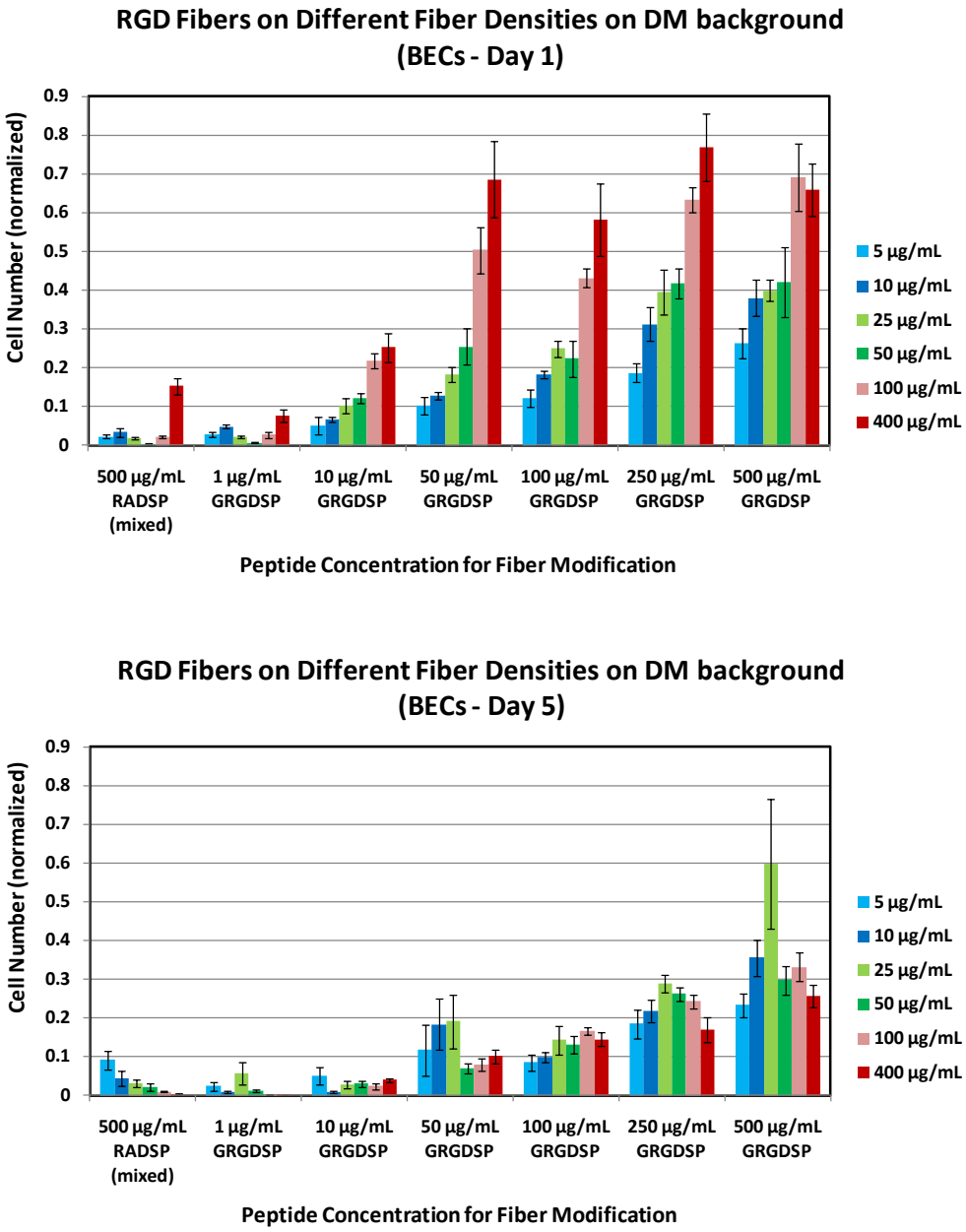

FIGURE 6.12. BEC proliferation on RGD-functionalized fibers on passivated (DM) background, varying RGD density and fiber surface density – 1 and 5 day. Cell number is normalized versus flat PLL surfaces. Error bars: standard error.

For BECs, after 5 days, greater amount of cell proliferation was observed on fibers with higher amounts of attached RGD (Figure 6.12). This day 1 and day 5 trend can be seen in the corresponding fluorescent images of Figure 6.14B.

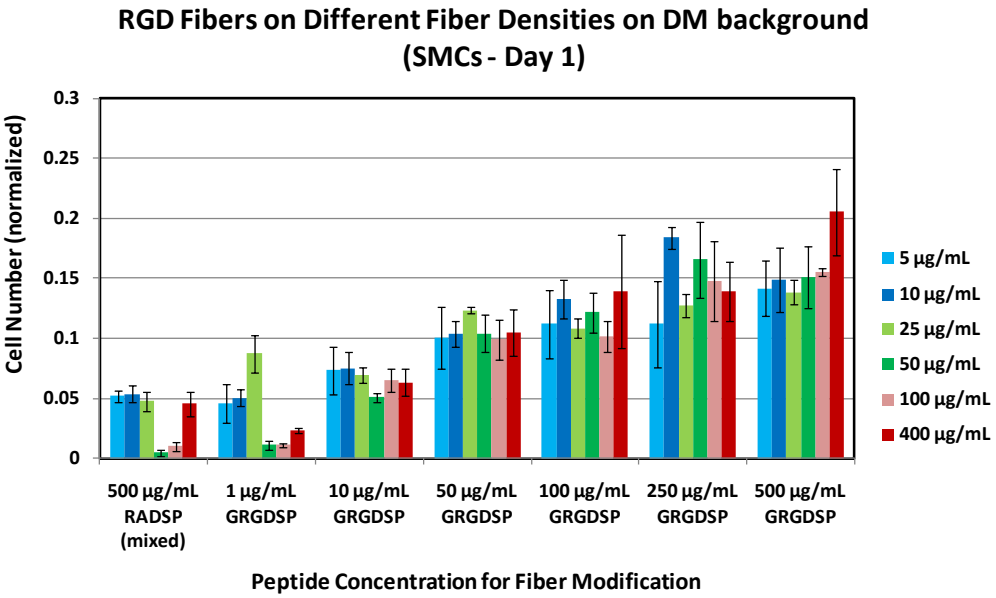

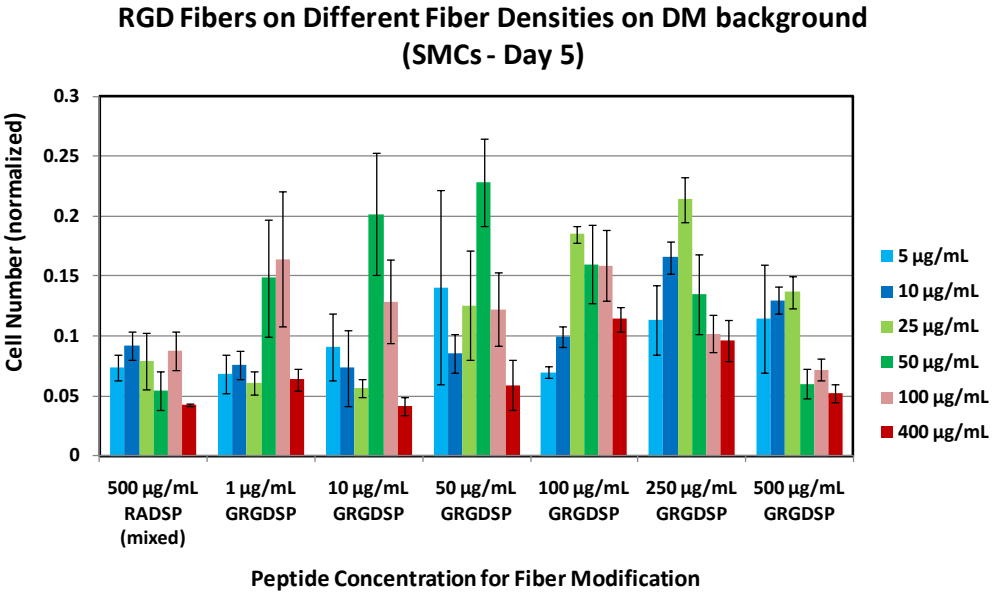

FIGURE 6.13. SMC proliferation on RGD-functionalized fibers on passivated (DM) background, varying RGD density and fiber surface density – 1 and 5 day. Cell number is normalized versus flat PLL surfaces. Error bars: standard error.

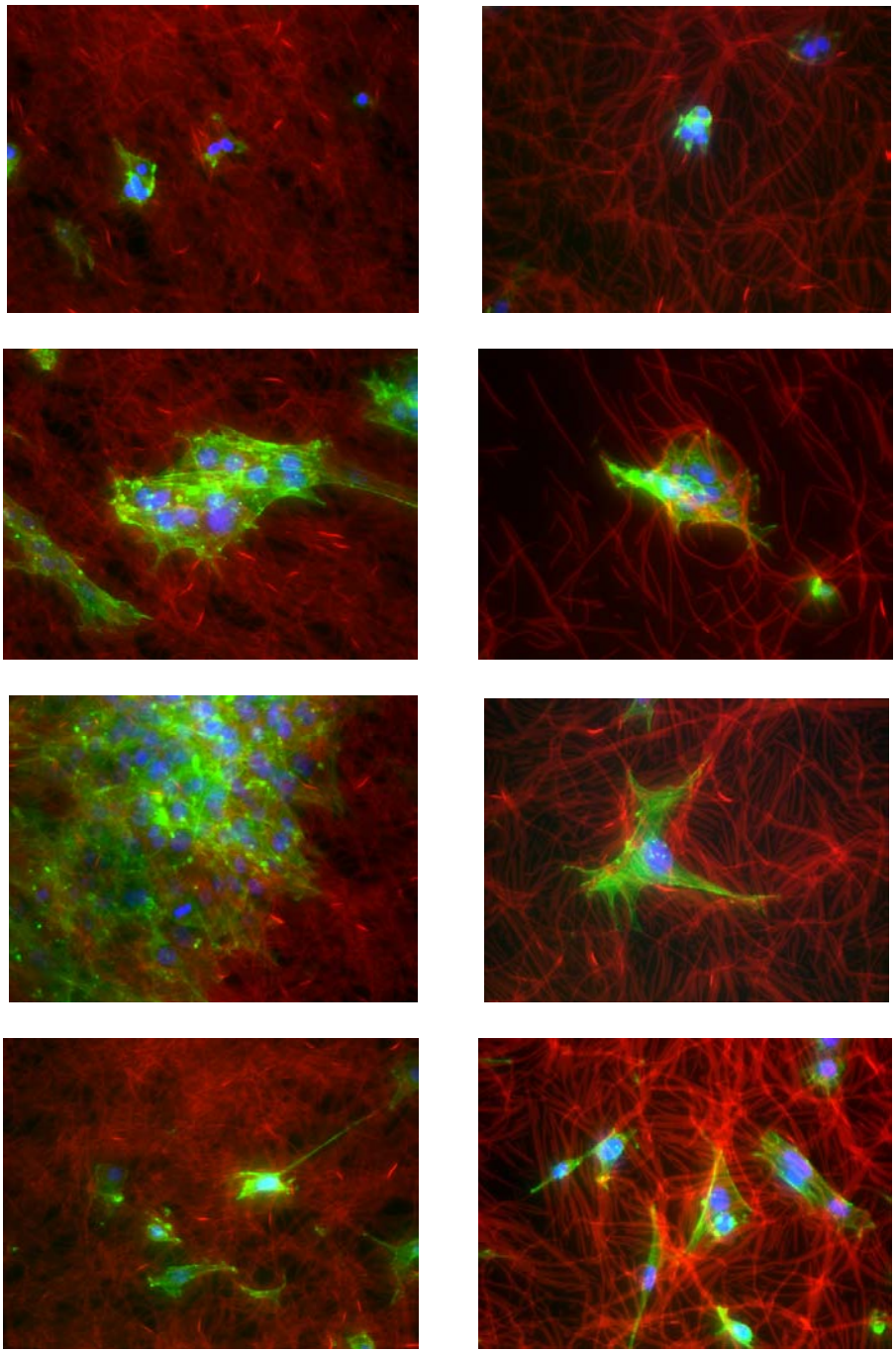

FIGURE 6.14A. 3T3s cultured on RGD-functionalized fibers on passivated (DM) background, varying RGD density and fiber surface density. 3T3s were cultured 1 day on high surface density (lt. column, seeded @ 400 µg/mL) or a lower surface density (rt. column, seeded @ 100 µg/mL). Fibers were modified with different amounts of RGD, increasing from the 2nd row to 4th row (modified with 10 µg/mL, 100 µg/mL or 500 µg/mL RGD). Fibers in the 1st row were modified with 500 µg/mL GRADSP. Images are false-colored: Fibers – red, actin – green, and nucleus – blue. Inverted fluorescence microscope, 40x objective. Images are 188µm x 141 µm (W x H).

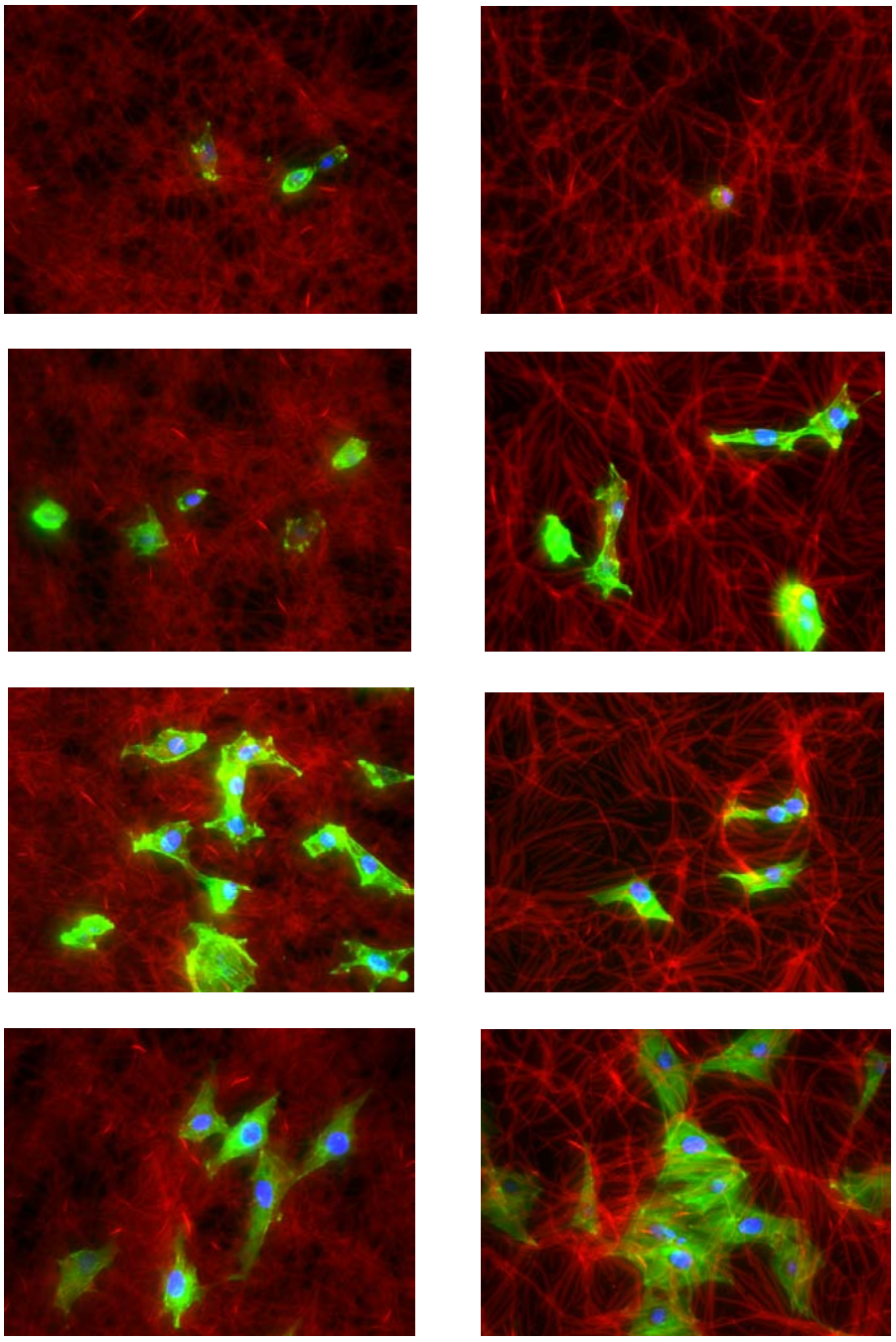

FIGURE 6.14B. BECs cultured on RGD-functionalized fibers on passivated (DM) background, varying RGD density and fiber surface density. BECs were cultured 1 day on high surface density (lt. column, seeded @ 400 µg/mL) or a lower surface density (rt. column, seeded @ 100 µg/mL). Fibers were modified with different amounts of RGD, increasing from the 2nd row to 4th row (modified with 10 µg/mL, 100 µg/mL or 500 µg/mL RGD). Fibers in the 1st row were modified with 500 µg/mL GRADSP. Images are false-colored: Fibers – red, actin – green, and nucleus – blue. Inverted fluorescence microscope, 40x objective. Images are 188µm x 141 µm (W x H).

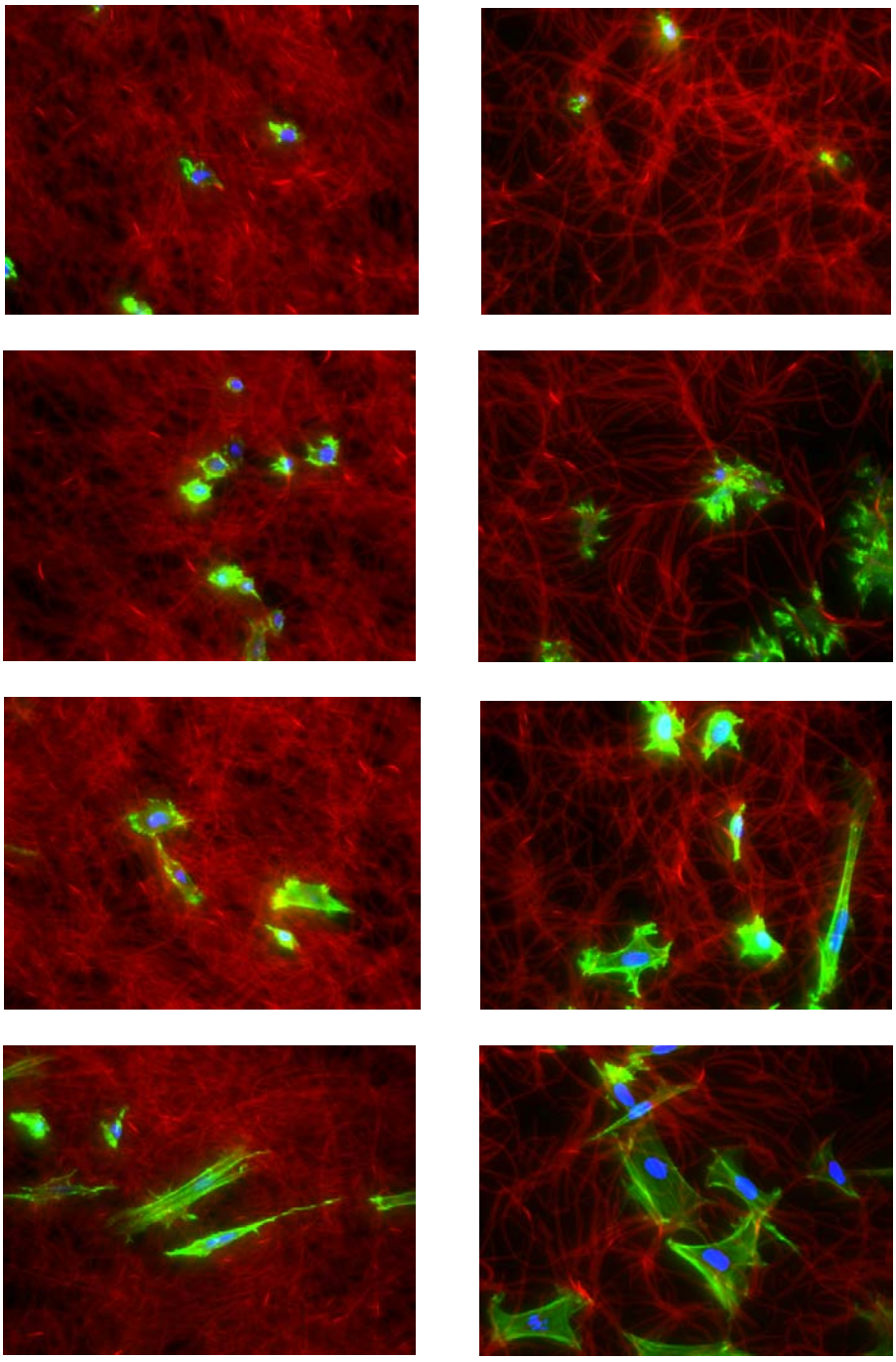

FIGURE 6.14C. SMCs cultured on RGD-functionalized fibers on passivated (DM) background, varying RGD density and fiber surface density. SMCs were cultured 1 day on high surface density (lt. column, seeded @ 400 µg/mL) or a lower surface density (rt. column, seeded @ 100 µg/mL). Fibers were modified with different amounts of RGD, increasing from the 2nd row to 4th row (modified with 10 µg/mL, 100 µg/mL or 500 µg/mL RGD). Fibers in the 1st row were modified with 500 µg/mL GRADSP. Images are false-colored: Fibers – red, actin – green, and nucleus – blue. Inverted fluorescence microscope, 40x objective. Images are 188µm x 141 µm (W x H).

3.4.2 Cell culture on RGD-functionalized fibers- varying fiber diameter and fibrous surface density

Mesh surface topographies were fabricated over a wide range of surface densities by varying fiber seeding concentration (10 µg/mL to 400 µg/mL). The amount of attached –RGD on a surface was varied by functionalizing surfaces at a constant –RGD concentrations (250 µg/mL –GRGDSP), but varying the diameter of attached fiber. Background substrate was passivated with a generally non-adhesive dextran monolayer.

Figures 6.15 shows the relative number of 3T3, BEC, and SMC cells measured for each surface after 5 days of culture, and corresponding fluorescent images are shown in Figures 6.16A, 6.16B and 6.16C.

Proliferation of 3T3s was severely limited on fibrous surfaces compared to the control PLL surface, with the highest amount of cell proliferation <10% that of control. In contrast, BECs experienced relatively high rates of proliferation, and formed the characteristic cobblestone appearance on many of the surfaces (Figure 6.16B). SMC cell proliferation was highest on lower density surfaces. Looking at the corresponding images in Figure 6.16C, SMCs on high density surfaces do not appear able to elongate; on low density surfaces, cells are able to spread and stretch in reaching from fiber to fiber.

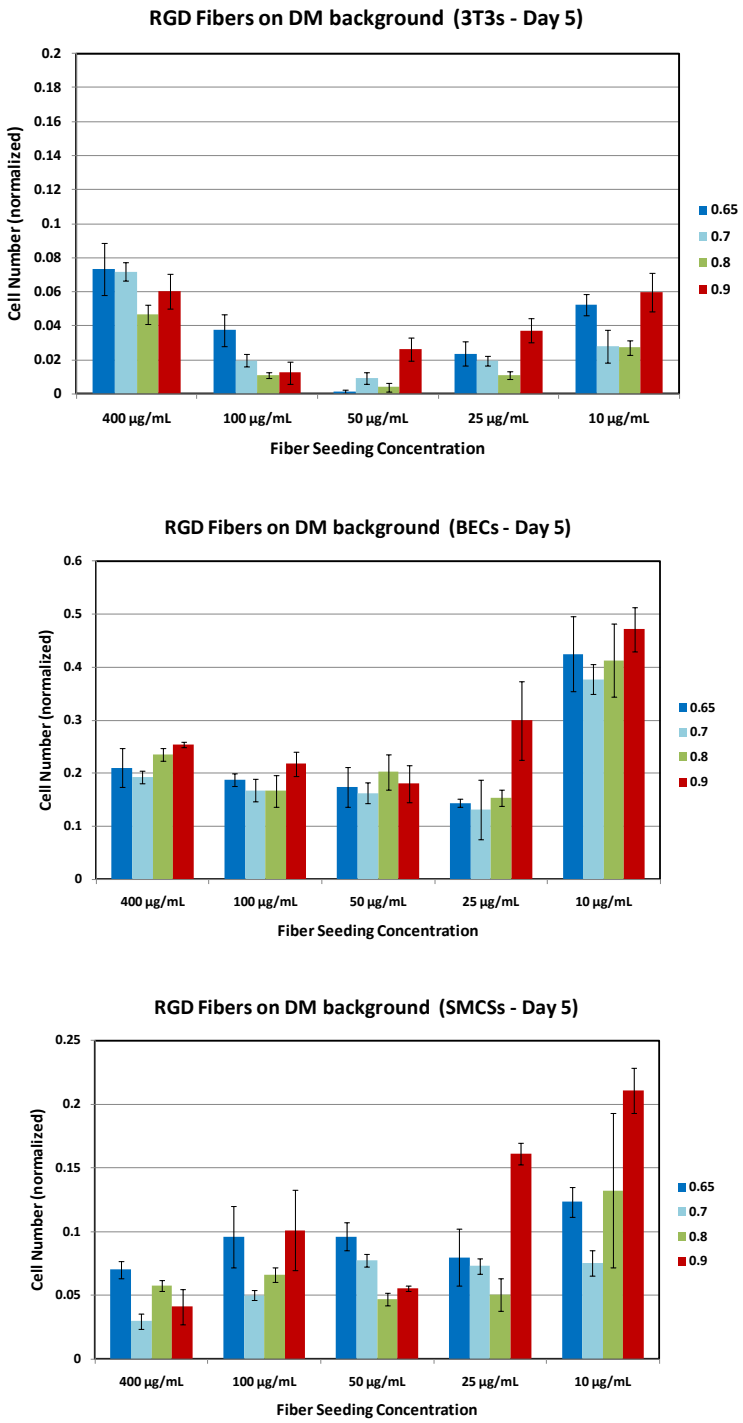

FIGURE 6.15. 3T3, BEC and SMC cell proliferation on RGD-functionalized fibers on passivated (DM) background, varying fiber diameter. Cells were cultured 5 days on a range of surface densities (seeding concentration from 10 to 400 µg/mL). All fibers were modified using the same RGD concentration (250 µg/mL). Fiber diameter ranged from nano-fibrous to micro-fibrous. Cell number is normalized versus flat PLL surfaces. Error bars: standard error.

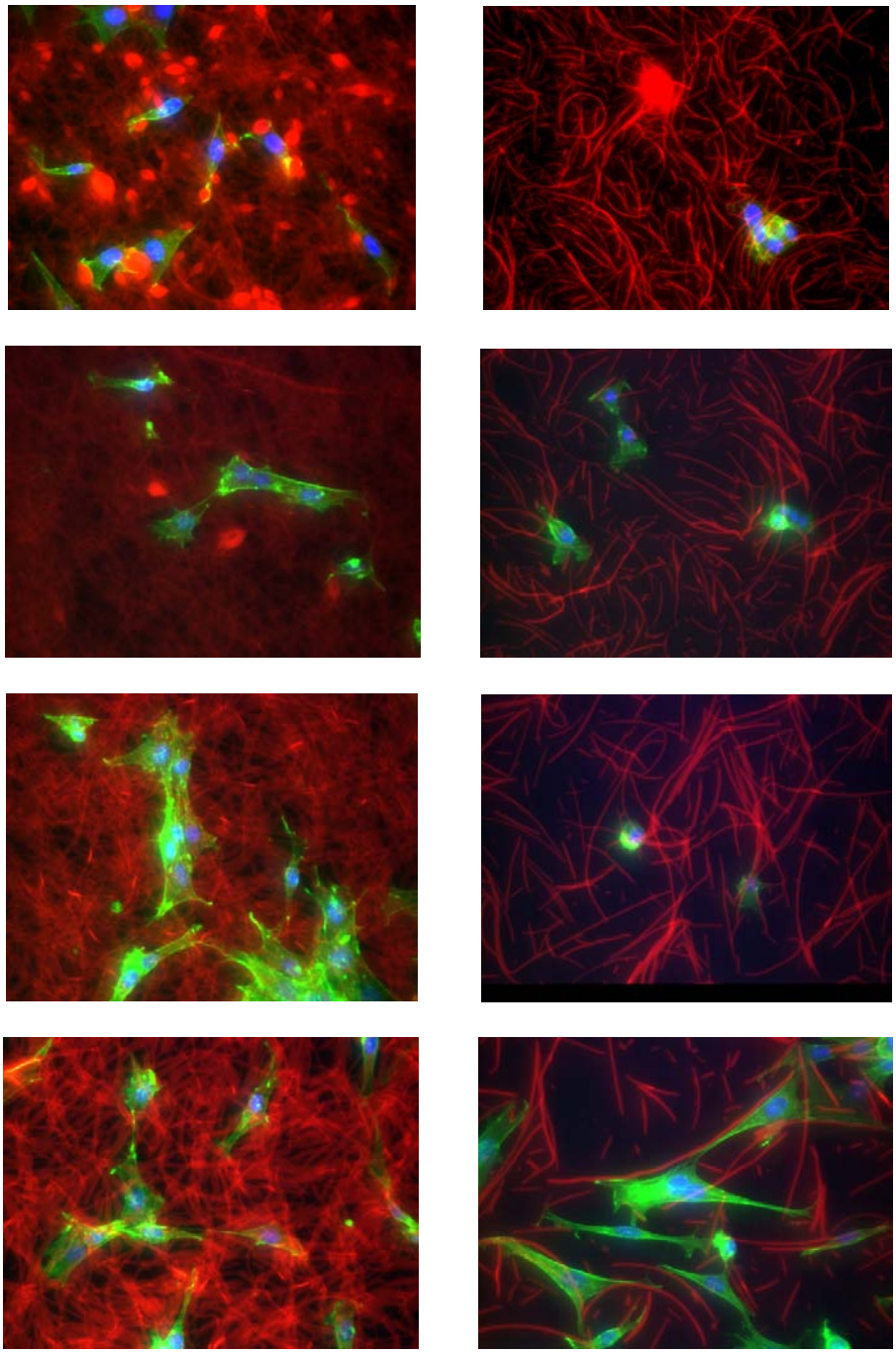

FIGURE 6.16A. 3T3s cultured on RGD-functionalized fibers on passivated (DM) background, varying fiber diameter. 3T3s were cultured 5 days on high surface density (left column, seeded @ 400 µg/mL) or a lower surface density (right column, seeded @ 25 µg/mL). Fibers were modified using the same RGD concentration (250 µg/mL). Fiber diameter ranged from nano-fibrous to micro-fibrous (increasing from 1st row to 4th row). Images are false-colored: Fibers – red, actin – green, and nucleus – blue. Inverted fluorescence microscope, 40x objective. Images are 188µm x 141 µm (W x H).

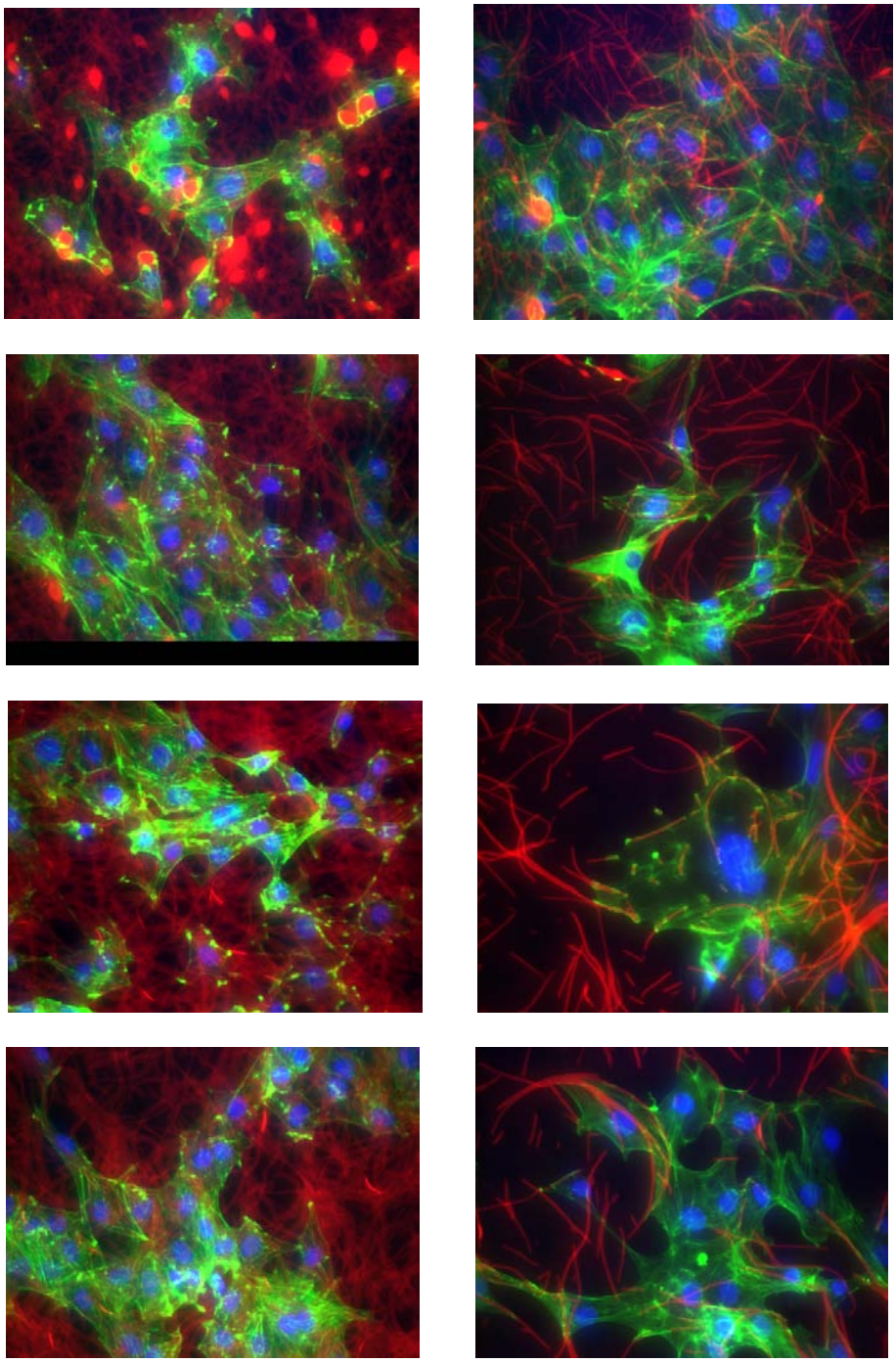

FIGURE 6.16B. BECs cultured on RGD-functionalized fibers on passivated (DM) background, varying fiber diameter. BECs were cultured 5 days on high surface density (left column, seeded @ 400 µg/mL) or a lower surface density (right column, seeded @ 25 µg/mL). Fibers were modified using the same RGD concentration (250 µg/mL). Fiber diameter ranged from nano-fibrous to micro-fibrous (increasing from 1st row to 4th row). Images are false-colored: Fibers – red, actin – green, and nucleus – blue. Inverted fluorescence microscope, 40x objective. Images are 188µm x 141 µm (W x H).

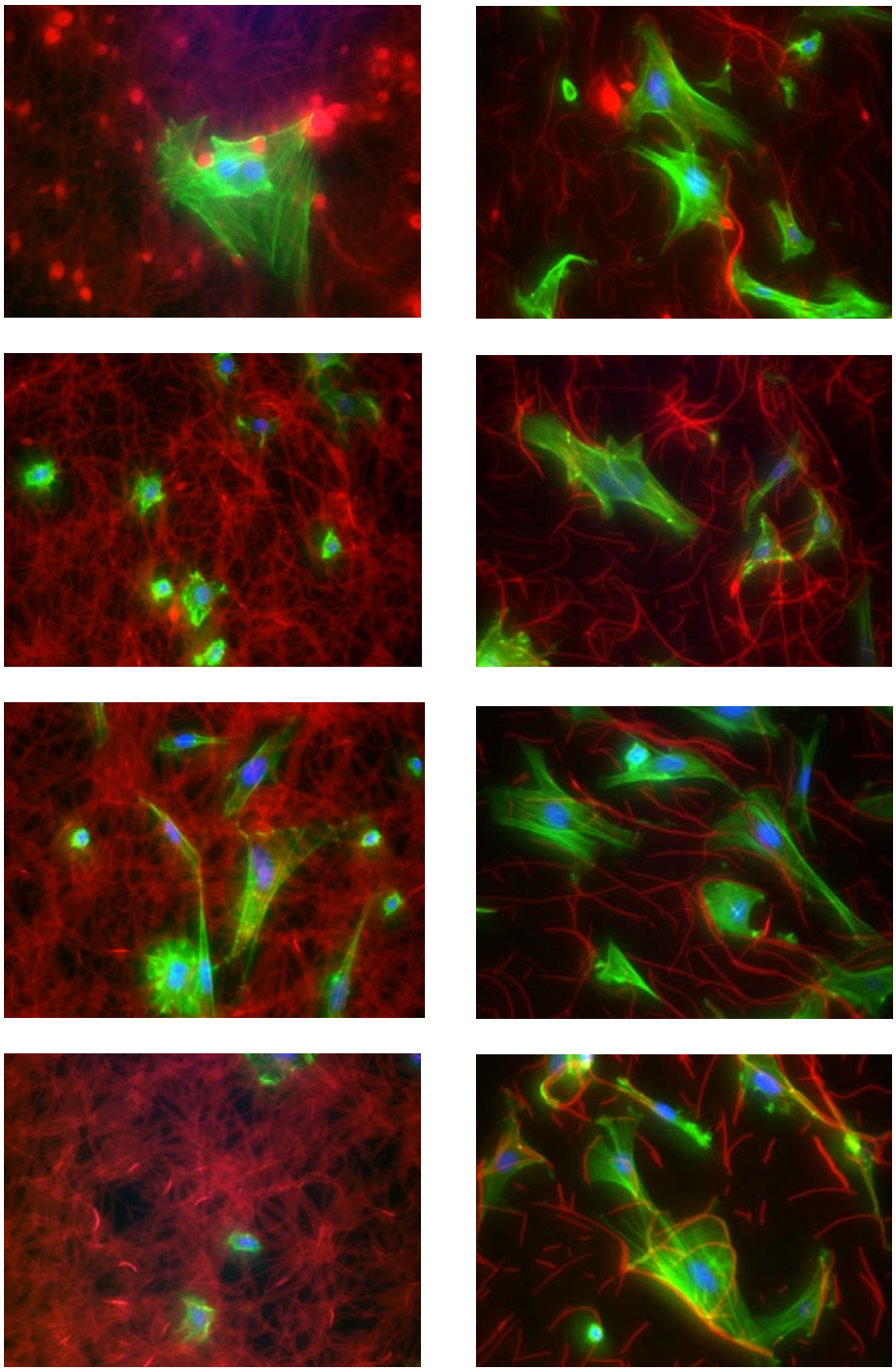

FIGURE 6.16C. SMCs cultured on RGD-functionalized fibers on passivated (DM) background, varying fiber diameter. SMCs were cultured 5 days on high surface density (left column, seeded @ 400 µg/mL) or a lower surface density (right column, seeded @ 25 µg/mL). Fibers were modified using the same RGD concentration (250 µg/mL). Fiber diameter ranged from nano-fibrous to micro-fibrous (increasing from 1st row to 4th row). Images are false-colored: Fibers – red, actin – green, and nucleus – blue. Inverted fluorescence microscope, 40x objective. Images are 188µm x 141 µm (W x H).

4. Conclusions

In this work, cell adhesion, proliferation and morphology were modulated via topography and surface chemistry. A variety of surface coatings were generated using fiber fragments (bristles) with diameters ranging from hundreds of nanometers to several microns. By minimizing PLL surface availability, higher fiber densities resulted in an overall decrease in cell adhesion. The non-adhesive fibers acted as a barrier, physically restricting cells from contacting the underlying adhesive surface. This property was most prominent on high-density fibrous mesh surfaces, which severely limited cell proliferation. On these particular surfaces, fibers covered the greatest adhesive surface area and minimized the spacing between fibers to which cells could attach.

These surface coatings were further modified for attachment of bioactive components (-RGD) to exert a greater degree of control over the cellular response. Overall, each cell type exhibited vastly different behavior from other cell types, and in response to the particular topography and amount of –RGD attached to the surface. These preliminary findings indicate that surfaces can be designed that limit fibroblast proliferation but promote endothelial cells. This is important for many medical applications (e.g. vascular grafts or general tissue regeneration), in which fibrosis needs to be prevented while native tissue cells infiltrate and restore tissue. These results can be utilized in the design of surfaces customized for specific applications.

CHAPTER 7

Conclusions and Future Work

1. Conclusions

In this work, fibrous hydrogel surfaces were developed that served as bioactive substrates for exerting fine control over the cellular response. Studies performed characterized the material, and provided numerous techniques for custom design of material properties and bioactivity. At a fundamental level, the surfaces were used to evaluate cellular response to nano- and micro- fibrous topography and surface chemistry; these results were then used to determine surface characteristics optimal for non-fouling materials or eliciting a specific cellular response.

The results of this work provide a mechanism by which materials implanted within the body can be shielded from eliciting an immune response and consequent rejection. This is a crucial requirement for numerous biomedical applications, including dialysis, filtration, contact lenses, drug delivery, tissue engineering constructs, and implants (stents, catheters, grafts, pacemakers, electrodes, organ transplants, bone screws, etc).

Effectiveness of these applications requires seamless integration of the implanted material within the body, without triggering an inflammatory response. An inflammatory response typically occurs when certain proteins or immune cells (e.g. white blood cells) recognize and adhere to a foreign material. This leads into

the foreign body reaction and subsequent fibrosis, thrombosis, or pathological inflammation, and ultimate rejection of the implanted material.

While this natural response is desirable for wound healing or ridding the body of something like a splinter, the foreign body response is detrimental for implanted materials and devices. Formation of a fibrotic barrier around electrodes or pacemakers severely limits device integration and *in vivo* performance. For blood-contacting devices, such as stents or vascular grafts, components in the blood may initiate an inflammatory cascade of events leading to platelet adhesion, thrombus formation, recruitment and adhesion of white blood cells (inflammation), and subsequent occlusion of the vessel over time.

These detrimental responses can be prevented by rendering materials "invisible" to the immune system. This requirement is fulfilled by the dex-PAA fibrous structures developed in this work. In this work, a fibrous hydrogel coating is applied to a material's surface. Depending on particular modifications made to the fibers, the coating functions either as a (1) ***barrier***, effectively shielding the underlying material from immune cells and potential inflammatory response or (2) ***bridge***, inducing the body's cells to interact with the coating in a specific, desirable manner and result in seamless integration of the underlying material within the body.

The fibrous coatings developed in this work operate by mediating the interfacial interaction between the body (cellular response/biological components) and underlying implanted material. This takes place at three levels of complexity – chemical, topographical and mechanical properties. In this work, these three

properties are tunable and can be optimized to tailor the body's response towards acceptance of the implanted material.

The surface coating itself is constructed from nanofibers and microfibers of dextran and poly(acrylic acid) (PAA) polymers, generated via a process of electrospinning. Long electrospun dextran-PAA fibers are cross-linked for aqueous stability, creating dex-PAA *hydrogel* fibers, which are then fragmented into short fiber segments. The end result of this process is a collection of very short dex-PAA hydrogel fibers, or "bristles," tunable in size between 400nm-4μm in diameter and 1μm-1mm in length. Immobilizing these fibrous "bristles" onto the surface of an implantable material forms a coating that functions as a camouflaging *barrier* or *bridge*.

When fibers are implemented as a ***barrier*** coating, they are customized to resist both protein adsorption and cell adhesion. These are events that instigate inflammatory responses that lead to implant rejection. For these coatings, the fibers are modified to display chemical groups to which proteins minimally adhere. This work demonstrated the protein-repellant nature of dex-PAA fibers, and that protein-repellant surfaces were also resistant to cell adhesion.

A further level of resistance to cell adhesion is achieved by optimizing fiber topography and coating density. This work demonstrates the cell-resistant nature for fibrous coatings applied at high surface density or constructed using micro-scale fiber diameters. Synergistically combining protein-resistant chemistry and cell-resistant topographies and coating densities results in a surface coating that can be applied as a resilient barrier to the immune system.

Camouflaged by this protein- and cell-resistant fibrous barrier, the underlying implanted material is able to appear "invisible" to the immune system, evading recognition as a foreign body and ultimate rejection.

When fibers are implemented as a ***bridge*** coating, they are customized to interact with the body's cells to promote natural incorporation of the material. For these coatings, the fibers display topographical and chemical cues derived from the native extracellular environment. This mimicry of the native environment provides signals to the body's cells, inducing them to integrate the fiber-coated, implanted material within the body. This work demonstrates that surface coatings can be fabricated to resemble the fibrous, often mesh-like, nature of native extracellular matrix.

The topographical and chemical cues exposed to cells direct the interaction between cells and the fibrous coating. The cellular response changes and can be directed towards that which exists in native tissue. In this usage of the fibrous coating, the coating serves as a bridge between the implanted material and body. By camouflaging the implanted material to mimic natural extracellular environments, the body's cells may seamlessly integrate the implanted material with native tissue.

Most therapeutic approaches rely on *systemic* suppression of the immune system to prevent implant rejection (e.g. NSAIDs, glucocorticoids). Although often effective, these systemic treatments compromise the overall integrity of an individual's immune system. This leaves the entire body susceptible to attack by infection and disease. The work developed here differentiates itself by affecting

the immune system only *locally a*round the implanted material. The immune system does not react towards the implant, but is still free to protect the remainder of the body, acting normally to combat infections and disease. Versus other localized therapies, the fibrous surface coatings in this work have unique, new characteristics giving them resistance to commonly encountered problems. Alternative implant coatings are typically comprised of (1) thin, monolayer chemical coatings or (2) slab gel coatings.

Thin chemical coatings often lose effectiveness from slight defects, such as imperfect coverage or chemical changes that occur post-implantation or from sterilization. These defects create a weak point permitting the invasion of immune cells and proteins to the underlying implanted material. In contrast, the dex-PAA fibrous coatings remain effective despite these defects. Since the fibrous coatings synergistically use topography, surface coverage, mechanical properties and chemistry to function, a defect damaging one of these levels of functionality does not destroy the remaining levels of activity. Even when coating defects allow proteins to reach the implanted material, fibrous topography still provides an effective barrier against the invading cells.

Gel coatings have problems with cracking and detachment from the implanted material. Gels tend to have a sponge-like nature, expanding and contracting according to environmental conditions that change liquid availability. As water is absorbed or lost by a slab-gel coating, dramatic size changes cause the gel to crack or detach. In contrast, due to the small size scale and innate

discontinuous coverage of the individual gel fibers comprising the work described here, the fibrous-gel coating does not crack or detach.

New improvements to biomaterial coating technology are realized by this research. This technology represents a shift from coating a material with a continuous phase to coating a material with a fibrous, tunable surface that can be customized to either bridge a material with native tissue, or form a barrier around the material to shield off immune system attack. Fibrous surface coatings outperform other surfaces in terms of stability, control over cell adhesion and protein adsorption, and ease of attachment. Other coatings do not allow the wide range of structures attainable with fiber coatings, which are tunable over multiple levels of complexity, including chemistry, density, topography and mechanical properties.

Potential benefits of this research include (1) the ability to implant therapeutic devices not previously possible, and (2) improved outcomes when implanting traditional materials, such as vascular grafts, electrodes or pacemakers. At a bare minimum, results of this work will help improve the longevity of implanted materials. Realizing the full potential of these coatings will allow the successful incorporation of virtually any material previously rejected by the immune system. Results of this work could potentially reduce the economic burden on the health care system by obviating the need for systemic anti-inflammatory and immunosuppressive drugs typically required for implanted devices, and avoiding the adverse side effects typically associated with these

drugs. Societal benefits include improvements in medicine, with a greater range of effective, implantable materials and devices available.

2. Future Work

In this work, a broad overview of surface and scaffolding fabrication using dex-PAA fibers was thoroughly characterized and methods developed for custom-design of mechanical, chemical and morphological properties. This provides a solid foundation for future work that involves the custom design of finely tuned fibrous scaffolding oriented towards a specific biomedical application.

REFERENCES

1. Ye, S. H.; Watanabe, J.; Iwasaki, Y.; Ishihara, K., Antifouling blood purification membrane composed of cellulose acetate and phospholipid polymer. *Biomaterials* **2003,** *24* (23), 4143-52.

2. Herrwerth, S.; Eck, W.; Reinhardt, S.; Grunze, M., Factors that determine the protein resistance of oligoether self-assembled monolayers --internal hydrophilicity, terminal hydrophilicity, and lateral packing density. *J Am Chem Soc* **2003,** *125* (31), 9359-66.

3. McArthur, S. L.; McLean, K. M.; St John, H. A.; Griesser, H. J., XPS and surface-MALDI-MS characterisation of worn HEMA-based contact lenses. *Biomaterials* **2001,** *22* (24), 3295-304.

4. Kodjikian, L.; Casoli-Bergeron, E.; Malet, F.; Janin-Manificat, H.; Freney, J.; Burillon, C.; Colin, J.; Steghens, J. P., Bacterial adhesion to conventional hydrogel and new silicone-hydrogel contact lens materials. *Graefes Arch Clin Exp Ophthalmol* **2008,** *246* (2), 267-73.

5. Keselowsky, B. G.; Bridges, A. W.; Burns, K. L.; Tate, C. C.; Babensee, J. E.; LaPlaca, M. C.; Garcia, A. J., Role of plasma fibronectin in the foreign body response to biomaterials. *Biomaterials* **2007,** *28* (25), 3626-31.

6. Morra, M.; Cassinelli, C., Biomaterials surface characterization and modification. *Int J Artif Organs* **2006,** *29* (9), 824-33.

7. Bos, G. W.; Scharenborg, N. M.; Poot, A. A.; Engbers, G. H.; Beugeling, T.; van Aken, W. G.; Feijen, J., Proliferation of endothelial cells on surface-immobilized albumin-heparin conjugate loaded with basic fibroblast growth factor. *J Biomed Mater Res* **1999,** *44* (3), 330-40.

8. Irvine, D. J.; Mayes, A. M.; Satija, S. K.; Barker, J. G.; Sofia-Allgor, S. J.; Griffith, L. G., Comparison of tethered star and linear poly(ethylene oxide) for control of biomaterials surface properties. *J Biomed Mater Res* **1998,** *40* (3), 498-509.

9. Heyes, C. D.; Groll, J.; Moller, M.; Nienhaus, G. U., Synthesis, patterning and applications of star-shaped poly(ethylene glycol) biofunctionalized surfaces. *Mol Biosyst* **2007,** *3* (6), 419-30.

10. Pasche, S.; Voros, J.; Griesser, H. J.; Spencer, N. D.; Textor, M., Effects of ionic strength and surface charge on protein adsorption at PEGylated surfaces. *J Phys Chem B* **2005,** *109* (37), 17545-52.

11. Chen, H.; Hu, X.; Zhang, Y.; Li, D.; Wu, Z.; Zhang, T., Effect of chain density and conformation on protein adsorption at PEG-grafted polyurethane surfaces. *Colloids Surf B Biointerfaces* **2008,** *61* (2), 237-43.

12. Singh, N.; Bridges, A. W.; Garcia, A. J.; Lyon, L. A., Covalent tethering of functional microgel films onto poly(ethylene terephthalate) surfaces. *Biomacromolecules* **2007,** *8* (10), 3271-5.

13. Nolan, C. M.; Reyes, C. D.; Debord, J. D.; Garcia, A. J.; Lyon, L. A., Phase transition behavior, protein adsorption, and cell adhesion resistance of poly(ethylene glycol) cross-linked microgel particles. *Biomacromolecules* **2005,** *6* (4), 2032-9.

14. Gonzalez, A. L.; Gobin, A. S.; West, J. L.; McIntire, L. V.; Smith, C. W., Integrin interactions with immobilized peptides in polyethylene glycol diacrylate hydrogels. *Tissue Eng* **2004,** *10* (11-12), 1775-86.

15. Unsworth, L. D.; Sheardown, H.; Brash, J. L., Protein-resistant poly(ethylene oxide)-grafted surfaces: chain density-dependent multiple mechanisms of action. *Langmuir* **2008,** *24* (5), 1924-9.

16. Sofia, S. J.; Premnath, V. V.; Merrill, E. W., Poly(ethylene oxide) Grafted to Silicon Surfaces: Grafting Density and Protein Adsorption. *Macromolecules* **1998,** *31* (15), 5059-70.

17. Martwiset, S.; Koh, A. E.; Chen, W., Nonfouling characteristics of dextran-containing surfaces. *Langmuir* **2006,** *22* (19), 8192-6.

18. Massia, S. P.; Stark, J.; Letbetter, D. S., Surface-immobilized dextran limits cell adhesion and spreading. *Biomaterials* **2000,** *21* (22), 2253-61.

19. Tugulu, S.; Silacci, P.; Stergiopulos, N.; Klok, H. A., RGD-Functionalized polymer brushes as substrates for the integrin specific adhesion of human umbilical vein endothelial cells. *Biomaterials* **2007,** *28* (16), 2536-46.

20. Latour, R. A., Thermodynamic perspectives on the molecular mechanisms providing protein adsorption resistance that include protein-surface interactions. *J Biomed Mater Res A* **2006,** *78* (4), 843-54.

21. Lord, M. S.; Stenzel, M. H.; Simmons, A.; Milthorpe, B. K., The effect of charged groups on protein interactions with poly(HEMA) hydrogels. *Biomaterials* **2006,** *27* (4), 567-75.

22. Carignano, M. A.; Szleifer, I. I., Prevention of protein adsorption by flexible and rigid chain molecules. *Colloids Surf B Biointerfaces* **2000,** *18* (3-4), 169-182.

23. Hoffmann, J.; Groll, J.; Heuts, J.; Rong, H.; Klee, D.; Ziemer, G.; Moeller, M.; Wendel, H. P., Blood cell and plasma protein repellent properties of star-PEG-modified surfaces. *J Biomater Sci Polym Ed* **2006,** *17* (9), 985-96.

24. Groll, J.; Ademovic, Z.; Ameringer, T.; Klee, D.; Moeller, M., Comparison of coatings from reactive star shaped PEG-stat-PPG prepolymers and grafted linear PEG for biological and medical applications. *Biomacromolecules* **2005,** *6* (2), 956-62.

25. Jeon, S. I.; Lee, J. H.; Andrade, J. D.; Degennes, P. G., PROTEIN SURFACE INTERACTIONS IN THE PRESENCE OF POLYETHYLENE OXIDE .1. SIMPLIFIED THEORY. *J Colloid Interface Sci* **1991,** *142* (1), 149-158.

26. Kochkodan, V. M.; Hilal, N.; Goncharuk, V. V.; Al-Khatib, L.; Levadna, T. I., Effect of the surface modification of polymer membranes on their microbiological fouling. *Colloid Journal* **2006,** *68* (3), 267-273.

27. Khorasani, M. T.; Mirzadeh, H., In vitro blood compatibility of modified PDMS surfaces as superhydrophobic and superhydrophilic materials. *Journal of Applied Polymer Science* **2004,** *91* (3), 2042-2047.

28. Sun, T. L.; Tan, H.; Han, D.; Fu, Q.; Jiang, L., No platelet can adhere - Largely improved blood compatibility on nanostructured superhydrophobic surfaces. *Small* **2005,** *1* (10), 959-963.

29. Rosario, R.; Gust, D.; Garcia, A. A.; Hayes, M.; Taraci, J. L.; Clement, T.; Dailey, J. W.; Picraux, S. T., Lotus effect amplifies light-induced contact angle switching. *Journal of Physical Chemistry B* **2004,** *108* (34), 12640-12642.

30. Wang, Q.; Zhang, B. W.; Qu, M. N.; Zhang, J. Y.; He, D. Y., Fabrication of superhydrophobic surfaces on engineering material surfaces with stearic acid. *Applied Surface Science* **2008,** *254* (7), 2009-2012.

31. Zhu, Y.; Li, J. M.; Wan, M. X.; Jiang, L., Superhydrophobic 3D microstructures assembled from 1D nanofibers of polyaniline. *Macromolecular Rapid Communications* **2008,** *29* (3), 239-243.

32. Li, W.; Amirfazli, A., Hierarchical structures for natural superhydrophobic surfaces. *Soft Matter* **2008,** *4* (3), 462-466.

33. Fang, W.; Mayama, H.; Tsujii, K., Formation mechanism of super water-repellent fractal surfaces of alkylketene dimer. *Colloids and Surfaces a-Physicochemical and Engineering Aspects* **2008,** *316* (1-3), 258-265.

34. Gessner, A.; Paulke, B. R.; Muller, R. H.; Goppert, T. M., Protein rejecting properties of PEG-grafted nanoparticles: influence of PEG-chain length and surface density evaluated by two-dimensional electrophoresis and bicinchoninic acid (BCA)-proteinassay. *Pharmazie* **2006,** *61* (4), 293-7.

35. Mei, Y.; Wu, T.; Xu, C.; Langenbach, K. J.; Elliott, J. T.; Vogt, B. D.; Beers, K. L.; Amis, E. J.; Washburn, N. R., Tuning cell adhesion on gradient poly(2-hydroxyethyl methacrylate)-grafted surfaces. *Langmuir* **2005,** *21* (26), 12309-14.

36. Yoshikawa, C.; Goto, A.; Tsujii, Y.; Fukuda, T.; Kimura, T.; Yamamoto, K.; Kishida, A., Protein repellency of well-defined, concentrated poly(2-hydroxyethyl methacrylate) brushes by the size-exclusion effect. *Macromolecules* **2006,** *39* (6), 2284-2290.

37. Pertsin, A. J.; Grunze, M.; Garbuzova, I. A., Low-energy configurations of methoxy triethylene glycol terminated alkanethiol self-assembled monolayers and their relevance to protein adsorption. *Journal of Physical Chemistry B* **1998,** *102* (25), 4918-4926.

38. Dalby, M. J.; Riehle, M. O.; Johnstone, H. J. H.; Affrossman, S.; Curtis, A. S. G., Nonadhesive nanotopography: Fibroblast response to poly(n-butyl methacrylate)-poly(styrene) demixed surface features. *J. Biomed. Mater. Res. Part A* **2003,** *67A* (3), 1025-1032.

39. Thapa, A.; Miller, D. C.; Webster, T. J.; Haberstroh, K. M., Nano-structured polymers enhance bladder smooth muscle cell function. *Biomaterials* **2003,** *24* (17), 2915-26.

40. Miller, D. C.; Thapa, A.; Haberstroh, K. M.; Webster, T. J., Endothelial and vascular smooth muscle cell function on poly(lactic-co-glycolic acid) with nano-structured surface features. *Biomaterials* **2004,** *25* (1), 53-61.

41. Thapa, A.; Webster, T. J.; Haberstroh, K. M., Polymers with nano-dimensional surface features enhance bladder smooth muscle cell adhesion. *J Biomed Mater Res A* **2003,** *67* (4), 1374-83.

42. Vance, R. J.; Miller, D. C.; Thapa, A.; Haberstroh, K. M.; Webster, T. J., Decreased fibroblast cell density on chemically degraded poly-lactic-co-glycolic acid, polyurethane, and polycaprolactone. *Biomaterials* **2004,** *25* (11), 2095-103.

43. Kunzler, T. P.; Drobek, T.; Schuler, M.; Spencer, N. D., Systematic study of osteoblast and fibroblast response to roughness by means of surface-morphology gradients. *Biomaterials* **2007,** *28* (13), 2175-82.

44. Curtis, A. S. G.; Dalby, M.; Gadegaard, N., Cell signaling arising from nanotopography: implications for nanomedical devices. *Nanomedicine* **2006,** *1* (1), 67-72.

45. Dalby, M. J., Cellular response to low adhesion nanotopographies. *Int J Nanomedicine* **2007,** *2* (3), 373-81.

46. Lim, J. Y.; Donahue, H. J., Cell sensing and response to micro- and nanostructured surfaces produced by chemical and topographic patterning. *Tissue Eng* **2007,** *13* (8), 1879-91.

47. Discher, D. E.; Janmey, P.; Wang, Y. L., Tissue cells feel and respond to the stiffness of their substrate. *Science* **2005,** *310* (5751), 1139-43.

48. Yeung, T.; Georges, P. C.; Flanagan, L. A.; Marg, B.; Ortiz, M.; Funaki, M.; Zahir, N.; Ming, W. Y.; Weaver, V.; Janmey, P. A., Effects of substrate stiffness on cell morphology, cytoskeletal structure, and adhesion. *Cell Motility and the Cytoskeleton* **2005,** *60* (1), 24-34.

49. Ghosh, K.; Pan, Z.; Guan, E.; Ge, S.; Liu, Y.; Nakamura, T.; Ren, X. D.; Rafailovich, M.; Clark, R. A., Cell adaptation to a physiologically relevant ECM mimic with different viscoelastic properties. *Biomaterials* **2007,** *28* (4), 671-9.

50. Engler, A. J.; Richert, L.; Wong, J. Y.; Picart, C.; Discher, D. E., Surface probe measurements of the elasticity of sectioned tissue, thin gels and polyelectrolyte multilayer films: Correlations between substrate stiffness and cell adhesion. *Surface Science* **2004,** *570* (1-2), 142-154.

51. Flanagan, L. A.; Ju, Y. E.; Marg, B.; Osterfield, M.; Janmey, P. A., Neurite branching on deformable substrates. *Neuroreport* **2002,** *13* (18), 2411-2415.

52. Flanagan, L. A.; Ju, Y. E.; Marg, B.; Osterfield, M.; Janmey, P. A., Neurite branching on deformable substrates. *Neuroreport* **2002,** *13* (18), 2411-5.

53. Sakiyama-Elbert, S. E.; Hubbell, J. A., Functional biomaterials: Design of novel biomaterials. *Annual Review of Materials Research* **2001,** *31*, 183-201.

54. Ma, P. X., Biomimetic materials for tissue engineering. *Adv Drug Deliv Rev* **2008,** *60* (2), 184-198.

55. Hubbell, J. A., Bioactive biomaterials. *Current Opinion in Biotechnology* **1999,** *10* (2), 123-129.

56. Keselowsky, B. G.; Collard, D. M.; Garcia, A. J., Surface chemistry modulates fibronectin conformation and directs integrin binding and specificity to control cell adhesion. *J Biomed Mater Res A* **2003,** *66* (2), 247-59.

57. Tziampazis, E.; Kohn, J.; Moghe, P. V., PEG-variant biomaterials as selectively adhesive protein templates: model surfaces for controlled cell adhesion and migration. *Biomaterials* **2000,** *21* (5), 511-20.

58. Hollmann, O.; Reichhart, C.; Czeslik, C., Kinetics of protein adsorption at a poly(acrylic acid) brush studied by surface plasmon resonance spectroscopy. *Zeitschrift Fur Physikalische Chemie-International Journal of Research in Physical Chemistry & Chemical Physics* **2008,** *222* (1), 205-215.

59. Hollmann, O.; Czeslik, C., Characterization of a planar poly(acrylic acid) brush as a materials coating for controlled protein immobilization. *Langmuir* **2006,** *22* (7), 3300-3305.

60. Schweikl, H.; Muller, R.; Englert, C.; Hiller, K. A.; Kujat, R.; Nerlich, M.; Schmalz, G., Proliferation of osteoblasts and fibroblasts on model surfaces of varying roughness and surface chemistry. *J Mater Sci Mater Med* **2007,** *18* (10), 1895-905.

61. Kodjikian, L.; Garweg, J. G.; Freney, J.; Burillon, C., Intraoperative antibiotics and bacterial contamination of the anterior chamber. *Eur J Ophthalmol* **2005,** *15* (1), 173; author reply 174.

62. Xu, F.; Persson, B.; Lofas, S.; Knoll, W., Surface plasmon optical studies of carboxymethyl dextran brushes versus networks. *Langmuir* **2006,** *22* (7), 3352-7.

63. Bulmus, V.; Chan, Y.; Nguyen, Q.; Tran, H. L., Synthesis and characterization of degradable p(HEMA) microgels: use of acid-labile crosslinkers. *Macromol Biosci* **2007,** *7* (4), 446-55.

64. Cooke, M. J.; Phillips, S.; Shah, D. S.; Athey, D.; Lakey, J. H.; Przyborski, S. A., Presentation of extracellular matrix motifs by biomimetic substrates to control cellular attachment and differentiation. *Journal of Anatomy* **2008,** *212* (1), 89-89.

65. Massia, S. P.; Stark, J., Immobilized RGD peptides on surface-grafted dextran promote biospecific cell attachment. *J Biomed Mater Res* **2001,** *56* (3), 390-399.

66. Mann, B. K.; West, J. L., Cell adhesion peptides alter smooth muscle cell adhesion, proliferation, migration, and matrix protein synthesis on modified surfaces and in polymer scaffolds. *J Biomed Mater Res* **2002,** *60* (1), 86-93.

67. Groll, J.; Fiedler, J.; Engelhard, E.; Ameringer, T.; Tugulu, S.; Klok, H. A.; Brenner, R. E.; Moeller, M., A novel star PEG-derived surface coating for specific cell adhesion. *J. Biomed. Mater. Res. Part A* **2005,** *74A* (4), 607-617.

68. Lee, K. Y.; Alsberg, E.; Hsiong, S.; Comisar, W.; Linderman, J.; Ziff, R.; Mooney, D., Nanoscale adhesion ligand organization regulates osteoblast proliferation and differentiation. *Nano Lett* **2004,** *4* (8), 1501-1506.

69. Lutolf, M. P.; Hubbell, J. A., Synthetic biomaterials as instructive extracellular microenvironments for morphogenesis in tissue engineering. *Nature Biotechnology* **2005,** *23* (1), 47-55.

70. Maheshwari, G.; Brown, G.; Lauffenburger, D. A.; Wells, A.; Griffith, L. G., Cell adhesion and motility depend on nanoscale RGD clustering. *J Cell Sci* **2000,** *113* (10), 1677-1686.

71. Zong, X.; Bien, H.; Chung, C. Y.; Yin, L.; Fang, D.; Hsiao, B. S.; Chu, B.; Entcheva, E., Electrospun fine-textured scaffolds for heart tissue constructs. *Biomaterials* **2005,** *26* (26), 5330-8.

72. Yang, S.; Leong, K. F.; Du, Z.; Chua, C. K., The design of scaffolds for use in tissue engineering. Part I. Traditional factors. *Tissue Eng* **2001,** *7* (6), 679-89.

73. Tuzlakoglu, K.; Bolgen, N.; Salgado, A. J.; Gomes, M. E.; Piskin, E.; Reis, R. L., Nano- and micro-fiber combined scaffolds: a new architecture for bone tissue engineering. *J Mater Sci Mater Med* **2005,** *16* (12), 1099-104.

74. Khang, G.; Lee, S. J.; Lee, J. H.; Lee, H. B., Interaction of fibroblast cells onto fibers with different diameter. *Korea Polymer Journal* **1999,** *7* (2), 102-107.

75. Pham, Q. P.; Sharma, U.; Mikos, A. G., Electrospun poly(epsilon-caprolactone) microfiber and multilayer nanofiber/microfiber scaffolds: Characterization of scaffolds and measurement of cellular infiltration. *Biomacromolecules* **2006,** *7* (10), 2796-2805.

76. Liao, S.; Li, B.; Ma, Z.; Wei, H.; Chan, C.; Ramakrishna, S., Biomimetic electrospun nanofibers for tissue regeneration. *Biomed Mater* **2006,** *1* (3), R45-53.

77. Norman, J. J.; Desai, T. A., Methods for fabrication of nanoscale topography for tissue engineering scaffolds. *Ann Biomed Eng* **2006,** *34* (1), 89-101.

78. Chen, R.; Hunt, J. A., Biomimetic materials processing for tissue-engineering processes. *Journal of Materials Chemistry* **2007,** *17* (38), 3974-3979.

79. Li, D.; Xia, Y. N., Electrospinning of nanofibers: Reinventing the wheel? *Advanced Materials* **2004,** *16* (14), 1151-1170.

80. Pham, Q. P.; Sharma, U.; Mikos, A. G., Electrospinning of polymeric nanofibers for tissue engineering applications: a review. *Tissue Eng* **2006,** *12* (5), 1197-211.

81. Sell, S.; Barnes, C.; Smith, M.; McClure, M.; Madurantakam, P.; Grant, J.; McManus, M.; Bowlin, G., Extracellular matrix regenerated: tissue engineering via electrospun biomimetic nanofibers. *Polymer International* **2007,** *56* (11), 1349-1360.

82. Pham, Q. P.; Sharma, U.; Mikos, A. G., Electrospinning of polymeric nanofibers for tissue engineering applications: A review. *Tissue Eng* **2006,** *12* (5), 1197-1211.

83. Tirtaatmadja, V.; Dunstan, D. E.; Roger, D. V., Rheology of dextran solutions. *Journal of Non-Newtonian Fluid Mechanics* **2001,** *97* (2-3), 295-301.

84. Kim, S. H.; Won, C. Y.; Chu, C. C., Synthesis and characterization of dextran-based hydrogel prepared by photocrosslinking. *Carbohydrate Polymers* **1999,** *40* (3), 183-190.

85. Lindberg, B.; Svensson, S., STRUCTURAL STUDIES ON DEXTRAN FROM LEUCONOSTOC MESENTEROIDES NRRL B-512. *Acta Chemica Scandinavica* **1968,** *22* (6), 1907-&.

86. Heinze, T.; Liebert, T.; Heublein, B.; Hornig, S., Functional polymers based on dextran. In *Polysaccharides Ii*, Springer-Verlag Berlin: Berlin, 2006; Vol. 205, pp 199-291.

87. Cadee, J. A.; van Luyn, M. J. A.; Brouwer, L. A.; Plantinga, J. A.; van Wachem, P. B.; de Groot, C. J.; den Otter, W.; Hennink, W. E., In vivo biocompatibility of dextran-based hydrogels. *J Biomed Mater Res* **2000,** *50* (3), 397-404.

88. Van Tomme, S. R.; Hennink, W. E., Biodegradable dextran hydrogels for protein delivery applications. *Expert Rev Med Devices* **2007,** *4* (2), 147-64.

89. Ifkovits, J. L.; Burdick, J. A., Review: photopolymerizable and degradable biomaterials for tissue engineering applications. *Tissue Eng* **2007,** *13* (10), 2369-85.

90. Jiang, H.; Fang, D.; Hsiao, B. S.; Chu, B.; Chen, W., Optimization and characterization of dextran membranes prepared by electrospinning. *Biomacromolecules* **2004,** *5* (2), 326-33.

91. Zong, X. H.; Kim, K.; Fang, D. F.; Ran, S. F.; Hsiao, B. S.; Chu, B., Structure and process relationship of electrospun bioabsorbable nanofiber membranes. *Polymer* **2002,** *43* (16), 4403-4412.

92. Chen, H.; Hsieh, Y. L., Ultrafine hydrogel fibers with dual temperature- and pH-responsive swelling behaviors. *Journal of Polymer Science Part a-Polymer Chemistry* **2004,** *42* (24), 6331-6339.

93. Nakajima, N.; Ikada, Y., Mechanism of amide formation by carbodiimide for bioconjugation in aqueous media. *Bioconjug Chem* **1995,** *6* (1), 123-30.

94. Uchida, E.; Uyama, Y.; Ikada, Y., SORPTION OF LOW-MOLECULAR-WEIGHT ANIONS INTO THIN POLYCATION LAYERS GRAFTED ONTO A FILM. *Langmuir* **1993,** *9* (4), 1121-1124.

95. Arndt, K. F.; Richter, A.; Ludwig, S.; Zimmermann, J.; Kressler, J.; Kuckling, D.; Adler, H. J., Poly(vinyl alcohol)/poly(acrylic acid) hydrogels: FT-IR spectroscopic characterization of crosslinking reaction and work at transition point. *Acta Polymerica* **1999,** *50* (11-12), 383-390.